IN-31
067135

NASA Contractor Report 204147
RD97–129

Precision Casting via Advanced Simulation and Manufacturing

Summary of Research

September 1997

Prepared for
Lewis Research Center
Under Cooperative Agreement NCC3–386

National Aeronautics and
Space Administration

RD97-129

Aerospace Industry Technology Program (AITP)

PRECISION CASTING VIA ADVANCED SIMULATION AND MANUFACTURING

Summary of Research

Period of Performance
March 1995 to February 1997

Rocketdyne Division
Boeing North American, Inc.
6633 Canoga Avenue
Canoga Park, CA 91303

Cooperative Agreement Number
NCC3-386

FOREWORD

The work reported herein was performed under the National Aeronautics and Space Administration Cooperative Agreement, NCC3-386. Dr. Bob Dreshfield and Bob Titran served as the NASA Project Managers.

ABSTRACT

A two-year program was conducted to develop and commercially implement selected casting manufacturing technologies to:

- Enable significant reductions in the costs of castings,
- Increase the complexity and dimensional accuracy of castings, and
- Reduce the development times for delivery of high quality castings.

The industry-led R&D project was cost shared with NASA's Aerospace Industry Technology Program (AITP). The Rocketdyne Division of Boeing North American, Inc. served as the team lead with participation from Lockheed Martin, Ford Motor Company, Howmet Corporation, PCC Airfoils, General Electric, UES, Inc., University of Alabama, Auburn University, Robinson, Inc., Aracor, and NASA-LeRC. The technical effort was organized into four distinct tasks. The accomplishments reported herein.

Task 1.0 developed advanced simulation technology for core molding. Ford headed up this task. On this program, a specialized core machine was designed and built. Task 2.0 focused on intelligent process control for precision core molding. Howmet led this effort. The primary focus of these experimental efforts was to characterize the process parameters that have a strong impact on dimensional control issues of injection molded cores during their fabrication. Task 3.0 developed and applied rapid prototyping to produce near net shape castings. Rocketdyne was responsible for this task. CAD files were generated using reverse engineering, rapid prototype patterns were fabricated using SLS and SLA, and castings produced and evaluated. Task 4.0 was aimed at developing technology transfer. Rocketdyne coordinated this task. Casting related technology, explored and evaluated in the first three tasks of this program, was implemented into manufacturing processes.

TABLE OF CONTENTS

	Page
FOREWORD	ii
ABSTRACT	ii
TABLE OF CONTENTS	iii
LIST OF FIGURES	v
LIST OF ACRONYMS	x
1.0 EXECUTIVE SUMMARY	1-1
1.1 Introduction	1-1
1.1.1 The Team	1-1
1.1.2 Technical Objectives and Schedule	1-1
1.2 Summary	1-3
1.2.1 Task 1.0 – Advanced Simulation Technology for Core Molding	1-3
1.2.2 Task 2.0 – Simulation and Control of Injection Molded Cores	1-4
1.2.3 Task 3.0 – Rapid, Near-Net Shape Casting	1-5
1.2.4 Task 4.0 – Technology Transfer and Implementation	1-7
2.0 INTRODUCTION	2-1
2.1 The Team	2-1
2.2 Technical Objectives and Schedule	2-2
3.0 TASK DESCRIPTIONS	3-1
3.1 Task 1.0 – Advanced Simulation and Technology for Core Molding (Ford)	3-1
3.1.1 Introduction and Summary	3-1
3.1.2 Procedures and Results	3-2
3.1.2.1 Task 1.1 - Analysis of Process Variability (Ford)	3-2
3.1.2.2 Task 1.2 - Core Cure Kinetics (University of Alabama)	3-6
3.1.2.3 Task 1.3 - Densification and Deformation Models (Auburn University)	3-9
3.1.2.4 Task 1.4 - Compressible Flow Model Development (NASA-LeRC)	3-12
3.1.2.5 Task 1.5 - Core Box Fill (One Phase) Model Development (Ford)	3-17
3.2 Task 2.0 – Simulation and Control of Injection Molded Cores (Howmet)	3-23
3.2.1 Introduction and Summary	3-23
3.2.2 Procedures and Results	3-25
3.2.2.1 Task 2.1 - Analysis of Core Injection Molding Defects (Howmet)	3-25
3.2.2.2 Task 2.2 - Analysis of Core Injectiodn Molding Defects (PCC)	3-28
3.2.2.3 Task 2.3 - Core Injection Molding Model Development (UES)	3-30

TABLE OF CONTENTS (CONTINUED)

Page

3.2.2.4 Task 2.4 - Sintering Modeling Development (Auburn University)... 3-35

3.2.2.5 Task 2.5 - 2.5D X-Ray Measurement Software (GE) 3-38

3.2.2.6 Task 2.6 - 2.5D X-Ray Measurement Hardware (ARACOR/Howmet)... 3-41

3.3 Task 3.0 – Rapid, Near-Net Shape Casting (Rocketdyne)................................ 3-42

3.3.1 Introduction and Summary.. 3-42

3.3.2 Procedures and Results... 3-43

3.3.2.1 CT Scan of Rocket Engine Parts (Rocketdyne)........................ 3-43

3.3.2.2 Rapid Prototype Design and Process (Rocketdyne).................... 3-48

3.3.2.3 Rapid Prototype Design and Process (Lockheed Martin).............. 3-52

3.3.2.4 Cast Rocket Engine Parts (Rocketdyne) 3-57

3.3.2.5 Cast Launch Vehicle Component (Lockheed Martin) 3-58

3.4 Task 4.0 – Technology Validation and Transfer (Rocketdyne)............................ 3-68

3.4.1 Introduction and Summary.. 3-68

3.4.2 Procedures and Results... 3-68

3.4.2.1 Implementation (Ford) 3-68

3.4.2.2 Injection Molded Cores (Howmet) 3-68

3.4.2.3 Injection Molded Cores (PCC)... 3-70

3.4.2.4 Rapid Casting (Rocketdyne) 3-70

3.4.2.5 Rapid Casting (Lockheed Martin) 3-79

3.4.3 Casting Design Guidelines (Robinson Products) 3-86

4.0 SUMMARY.. 4-1

APPENDIX A

APPENDIX B

APPENDIX C

LIST OF FIGURES

		Page
1-1	Technical Barriers to Near-Net Shape Casting	1-1
1-2a	Program Schedule	1-2
1-2b	Program Schedule	1-3
1-3	AITP Precision Casting Work Breakdown Structure	1-3
1-4	Approach to Reverse Engineer Component Using CT	1-6
1-5	Approach to Produce Metallic Component Directly Using Selective Sintering	1-6
2-1	The Near-Net Shape Casting Cooperative Team	2-1
2-2	Technical Barriers to Near-Net Shape Casting	2-2
2-3	The Cost Effectiveness of Castings Increases with Casting Size and Complexity!	2-2
2-4	Essential Process Steps in Core Making for (A) Aerospace Applications and (B) Automotive Applications	2-3
2-5a	Program Schedule	2-4
2-5b	Program Schedule	2-5
2-6	AITP Precision Casting Work Breakdown Structure	2-5
3-1	Gauging System	3-4
3-2	Density Measurement System	3-4
3-3	Laser Scan System for Core Box Wear	3-5
3-4	Permeability Fixture	3-6
3-5	Diffusivity Fixture	3-6
3-6	Experiment Design	3-7
3-7	Cure Rate Experimental Apparatus	3-7
3-8	Results of Designed Experiment	3-8
3-9	Effects of Parameters on K and D_e	3-8
3-10	Chromatographic Effect	3-8
3-11	Curing with Various TEA Amounts	3-8
3-12	Capillary Tube Viscometer	3-9
3-13	Rotational Viscometer	3-9
3-14a	Apparent Viscosity of Sand Bed as a Function of the Apparent Shear Rate	3-11
3-14b	Apparent Viscosity of Binded Sand as a Function of the Apparent Shear Rate	3-12
3-15	Filling Pattern at Four Successive Times in the Filling Process, as Calculated by the Micro/Macro Model (3D Results). Arrows Indicate Air/Sand Flow Entering or Air Flow Leaving the Mold	3-15
3-16	Pressure and Density at the Walls Near the End of the Core Filling Process	3-16
3-17	Sand Flow Property Test	3-17

LIST OF FIGURES (CONTINUED)

		Page
3-18	Sand Permeability Test	3-17
3-19	Simulation Software System	3-18
3-20	Single Chamber Core Box Verification Test Setup	3-19
3-21	Density Pattern Comparison	3-20
3-22	TEA Moving Front Result Comparison	3-20
3-23	2.3L Ranger Slab Core	3-21
3-24	2.3L Ranger Slab Core Density Comparison	3-21
3-25	Gassing TEA Moving Front Comparison	3-22
3-26	Typical Injection Molded Core Fabrication Process Steps	3-23
3-27	Effects of Injection Parameter Variations on Core Quality Measures	3-26
3-28	Effects of Injection Parameters with Different Compound Solids Levels	3-27
3-29	Relationship Between Local Measure of Green Core Binder Content and Fired Core Porosity	3-27
3-30	Dimensional Comparison of Two PCC Core Compound Types	3-29
3-31	Gage Yield Comparison by PCC Part Number and Mix type	3-30
3-32	Typical Process Yields with Different Controls on Injection Cycle	3-30
3-33	Generic PIT Turbine Blade Core Finite Element Mesh	3-32
3-34	PIT Core Temperature Contours During Filling	3-33
3-35	PIT Core Shear Rate Contours During Filling	3-33
3-36	PIT Core Fraction Solid Contours Just After Filling	3-34
3-37	Zigzag and Expansion Die Finite Element Mesh	3-34
3-38	Auburn Sintering Furnace and Experimental Setup Schematic	3-36
3-39	Core Sample Shrinkage Relative to Sintering Temperature with Time t_0	3-37
3-40	Core Sample Shrinkage Relative to Sintering Temperature with Time $3t_0$	3-37
3-41	Summary Chart of Sample Shrinkage in Air and Moist CO_2	3-38
3-42	Recovery and Application of Deformation Parameters	3-40
3-43	PIT Blade Radiographic Image Showing Core Passage Detail	3-41
3-44	Low Cost Manufacturing Approach via the Rapid, Near-Net Shape Casting Process	3-42
3-45	Selective Laser Sintering (SLS) Process	3-44
3-46	Approach to Reverse Engineer a Component Using CT	3-44
3-47	Selection Criteria Used to Evaluate Candidate Hardware	3-45
3-48a	Gas Generator Housing Design	3-46
3-48b	Gas Generator Housing	3-46

LIST OF FIGURES (CONTINUED)

		Page
3-49	Pro-E CAD Image of the Gas Generator Housing	3-47
3-50	SLS Polycarbonate Rapid Prototype Pattern	3-48
3-51	Photograph of DTM Sinterstation 2000 Used to Produce Metallic Components Directly	3-50
3-52	Processing Parameters	3-51
3-53	Photograph Metallic Parts Produced Directly with SLS	3-52
3-54	Photograph of the 321 Stainless Steel LO_2 Tank Elbow (11 in. ID) Joined to the Wall of the Atlas IIAS Booster	3-52
3-55	Summary of the Conventional Design Compared to the Casting Design of the LO_2 Tank Elbow	3-53
3-56	Schematic of Meshed Gating System and Casting for the LO_2 Tank Elbow	3-55
3-57	An Example of a Temperature Fringe Plot of the Static LO_2 Tank Elbow Casting (0.100 in. Thick Wall) Solidification Model (at 2 sec After Start of Pour Using a Fill Time of 2 sec (Pour Velocity of 3 m/s))	3-56
3-58	Gating Design for 0.100 in. Thick Walled LO_2 Tank Elbow Static Investment Casting. Schematic Also Shows the Differential Wrap of Insulation Used to Extend Feed Distances.	3-56
3-59	Photograph of a Stereolithography (QuickCast™) Pattern of the LO_2 Tank Elbow Casting (11 in. ID, 0.100 in. Wall Thickness)	3-57
3-60	Photo Showing the Gating of the First 0.100 in. Thick Walled LO_2 Tank Elbow	3-59
3-61	Fabrication Process and Materials Used for Production of the Investment Casting Shell for the 0.100 in. Thick Walled LO_2 Tank Elbow	3-59
3-62	Photos of First Elbow Casting (Lot #1) After Ceramic Removal and Shot Blasting, Showing Extensive Area of Nonfill	3-60
3-63	Photos of Second Elbow Casting (Lot #2) After Ceramic Removal and Shot Blasting, Showing Extensive Area of Nonfill	3-61
3-64	Schematic Showing Results of PCC Airfoils' Reverse Engineering of the Heat Transfer Coefficient for the 0.100 in. Thick Wall LO_2 Tank Elbow. Areas of Nonfill/Misrun Predicted by the Solidification Model are Similar to Those Observed in the Casting	3-62
3-65	Schematic Representation of Precision Castparts Corporation's Thermally Controlled Solidification Furnace	3-63
3-66	Overview of the TCS Process Development Study	3-65
3-67	Steps Used for Producing TCS Process Development Castings. Note that Castings were Procured to Meet the General Requirements of AMS 5362 and Inspection Requirements of MIL-STD-2175 Class 1, Grade B	3-65
3-68	SLA QuickCast™ Pattern for the 0.055 in. Thick Wall LO_2 Tank Elbow Casting Used in the TCS Process Development. Note that Some Portions of the Gating Design are Also Shown	3-66

LIST OF FIGURES (CONTINUED)

Page

3-69 Lot 001 of the Thin-Walled (0.055 in.) 11 in. ID LO_2 Tank Elbow Casting (Alloy CF-8C SHT) Produced via the TCS Process ... 3-67

3-70 Zigzag and Expansion Die Tooling and CAD Models ... 3-69

3-71 PIT Core Simplified Unigraphics CAD Model ... 3-69

3-72 Pressure Relief Valve Component Scans ... 3-72

3-73 CT Scan Image of Hardware ... 3-72

3-74 CAD Image of the Scanned Hardware and the Final Rapid Prototype Hardware Next to the Existing Hardware ... 3-74

3-75 Cast Inconel 718 Tensile Data ... 3-75

3-76 Fracture Analysis of pre-HIP and Homogenization Specimen (L Sample) Reveals Extensive Presence of Voids Due to Casting Shrinkage. The View on the Right is Magnified at 750X ... 3-76

3-77 Significant Reduction in the Porosity Levels are Evident in the 100X Metallography Samples Shown of Samples Before and After Homogenization and HIP'ing ... 3-76

3-78 Fracture Analysis of Post-HIP and Homogenization "T" Specimen Reveals Little to No Porosity Due to Shrinkage. The View on the Right is of the Initiation Site Magnified at 600X ... 3-76

3-79 STL Pattern and Casting of the Turbine Discharge Housing Cast Using PCC's TCS Process ... 3-77

3-80 Center Jet Casting Produced Through the TCS Process ... 3-78

3-81 Chemical Compositions for Each Casting Lot, as Measured by PCC, as Compared to the Requirements of ASTM A743 for the CF-8C Casting Alloy ... 3-79

3-82 Photomicrograph of Representative TCS Casting (left) and Conventional Air Casting (Right) Showing Duplex Ferrite-in-Austenite Microstructure of CF-8C. (TCS Casting Etch: 10% Oxalic, Electrolytic - Air Casting Etch: 20% NaOH, Electrolytic). 3-80

3-83 Test Specimen Configurations for Performing the Room Temperature and -320°F Tensile Tests of Lot 006 [TCS LO_2 Tank Elbow Casting (CF-8C SHT Condition)] ... 3-80

3-84 Average Test Results for Excised Tensile Specimens Taken from Lot 006 [TCS LO_2 Tank Elbow Casting (CF-8C SHT Condition)] Tested at 70°F and -320°F. Note that the Minimum Required Tensile Properties at Room Temperature per AMS 5362 were Met or Exceeded ... 3-81

3-85 Test Conditions for Pressurization Testing of 0.055 in. Thick Wall, 11 ID LO_2 Tank Elbow Casting (CF-8C SHT Condition) (Lot 006) ... 3-81

3-86 Pressurization Test Setup for Testing the TCS Cast 0.055 in. Thick Walled, 11 in. ID LO_2 Tank Elbow (Alloy CF-8C, SHT) ... 3-82

LIST OF FIGURES (CONTINUED)

Page

3-87 Photograph of the TCS Cast 0.055 in. Thick Walled, 11 in. ID LO_2 Tank Elbow (Alloy CF-8C, SHT) Following Successful Burst Testing. Test Completed at 304 psi vs the Designed Burst Pressure of 213 psi. Note that the Thin-Walled Casting is Completely Intact 3-82

3-88 Comparison of the Recurring Cost (Normalized) of the 11 in. LO_2 Tank Elbow Fabricated Both Conventionally and as a Casting 3-83

3-89 Estimated Cycle for Development of the Thin-Walled 11 in. ID LO_2 Tank Elbow Casting Using the Rapid, Near-Net Shape Casting Approach 3-84

3-90 Examples of Various Lockheed Martin Applications Evaluated for or Fabricated with the Rapid, Near-Net Shape Casting Process 3-85

LIST OF ACRONYMS

AGS	Air Gauging System
AITP	Aerospace Industry Technology Program
CAD	Computer Aided Design
CAE	Computer Aided Engineering
CCP	Cleveland Casting Plant
CFO	Casting and Forging Operations
CML	Computational Materials Laboratory
CMM	Coordinate Measurement Machine
CPU	Central Processing Unit
CT	Computer Tomography
DLL	Dynamic Link Library
DR	Digital Radiography
EELV	Evolutionary Expendable Launch Vehicle
ELV	Expendable Launch Vehicle
FEM	Finite Element Model
FIDAP	Fluid Dynamics Analysis Package
FTP	File Transfer Protocol
HC	Howmet Corporation
HIP	Hot Isostatic Pressing
IR	Infrared
IT	Information Technology, Rocketdyne Division
MEV	Million Electron Volts
MIMICS	Materialise's Interactive Medical Image Control System
MS	Microsoft
NDT	Non-Destructive Test
OD	Outside Diameter
PCC	PCC Airfoils
PIT	Process Improvement Team
PLC	Programmable Logic Controller
S/N	Signal-to-Noise
SLS	Selective Laser Sintering
STL	Stereolithography
TCD	Thermal Conductivity Detector

LIST OF ACRONYMS (CONTINUED)

TCS	Thermally Controlled Solidification
TEA	Triethylamine
UG	Unigraphics

1.0 EXECUTIVE SUMMARY

1.1 INTRODUCTION

A two-year program was conducted to develop and commercially implement selected casting manufacturing technologies to:

- Enable significant reductions in the costs of castings,
- Increase the complexity and dimensional accuracy of castings, and
- Reduce the development times for delivery of high quality castings.

1.1.1 The Team

The industry-led R&D project was cost shared with NASA's Aerospace Industry Technology Program (AITP). The Rocketdyne Division of Boeing North American, Inc. served as the team lead with participation from Lockheed Martin, Ford Motor Company, Howmet Corporation, PCC Airfoils, General Electric, UES, Inc., University of Alabama, Auburn University, Robinson Products, Inc, Aracor and NASA-LeRC.

1.1.2 Technical Objectives and Schedule

The overall objective of this program was to develop technology to increase the competitiveness of the U.S. casting industry. Several barriers had been identified that would have to be overcome to meet this overall objective. These barriers are listed in Figure 1-1.

Figure 1-1. Technical Barriers to Near-Net Shape Casting

- Lack of a quantitative understanding of the process physics and predictive capabilities for foundry core molding
- Lack of a robust, integrated measurement and control technology for closed loop feedback control of dimensions
- Lack of a rapid, near-net shape casting capability to certify pilot production processes.

The first barrier is the result of the "art" of foundry core making. Cores are produced by blowing or injecting a mixture of ceramic aggregate and free flowing carrier into a die. Computational methods based upon the physics of the process that offer the potential of enhancing the process design, reducing variabilities, improving quality, and lowering costs were investigated as part of this program. This effort was led by Ford.

The second barrier to near net shape casting is the inability of foundries to robustly monitor and control both internal and external dimensions of their cores and castings in real time. Real-time process monitoring and control were explored and evaluated to minimize dimensional variability. This effort was led by Howmet.

The third barrier to successfully produce near net shape casting involves the long production lead times required for foundries to qualify their processes. This technology was explored on the program to significantly shorten development time for castings. This effort was led by Rocketdyne.

The technical plan was divided into three major thrust areas to address each of the technical barriers:

- Advanced Simulation Technology for Core Molding,
- Simulation and Control of Injection Molded Cores, and
- Rapid, Near-Net Shape Casting.

These three technical thrust areas were directly linked to solving the three technical barriers above. In addition, a fourth thrust area was established to help provide technology transfer and implementation. The overall technical approach and schedule are shown in Figure 1-2. The work breakdown structure for each task along with the responsible organization is shown in Figure 1-3.

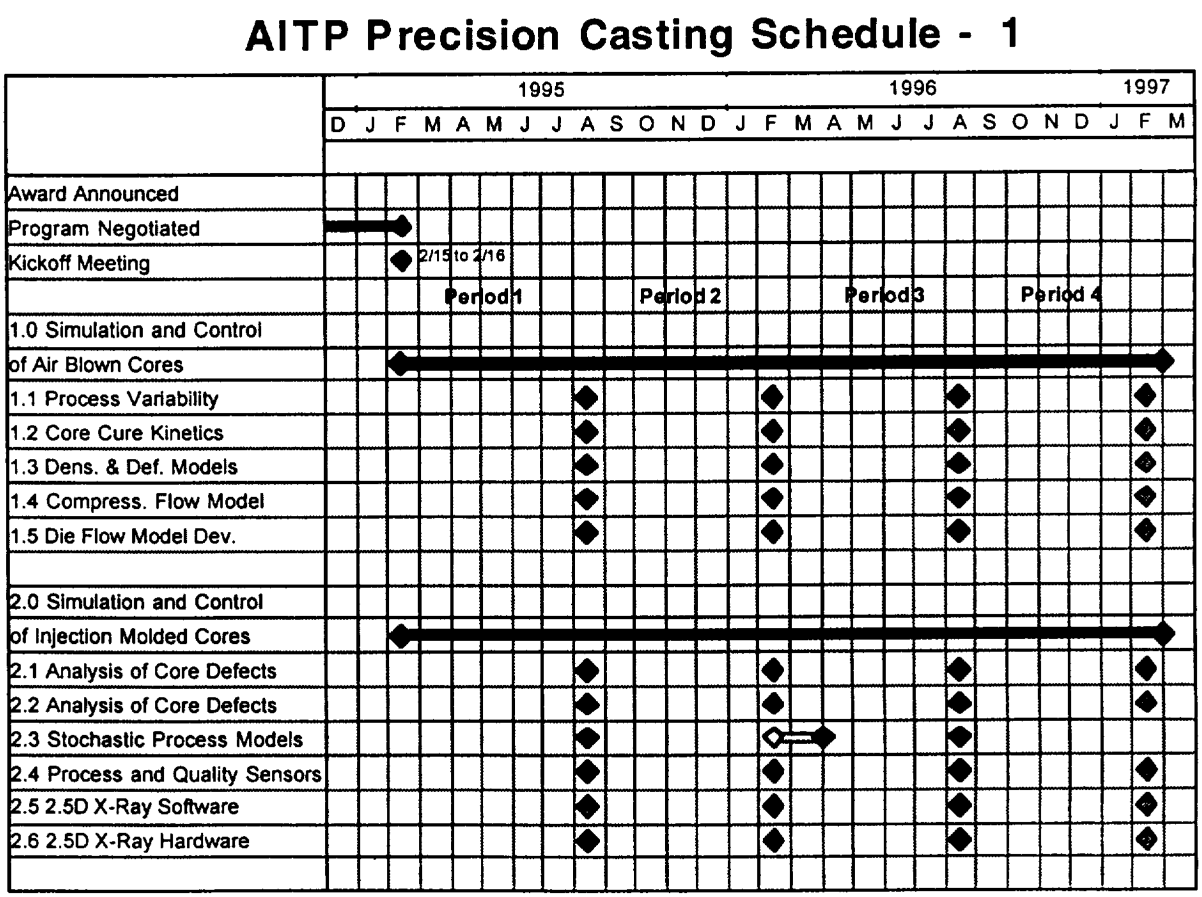

Figure 1-2a. Program Schedule

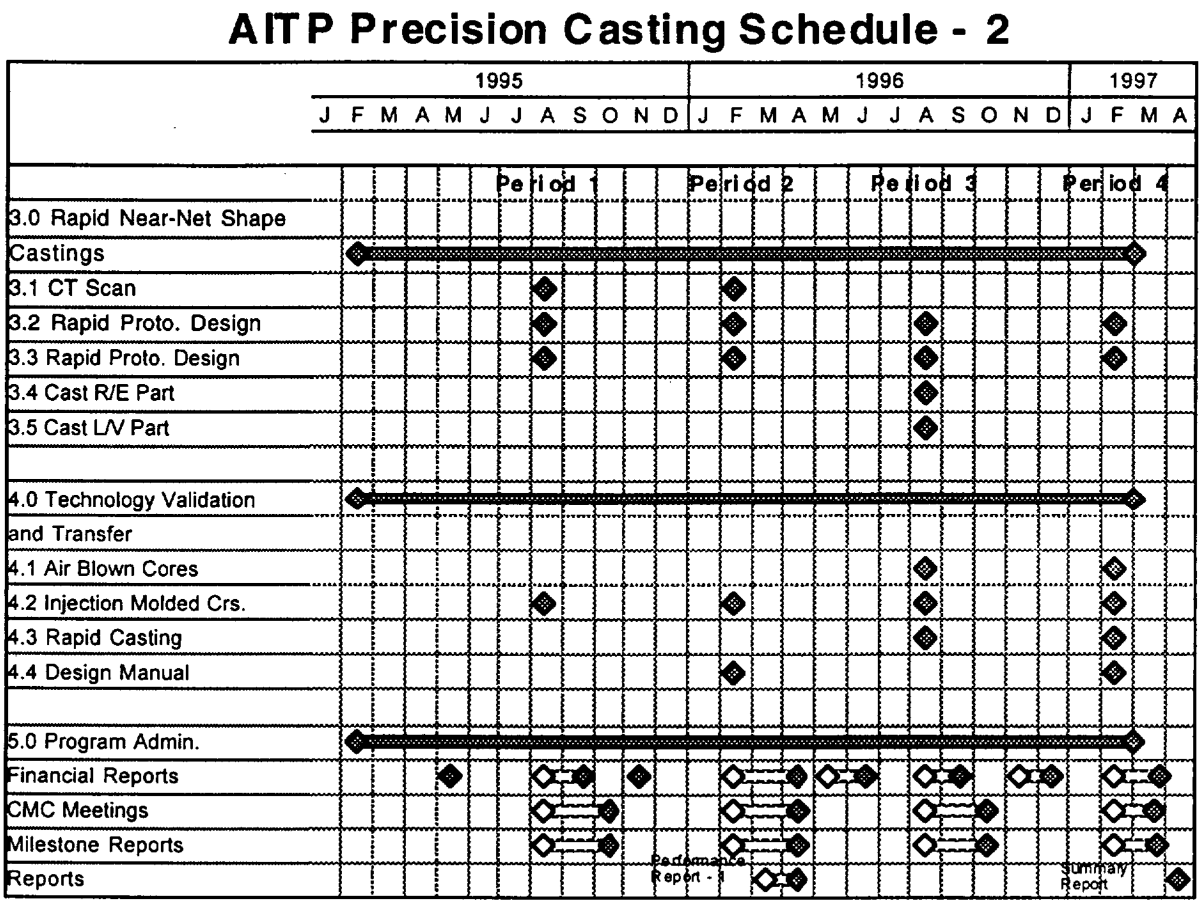

Figure 1-2b. Program Schedule

Figure 1-3. AITP Precision Casting Work Breakdown Structure

Task 1.0	Simulation and Control of Air Blown Cores – Ford Motor Company
Task 2.0	Simulation and Control of Injection Molded Cores – Howmet
Task 3.0	Rapid Near Net Shape Casting – Rocketdyne
Task 4.0	Technology Validation and Transfer – Rocketdyne

1.2 SUMMARY

1.2.1 Task 1.0 – Advanced Simulation Technology for Core Molding

The objective of this effort was to investigate and apply computer aided engineering (CAE) tools and methods in the design and manufacture of air blown sand cores, associated core box tooling and real-time process controls. Ford Casting and Forging Operations conducted empirical studies of the physical phenomena associated with the core making process and developed analytical computer models. Three distinct, but interrelated efforts, were performed at Ford. One team focused on the analysis of process variability; they developed dynamic process controls for application on the experimental core machine. A second team studied the ability of analytical modeling to improve tooling based on better knowledge of sand behavior as determined by laboratory experiments. A third team integrated the knowledge gained and the developments achieved in test and measurement systems into an experimental core machine. Test results provide a means to verify the accuracy of CAE models.

An experimental core machine was designed and built, real-time non-destructive test methods were evaluated, methods to evaluate resin bond strength were explored, sensors for monitoring all aspects of the core blow process were investigated and control and data acquisition systems were evaluated. Best practices for these efforts and the integrated controls and measurements systems were transferred to the Cleveland Casting Plant (CCP) in the second year.

The University of Alabama was tasked with measuring physical properties that affected transport and reaction of catalyst gas in a resin core including permeability and effective diffusivity. During the first year, a resin binder was selected and equipment designed, built and tested for acquiring these properties. Screening experiments were conducted in the second year to determine which core properties had major impacts on transport properties.

Auburn University was tasked to develop a system for quantifying compaction characteristics and permeability of resin coated silicon aggregate as a function of pressure, particle size, particle angularity, and resin coatings. Experimental instrumentation was designed and fabricated and viscosity measurements made.

The NASA-LeRC Computational Materials Laboratory assessed two-phase flow to understand granular flow in the core filling process. The complexity of the numerical techniques made this approach impractical.

In addition, Ford worked with UES and Aracor to study sand density during filling analytically and anchored the models with computed tomography. Finally, Ford designed and built a core box with clear windows to photograph the sand core filling process. This system was used during the second year to develop experimental data on core filling.

1.2.2 Task 2.0 – Simulation and Control of Injection Molded Cores

The Task 2.0 effort for this AITP program included both experimental and analytical thrusts to better understand the core injection molding and sintering processes. Howmet Corporation (HC) and PCC Airfoils (PCC) independently conducted experimental efforts to develop a better understanding of the core injection molding process. The primary focus of these experimental efforts was to characterize the process parameters that have a strong impact on dimensional control issues of injection molded cores during their fabrication. Findings from the experimental efforts completed at these two companies as a part of this program were transitioned into the production core making facilities with favorable results.

UES was chartered to evaluate and develop analysis methods and tools within ProCast that can be used to analytically predict the core injection molding process, and provide insight into coupled fluid flow and heat transfer effects, such as, particle segregation (density variations), core porosity, and non-fill problems. These modified tools are available for core injection molding process modeling and die design. During the conduct of the program, it was found that the ceramic particle density variations within injection molded cores could not be adequately correlated to basic flowfield results. In order to accurately predict particle density variations a multiphase flow model would be required. Auburn University during the program developed an empirical data base to evaluate dimensional changes occurring in ceramic core materials during the sintering stage of core processing.

GE and ARACOR have developed the software and hardware to enable the use of 2.5D X-Ray techniques to enable near, real-time, three-dimensional evaluation of cores and/or castings during the production cycle. These tools allow direct comparison of actual part geometric data to known reference or CAD solid models and theoretically could be used to eliminate out of specification parts earlier in the casting production cycle and reduce casting scrap rates. Solid progress was made by all Task 2.0 participants during the AITP program.

1.2.3 Task 3.0 – Rapid, Near-Net Shape Casting

The objective of this task was to shorten the cycle time for the fabrication of high quality castings by utilizing rapid prototyping technology. The emphasis was on launch vehicle and rocket engine components, but the benefits apply to almost all commercial castings.

Two rocket engine and launch vehicle components that had previously been manufactured using conventional machining and welding techniques were selected. Two different approaches were used to achieve electronic designs of the hardware. The first approach, used a 2.5 million electron volts (MEV) Computer Tomography (CT) unit, located at Rocketdyne's Santa Susana Field Laboratory. CT scan data of existing rocket engine hardware was converted into a useable Computer Aided Design (CAD) file using Imageware software. The process flow to reverse engineer a part is shown in Figure 1-4. Application of this reverse engineering technical capability eliminates the need for extensive CAD work that is required for developing an electronic design of existing hardware. The second concurrent approach, applied the more traditional CAD techniques, to generate an electronic model of a systems component.

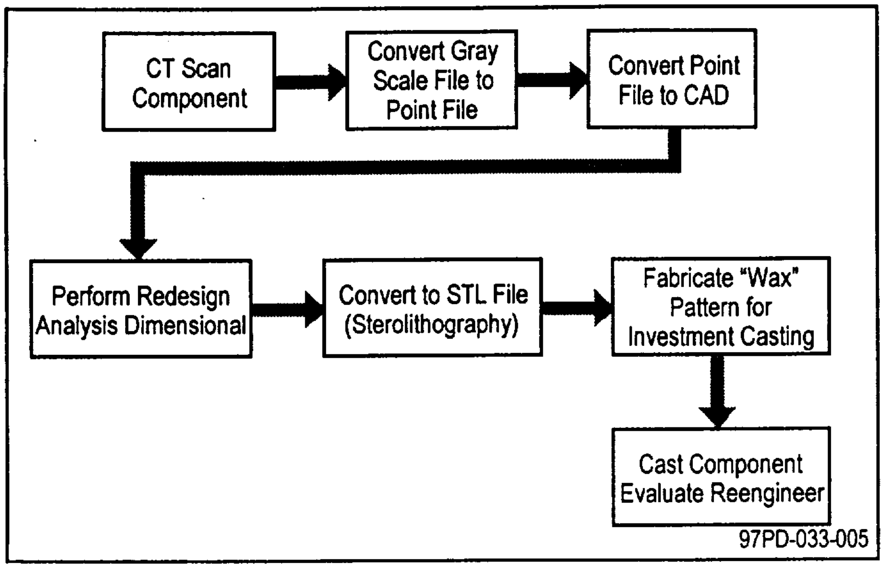

Figure 1-4. Approach to Reverse Engineer Component Using CT

CAD models, created with each technique, were used to generate Stereolithography (STL) files for the fabrication of rapid prototype patterns. These patterns were used in the second year to produce investment castings.

Rocketdyne also investigated Selective Laser Sintering (SLS) to produce metallic components directly from the CAD. The objective of this effort was to evaluate the feasibility of using Rapid Prototyping as a means of forming a green part which could be subsequently sintered to high density and near net shape. Figure 1-5 shows an overview of the fabrication process. Metallic powders are blended with a plastic binder; the binder is fused together during the SLS process, and then the binder is removed. The green part is then sintered to a near-net shape.

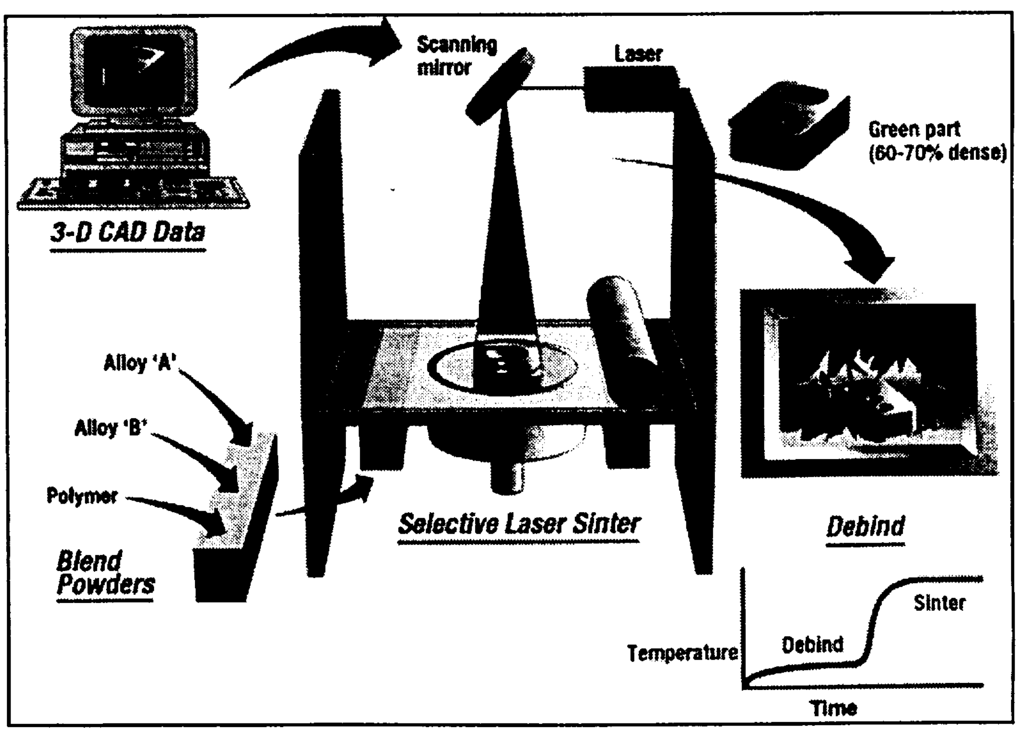

Figure 1-5. Approach to Produce Metallic Component Directly Using Selective Laser Sintering

SLS of metals has been demonstrated to be a potential method of Free Form Fabrication of parts and dies, but much work is still needed to refine the process as a production viable tool.

1.2.4 Task 4.0 – Technology Transfer and Implementation

The task was established to help provide a path to assure that, as the technology was developed on this program, it would be transferred into production. Ford, Howmet, PCC, Rocketdyne, and Lockheed Martin each had tasks to make sure the technology was implemented. In addition, Robinson Products, Inc. was tasked with assembly of a guide for applying rapid prototyping to produce castings.

Ford focused on implementing technology developed during the evaluation of their experimental core machine. The key piece of technology that was transferred into production was the laser inspection device to ensure core boxes were clean.

Howmet and PCC each used the statistical data acquired during measurement of the cores to improve the dimensional control of their ceramic cores. This technology was implemented on several different cores.

Rocketdyne and Lockheed Martin each focused on how to apply rapid prototyping to produce castings. Rocketdyne implemented Imageware software to help produce rapid prototyping patterns and both Rocketdyne and Lockheed Martin, in conjunction with PCC, implemented Thermally Controlled Solidification (TCS) technology to produce castings for production. TCS casting is a technique which uses rapid prototype patterns and a thermal gradient furnace to make extremely thin-walled casting. Finally, technology demonstrated on this program to make metallic rapid prototype parts at Rocketdyne will be used to produce injector bodies for an Air Force program.

2.0 INTRODUCTION

A two-year program was conducted to develop and commercially implement selected casting manufacturing technologies to:

- Enable significant reductions in the costs of castings,
- Increase the complexity and dimensional accuracy of castings, and
- Reduce the development times for delivery of high quality castings.

Many of the process problems in producing cost effective, near net shape castings are common whether or not the casting design is for 10 space launch vehicles, 100 aircraft, or 100,000 automobiles. The alloys, tolerances, quality criteria, and production volumes certainly differ, but the fundamental physics required to quantitatively understand and control the manufacturing processes is the same. The management of the companies in this Cooperative recognized this and committed to jointly develop the innovative manufacturing technologies necessary for their companies to compete world-wide in future markets.

2.1 THE TEAM

Our team, as shown in Figure 2-1, was both vertically and horizontally integrated and was assembled to aggressively remove specific technical and commercial barriers to the wider utilization of castings by U.S. manufacturers. The team's vision was to apply the diverse yet aggregated project resources to:

- Accelerate the understanding of critical manufacturing processes,
- Develop appropriate control technology to rigorously control the processes, and
- Develop the methodologies to apply reverse engineering and rapid prototyping to the manufacture of small lots of production castings.

Figure 2-1. The Near-Net Shape Casting Cooperative Team

Team Member	Expertise/Function
Rocketdyne, Canoga Park, CA	Team leader, rapid prototyping expertise, rocket engine manufacturing
Ford Motor Company, Dearborn, MI	Automotive casting expertise, stochastic process control
Howmet Corporation, Whitehall, MI	Investment casting expertise
PCC Airfoils Inc., Beachwood, OH	Investment casting expertise
General Electric, Schenectady, NY	Digital radiography imaging software
Lockheed Martin, Denver, CO	Launch vehicle manufacturing
UES Inc., Annapolis, MD	Casting process modelling software expertise
Aracor, Mountain View, CA	Computed tomography/digital radiography
Auburn Univ., Auburn, AL	Ceramic core manufacturing
Robinson Inc., Shaker Heights, OH	Casting technology
Univ. of Alabama, Tuscaloosa, AL	Environmental effects, reaction kinetics
NASA LeRC, Cleveland, OH	Computational simulation of complex process

2.2 TECHNICAL OBJECTIVES AND SCHEDULE

Casting product performance requirements are increasing, due primarily to customer demands for lighter weight, higher strength, and lower cost. The ability of the U.S. foundry industry to meet these demands with shorter, more flexible product cycles is placing tremendous competitive pressures on the industry. Since the cost effectiveness of castings actually increases as castings become larger and more complex, as shown schematically in Figure 2-2, one of the most promising capabilities requiring development is the cost-effective, near net shape casting of large parts. However, serious technical barriers prevent the U.S. foundry industry from possessing this capability. These barriers are shown in Figure 2-3.

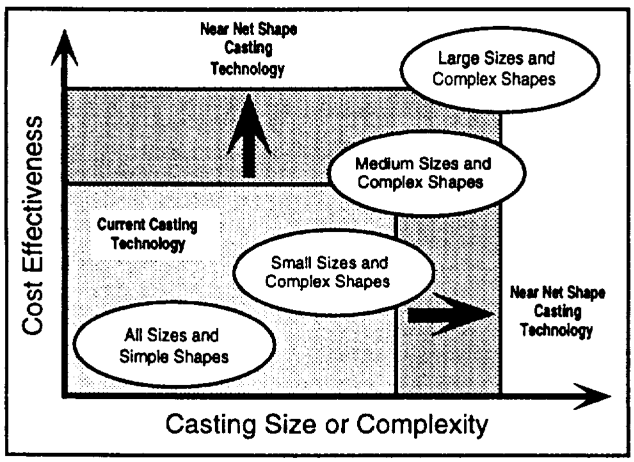

Figure 2-2. Technical Barriers to Near-Net Shape Casting

Figure 2-3. The Cost Effectiveness of Castings Increases with Casting Size and Complexity!

- Lack of a quantitative understanding of the process physics and predictive capabilities for foundry core molding
- Lack of a robust, integrated measurement and control technology for closed loop feedback control of dimensions
- Lack of a rapid near net shape casting capability to certify pilot production processes

The first barrier is the result of the "art" of foundry core making. Cores are produced by blowing or injecting a mixture of ceramic aggregate and free flowing carrier into a die. Cores for the investment casting industry are typically composed of silica or alumina which is injected into a die with a wax carrier. Note Figure 2-4(A). Cores for the automotive industry are typically composed of silica coated with a resin binder which is delivered to a die with air as shown in Figure 2-4(B). After molding, both types of cores must be strengthened by appropriate chemical or thermal reactions prior to casting. Currently the design of tooling and the selection of appropriate molding and curing process parameters are defined by trial-and-error techniques. This empirical approach leads to long process development lead times, poor process yields, and an inability to cost-effectively produce complex castings. Computational methods based upon the physics of the process that offer the potential of enhancing the process design, reducing variabilities, improving quality, and lowering costs were investigated as part of this program.

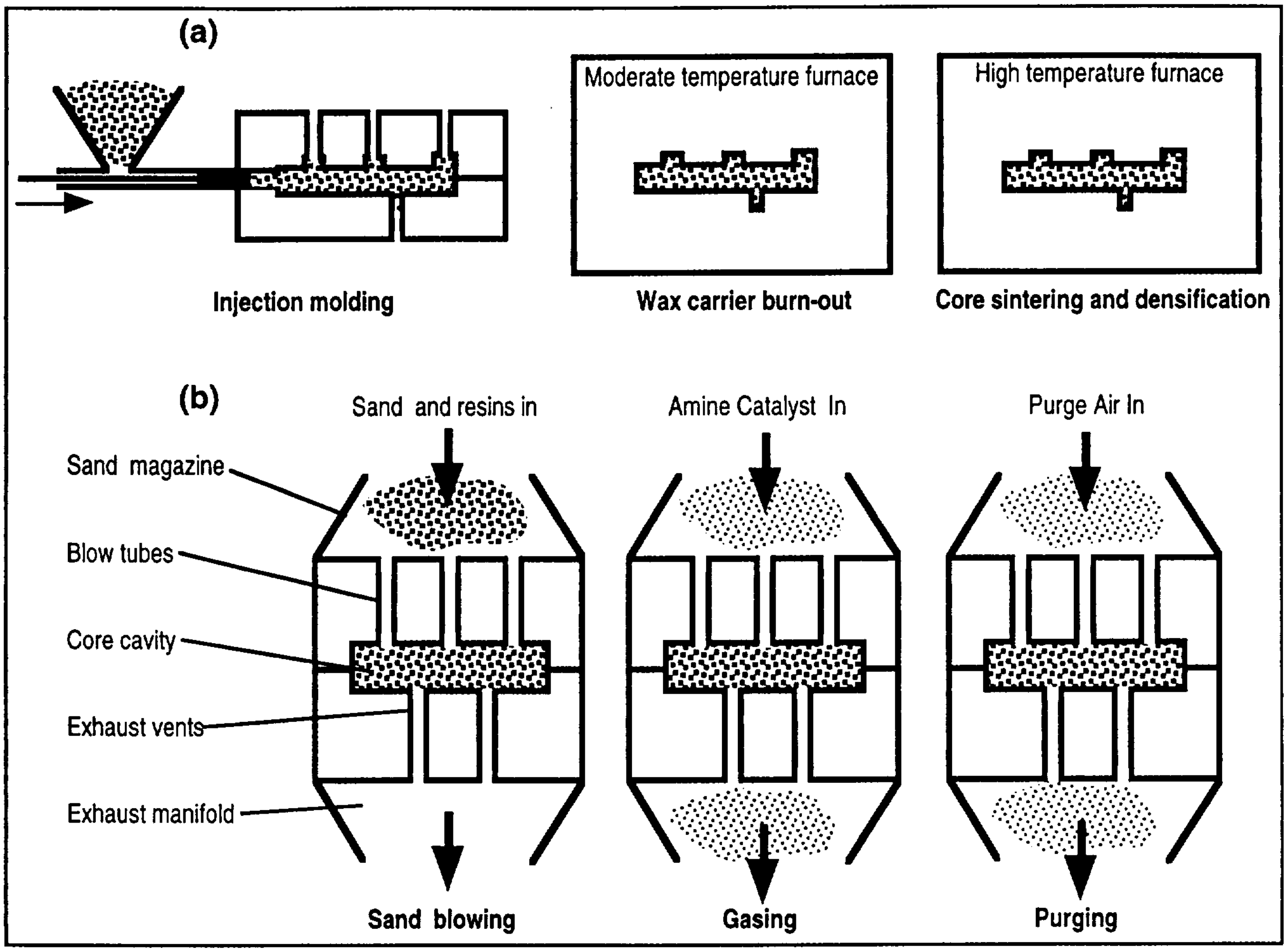

Figure 2-4. Essential Process Steps in Core Making for (A) Aerospace Applications and (B) Automotive Applications

The second barrier to near-net shape casting is the inability of foundries to robustly monitor and control both internal and external dimensions of their cores and castings in real time. Since the dimensions of complex castings are principally determined by the dimensions of the cores that shape the casting, reductions in the dimensional variability of cores will reduce the dimensional variability of metal castings. Foundry processes involve large numbers of coupled variables that are not quantitatively understood, are not routinely measured, and consequently, are not adequately controlled. Although foundries and their customers have accepted this "inherent variability" for years, economic pressures mandate that the foundry of the future utilize intelligent process control. Thus, real-time process monitoring and control were explored and evaluated to minimize dimensional variability.

The third barrier to successfully produce near-net shape casting involves the long production lead times required for foundries to qualify their processes. Complex automotive sand castings and structural aerospace castings routinely require three to four years to develop and certify. This is too long and expensive for the fast changing markets of today. Accurate prototype castings are needed within months, not years, for engineering certification tests. This technology was implemented on the program to significantly shorten development time for castings.

The technical plan was divided into three major thrust areas to address each of the technical barriers:

- Advanced Simulation Technology for Core Molding,
- Intelligent Process Control of Core Molding, and
- Rapid, Near-Net Shape Casting.

These three technical thrust areas were directly linked to solving the three technical barriers above. In addition, a fourth thrust area was established to help provide technology transfer and implementation. The overall technical approach and schedule are shown in Figure 2-5. The work breakdown structure for each task along with the responsible organization is shown in Figure 2-6.

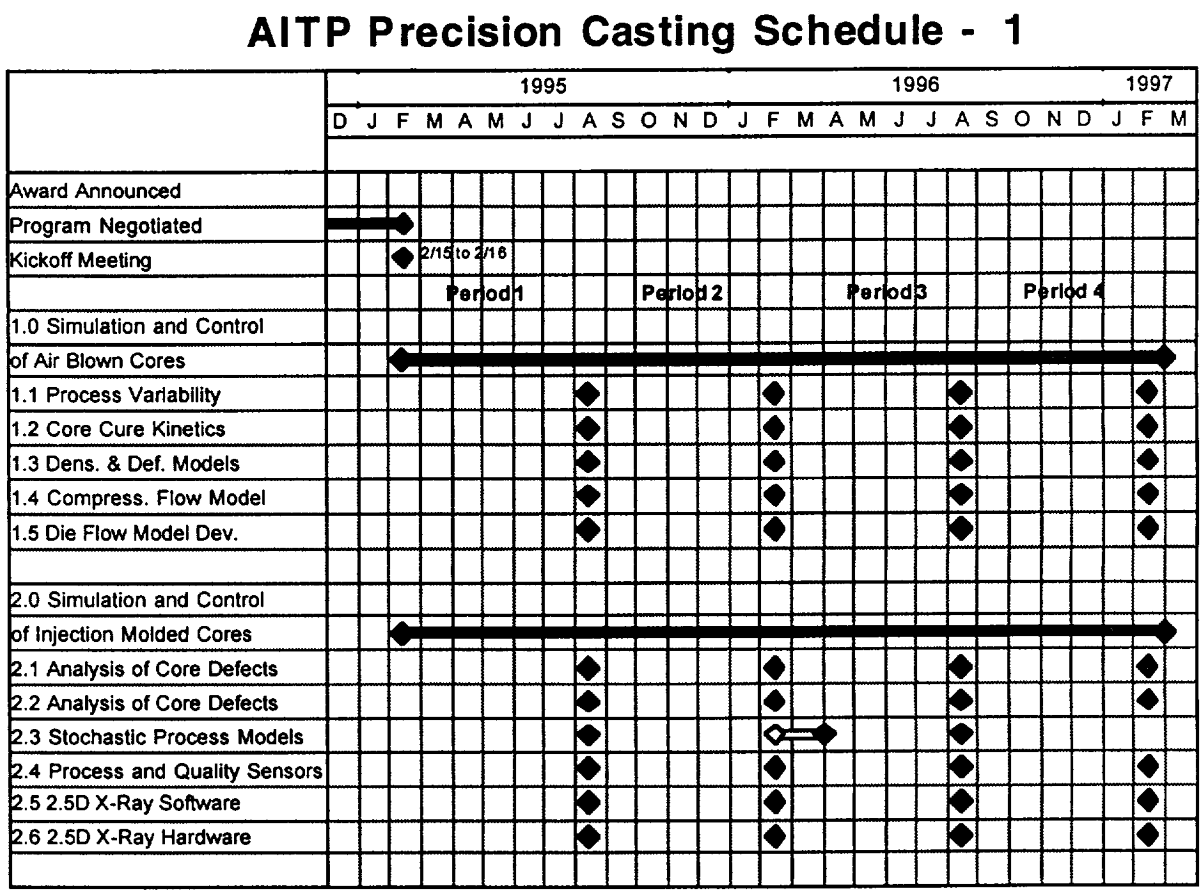

Figure 2-5a. Program Schedule

AITP Precision Casting Schedule - 2

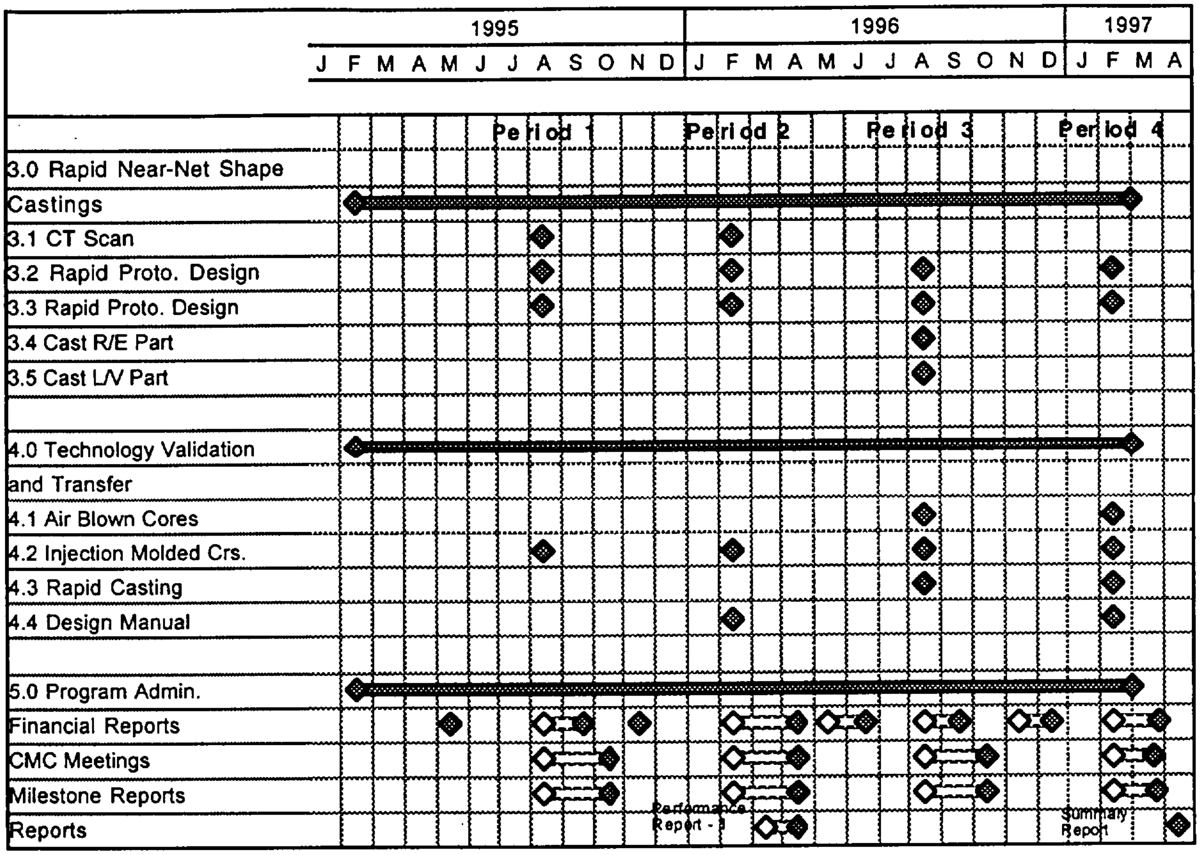

Figure 2-5b. Program Schedule

Figure 2-6. AITP Precision Casting Work Breakdown Structure

Task 1.0	Simulation and Control of Air Blown cores – Ford Motor Company
Task 2.0	Simulation and Control of Injection Molded Cores – Howmet Corporation
Task 3.0	Rapid Near Net Shape Casting – Rocketdyne
Task 4.0	Technology Validation and Transfer – Rocketdyne

3.0 TASK DESCRIPTIONS

3.1 TASK 1.0 – ADVANCED SIMULATION AND TECHNOLOGY FOR CORE MOLDING

3.1.1 Introduction and Summary

Casting and Forging Operations (CFO), a component of Ford Motor Company's Powertrain Operations, is an international producer of iron and aluminum castings for the automotive industry. To remain competitive in a global marketplace Ford Motor Company must continually reduce engineering lead-time, increase robustness and reusability, and improve manufacturing efficiencies.

CFO understands that maintaining the structural and dimensional integrity of sand cores used to produce internal features on increasingly complex engine castings is critical to supplying the customer with a quality product. Ford's participation in the AITP Precision Casting program addressed engineering lead-time and manufacturing efficiency by developing simulation and machine control tools for the design and manufacture of air-blown sand cores.

Task 1.0 focused on the development and implementation of computer-aided engineering tools to emulate core-box performance, control the core manufacturing process, and detect the cleanliness and wear of production core boxes.

Ford formed two cross-functional teams to investigate underlying technologies required to meet these objectives. The first team consisted of manufacturing, software, and controls engineers, and focused on the analysis of process variability, non-destructive quality measurement, and machine control. This group was also responsible for developing a real-time core box wear measurement system. The efforts of this team are summarized under Task 1.1.

The second team, product engineers and scientists form Ford, professors and graduate students from Auburn University and the University of Alabama, and scientists from the NASA Lewis Research Center, was responsible for the development of simulations for core blowing and curing processes. The efforts of this team are summarized in Tasks 1.2, 1.3, 1.4, and 1.5.

Both teams were successful in meeting technical objectives. Engineering expertise and cooperation among consortium members provided Ford with technologies for improving quality, lowering costs, and reducing engineering lead-times on new engine programs.

The manufacturing team developed a closed-loop control system for a production core machine that reacts to information provided in real-time by non-destructive tools measuring dimensional accuracy and density of production sand cores. A destructive method for measuring the strength of production cores (not lab samples) was also developed and integrated.

The manufacturing team also developed a non-contact, in-process method for measuring the wear of production core-boxes. The closed-loop control, and core-box wear measurement systems are scheduled for installation at Ford production facilities by fourth quarter 1997.

The product team successfully developed simulation tools for blowing and curing sand cores providing predictive quality information based on tool-design inputs (i.e., size and location of blow tubes and vents). This provided Ford with better first time capability and reduced iterative design changes at the prototype stage. These tools are currently being rolled out to product engineers for use on new and existing programs.

The following sections summarize the technical effort and achievements that led to the development of these tools.

- Task 1.1 – Analysis of Process Variability - Ford Manufacturing Team
- Task 1.2 – Core Curing Kinetics - University of Alabama
- Task 1.3 – Sand Densification and Deformation Properties - Auburn University
- Task 1.4 – Compressible (two-phase) Core Box Fill Model Development - NASA Lewis Research Center
- Task 1.5 – Core Box Fill (one-phase) Model Development - Ford Product Team

3.1.2 Procedures and Results

3.1.2.1 Task 1.1 – Analysis of Process Variability. The goal of the Ford manufacturing team was to measure, understand, and control, the variability in the sand-core manufacturing process. To accomplish this the team required quantitative data on the machine process variables, core quality, and tooling performance. Methods for capturing, exploring, and reporting on data needed to be developed. A control paradigm and the associated hardware and software tools to execute were also required.

To meet objectives the team concentrated efforts in five areas:

- Core Machine
- Core Quality
- Data Capture
- Closing the Process Control Loop
- Measure Tool Performance

Variability in core manufacturing can be attributed to three elements, the machine process, tooling performance, and ambient/environmental conditions. Measuring the individual components of these elements on production core machines would be an enormous task, burdening a plants labor, machine utilization, and bottom line. To control a machine, however, a thorough understanding of its behavior in process must be accomplished.

To facilitate this, a production core machine was purchased and installed at a Ford development facility. The machine, and supporting equipment, was configured as a make-like-production system, providing conditions as close as possible to an operating foundry.

To efficiently capture and organize data from a multitude of sensors, including a Programmable Logic Controller (PLC), the team integrated data acquisition hardware and software from National Instruments. The flexibility of the software provided engineers with a functional, albeit crude, platform for eventually controlling the machine.

While most process information was provided by the PLC and off-the-shelf devices, several sensors had to be developed/adapted to the core machine and foundry environment. These included mass-flow and real-time catalyst monitoring at tooling outlets, XYZ motion of tooling, and on-line measurement of moisture content in raw materials (sand).

Practical plant-floor implementation was one of the top criteria when selecting sensors for implementation/development. This was to ensure that variables being measured, should they prove vital to the control system, could be utilized in the foundry.

Two-way communication with the Allen-Bradley PLC5/40 was established using off-the-shelf hardware, and integrated into National Instrument's data acquisition system with little customization.

In parallel with development of process sensors the team worked on quantifying sand-core quality. Quantitative methods to date had been mostly destructive, an thus not suitable for production.

Through research of existing literature, and communication with industry experts, three physical properties of sand cores were target for in-process measurement:

- Dimensional
- Density
- Strength

Working with suppliers, the team developed three technologies that could provide this information real-time and withstand the harsh environment usually found in foundries. Each of these tools was customized, and integrated with the data acquisition system.

Production sand cores were dimensionally gauged using technology developed by Matrix Technologies. The AGS system (Figure 3-1) calculates gap distance by measuring pressure differences between sensors and a manifold. The pressure at the sensor varies depending on resistance to air flow caused by an object some distance from it. The operating pressure of the AGS system, approximately 1.5 psi, is non-destructive and provides a resolution of approximately 0.005 in. Sensors are mounted at strategic locations around the sand-core, and the data is compiled by the acquisition system.

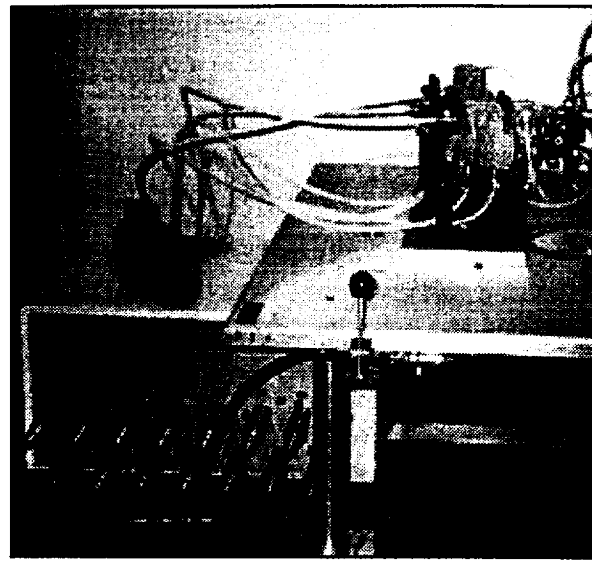

Figure 3-1. Gauging System

The core blow/cure simulation model (Task 1.5) provides Manufacturing with a predicted density map of the production sand core. Manufacturing felt this property important enough to measure in-process. Most methods for measuring density report bulk density, but they do not provide indication as to variability within the core. The team worked with Matrix Technologies to modify the AGS system (Figure 3-2). These modifications provided engineers with delta-voltage feedback based on the resistance to flow of the porous material. By strategically placing sensors, and scaling/calibration, actual density can be estimated. This information is collected by the acquisition system.

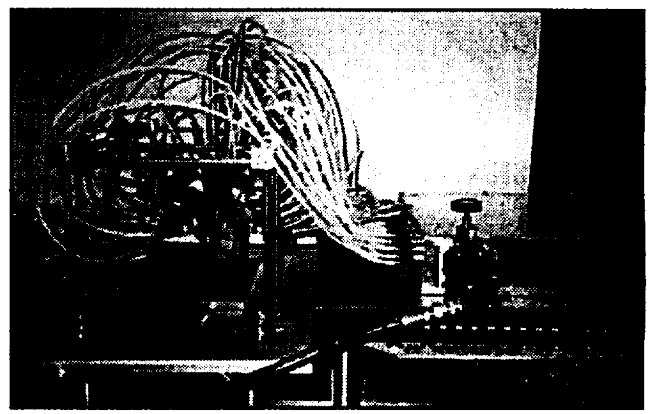

Figure 3-2. Density Measurement System

One of the most critical characteristics of production sand cores is strength. Strong cores are less likely to be damaged during material handling and withstand higher, less stable, pouring rates. The traditional technique for measuring strength is destructive, apply a force until failure, and record maximum force. This is usually accomplished using standard sand core samples produced in a lab. This information has proven valuable, but applying destructive tests to production cores does impact throughput and scrap. Another approach is to apply a known load, at a known rate, for a known time. If the production core survives, then confidence is high that the production core will withstand expected forces. If the core breaks, chances are it would not have made it through the plant. By scraping the core at this point, no added value is given to sub par components. Testing strength is accomplished with an off-the-shelf force/deflection gauge produced by Chatillon. Custom communications were developed to capture signatures for force and deflection.

Once process and core quality information are compiled, the data acquisition application stores it in an MS Access database. Signatures of some variables are also stored to ASCII files for future reference. Data analysis can easily be performed by any number of statistical/spreadsheet packages on the market today.

As a first line of defense, the engineer can visualize the data in a package called the "Automated Core Evaluation Center." This software allows process engineers to completely map characteristics of production tooling and to design experiments, perform the experiments, visualize the data, train control algorithms, and deploy advanced intelligent process control systems on production machines.

Deploying intelligent control algorithms involves the training of neural networks, and in some cases combining them with genetic algorithms for optimization. Neural Networks can be developed in several packages. Many of them have the capability to export networks to 'C' code or Visual Basic. It is this exported code that gets compiled into a Dynamic Link Library (DLL). This DLL then becomes a simple function call to the control system.

Also critical to sand core production is dimensional stability of core box tooling. Over time, steel tooling is eroded by the sand-blast effect of core blowing (Figure 3-3). This wear eventually creates dimensionally variant cores, which usually lead to scrap castings. Measuring systems for tool wear are traditionally located in a layout room, and thus are not used in production environments. Dimensional differences are to small to be detected by the naked eye, and thus tend to go undiscovered until a casting is CMM near inspection. The reader can extrapolate as to the value added to a bad core if they go unchecked.

The solution would be to measure tooling in-process. Such a system would have to be highly accurate, fast, and provide for quick set-up. Brown and Sharpe markets a product that has been used in other applications. Engineers are working closely with Brown and Sharpe to integrate the technology into the foundry environment.

The laser based system provides a point cloud, from which surfaces are generated. These surfaces can be compared to CAD models, or earlier scans to detect geometric differences. If a tool is out of tolerance, it is flagged–with a drawing indicating where trouble is–and forwarded to the layout room for repair.

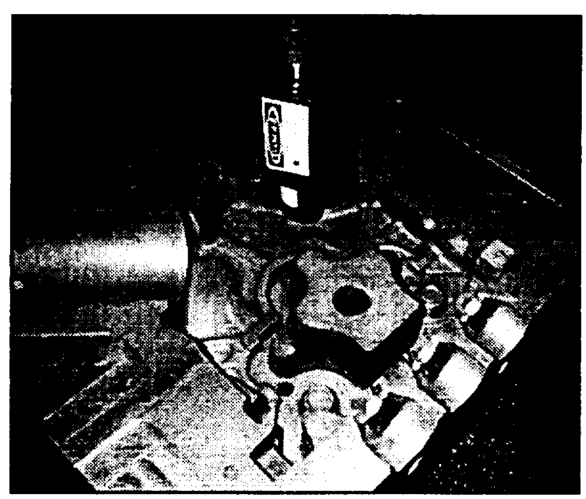

Figure 3-3. Laser Scan System for Core Box Wear

3.1.2.2 Task 1.2 – Core Cure Kinetics. The objective of this task was to measure the physical properties that affect transport and reaction of catalyst gas in a resin core. These data were needed for the predictive models being developed.

Ashland's ISOCURE™ system was used for the core binder. This is a mixture of polymeric diisocyanate and phenolic resins with triethylamine (TEA) catalyst gas. Samples of the resin were supplied by Ashland. Ford supplied a sample of Wedron sand, which was sieved to 30 and 50 mesh. 2 wt % resin was added to the sand. A 2" x 2" cylindrical core was made by ramming 200 g of sand in a steel mold.

Gas spreads through a sand core in response to a pressure gradient (as measured by the permeability) and a concentration gradient (as measured by the effective diffusivity). These are in part properties of the core and not the gas. Therefore, much of the experimental work was conducted with less hazardous gases, such as, helium and nitrogen.

Figure 3-4 is a diagram of the permeability apparatus. Nitrogen gas was applied to the top of the sample at various pressures. The pressure gradient across the sample was measured with a differential pressure transducer. The flow rate of gas was measured with a wet test meter which was checked against a calibrated water rotometer. Permeability was calculated using a modified form of Darcy's equation.

Effective diffusivity can be measured in a number of different ways including moment techniques which are fast and dependable. A diagram of the apparatus is shown in Figure 3-5. A carrier gas of nitrogen was passed over the top and bottom faces of the sand core. A differential pressure transducer was used to ensure that the pressure was the same on both sides of the core to eliminate convective flow. A small pulse of helium was passed over the top face of the core and most was swept out the vent. A portion diffused through the sample and was carried out the bottom through a thermal conductivity detector (TCD). The first moment of the pulse is related to the effective diffusivity.

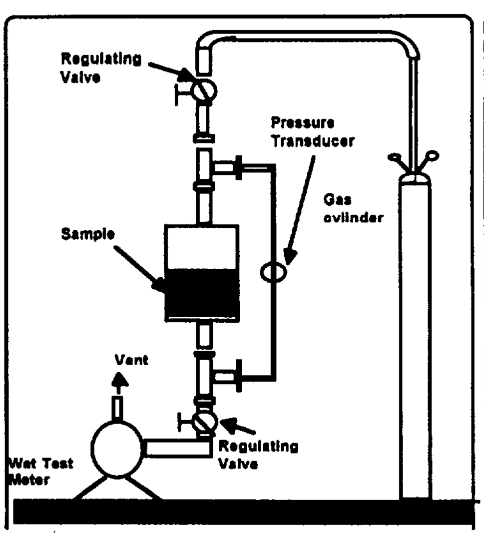

Figure 3-4. Permeability Fixture

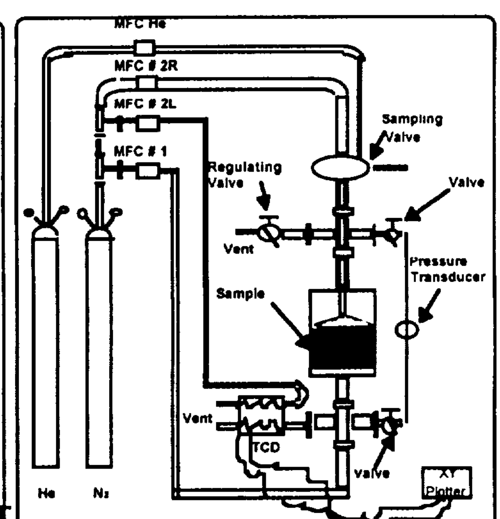

Figure 3-5. Diffusivity Fixture

A designed experiment was conducted to find the effect of sand variables on the transport properties. These variables and their levels were based on recommendations by Ford. They included grain size (30 or 50 mesh), moisture (0 or 5 wt. %) and degree of cure (cured or not). The design shows whether changing these variables causes a statistically significant effect. Interaction effects can also be detected. The experimental design is shown in Figure 3-6.

Figure 3-6. Experiment Design

Variables	Low Level	High Level
Mesh Size	30	50
H_2O (wt. %)	0	5
Cure	Cured	Uncured

Rather than extensive measurements of permeability and diffusivity, two other measurements were made. The first was to observe the "chromatographic effect." The TEA, in addition to flowing through the free area between sand grains, also is absorbed into the resin coating and then desorbs. A 1/4" glass tube was filled with sand. The sand could be coated with resin or not. The tube was connected to one leg of a TCD. Helium flow was introduced to both legs. A pulse of TEA/air was injected into the helium upstream of the glass tube and sensed by the TCD. This is very similar to the operation of a gas chromatograph.

The second measurement was to determine the rate of the curing reaction. The vendor and some users consider the reaction "instantaneous." Once the TEA gas reaches the resin, then complete reaction occurs. This may not be true at the low TEA concentrations expected in difficult-to-access regions of the core. The experimental apparatus is shown in Figure 3-7. The resin mixture was coated onto an infrared (IR) transparent salt plate and used as a window in a gas cell. The isocyanate adsorption peak was observed at 2270 cm^{-1} with an IR detector. The disappearance of this peak is an indication of the reaction between the hydroxyl groups in ISOCURE I resin and the isocyanate groups in the ISOCURE II resin. The TEA was injected into a recirculation loop driven by a peristaltic pump. The injection port was heated to vaporize the TEA but the rest of the system was kept at room temperature.

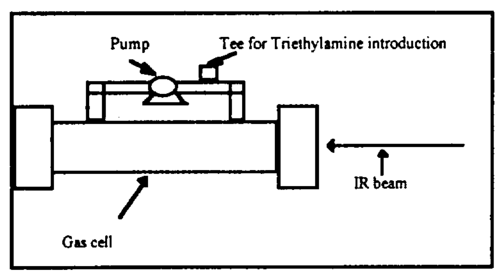

Figure 3-7. Cure Rate Experimental Apparatus

The transport properties and the effect of changing process parameters are shown in Figures 3-8 and 3-9. Curing the resin caused a significantly (in a statistical sense) higher permeability. However, its effect was small compared to the decreases caused by grain size and moisture. As the mesh size increases, the grains actually are smaller which reduces the free area available for flow. Excess moisture would also result in a more impenetrable sand. The positive effect of mesh-moisture interaction is not understood completely.

Figure 3-8. Results of Designed Experiment

Mesh	Moisture	Cure	K x 10^{-8}(ft^2)	D_e x 10^{-3} (cm^{-2}/s)
-30	0	Uncured	4.25	2.19
50	0	Uncured	2.25	1.95
-30	5	Uncured	3.53	1.95
50	5	Uncured	2.02	2.10
-30	0	Cured	4.50	2.44
50	0	Cured	2.35	2.32
-30	5	Cured	3.53	2.93
50	5	Cured	2.22	2.34
-30	0	Uncured	4.25	2.19
50	0	Uncured	2.25	1.95
-30	0	Uncured	3.53	1.95
50	5	Uncured	2.02	2.10
-30	0	Cured	4.50	2.44
50	0	Cured	2.35	2.32
-30	5	Cured	3.53	2.93
50	5	Cured	2.22	2.34

Curing had the only significant effect on diffusivity. This may be due to a chromatographic effect with the gas adsorbing/desorbing on the resin coating as it diffuses through the sand core. This is a phenomenon not accounted for in the current model of the curing process.

The specific values of permeability and effective diffusivity can be used in the verification trials of the curing simulation.

The range of values can be used in a sensitivity analysis to process conditions.

Figure 3-9. Effects of Parameters on K and D_e

Effect	K x 10^{-8}(ft^2)	D_e x 10^{-3} (cm^{-2}/s)
Mesh	-1.74	-1.83
Moisture	-0.54	1.29
Cure	0.14	4.18
Significant	0.03	3.32

Figure 3-10 shows the delay in TEA transport through a bed of sand when it is coated with resin. It took about 10 sec for the TEA to get through the column of dry sand and about 25 sec for the resin coated sand. This preliminary experiment only demonstrates the reality of the chromatographic effect.

Figure 3-11 shows the amount of uncured resin with time for various amounts (μL) of TEA injected into the system. 10 μL represents about a mmole/L in our system. Curing has a measurable rate and concentration dependence.

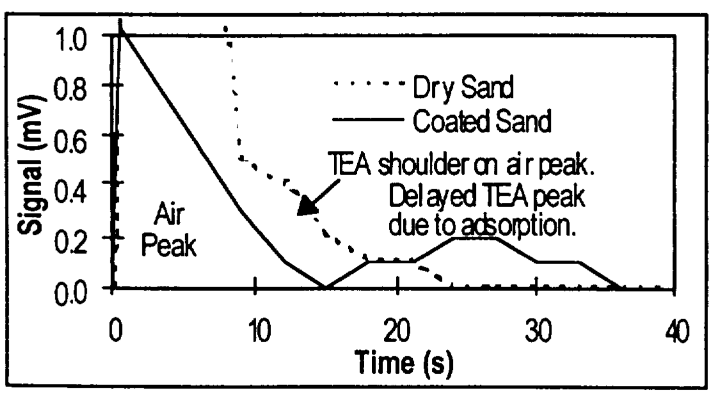

Figure 3-10. Chromatographic Effect

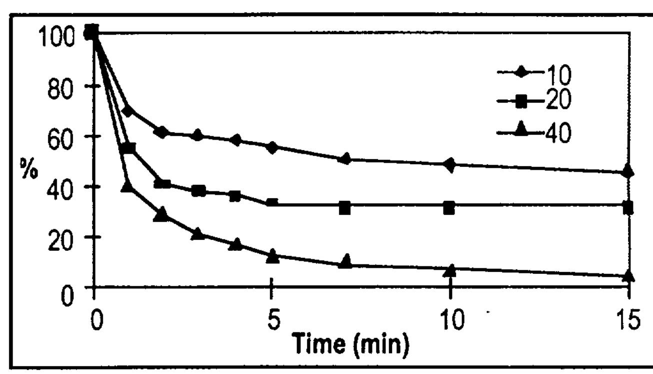

Figure 3-11. Curing with Various TEA Amounts

Recommendations. Transport properties can now be routinely measured. Curing kinetics and adsorption/desorption need to be investigated further.

3.1.2.3 Task 1.3 – Densification and Deformation Models. The goal of this work was to determine the apparent viscosity of fluidized sand. These data could then be used to validate predictive models. There are several different experimental approaches to the study of the transport properties of fluidized materials. The problem of the rheologist is the interpretation of the flow behavior of a fluidized material in terms of its physical and chemical properties and its state of fluidization. Simple mathematical models cannot at present describe the general flow behavior of fluidized materials. The apparent viscosity of a fluidized material is a multiparametric function and is dependent on the physical and chemical properties of both the solids and the aerating fluid. Fluidized materials are particularly complex and, if numerical simulations of the behavior are to be reliable, it is critical that the measured values be consistent regardless of the measurement techniques applied. This work was concerned with an experimental study of the apparent viscosity of fluidized sand utilizing both Poiseuille flows (capillary viscometer) and Couette flows (rotational viscometer). Capillary tube viscometers are preferred when the data are to be used for pipe flow problems, and rotational viscometers, which subject the material under test to a precise and uniform rate of shear, have definite advantages in the analysis of complex system, such as in sand molding processes.

Viscometric measurements by capillary tube viscometers were run in the system shown schematically in Figures 3-12 and 3-13. It consists of a clear acrylic cylindrical chamber 457.2 mm long and 69.85 mm in inside diameter which is sealed at the top and bottom. A funnel with the angle of approach 57°, 30' was attached at the bottom of the cylinder. Precision-bore copper capillary tubes of 4.7625 mm inside diameter and five different lengths (73 mm, 146 mm, 292.1 mm,

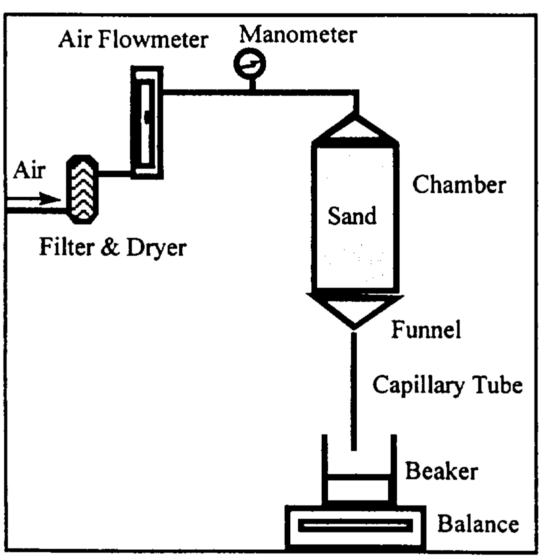

Figure 3-12. Capillary Tube Viscometer

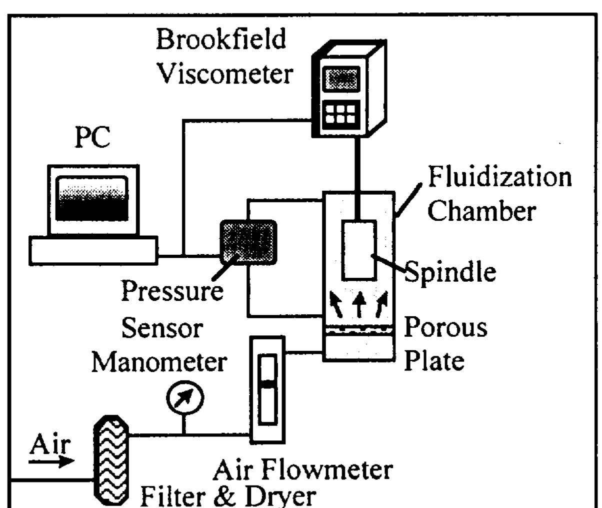

Figure 3-13. Rotational Viscometer

584.2 mm and 1168.4 mm) were screwed into the funnel exit. Air at a carefully controlled constant pressure was admitted through the top plug of the chamber. The rate of sand flow was typically measured by collecting a sample over a measured time and determining its mass. The experiments were run using capillary tubes coated (to prevent wall slippage) by sand of the same particle diameter of sample to be tested. As coated capillary tubes copper tubes were used of 7.9375 mm inside diameter and five different lengths (122 mm, 243 mm, 487 mm, 974 mm and 1947 mm). One of the main difficulties in capillary tube viscometry is in accurately determining the appropriate pressure drops. The corrections for the head of sample over the tube, for kinetic energy effects, and for entrance losses are required. The first correction is straightforward. The other two were respectively estimated by (1) repeating experiments in capillary tubes of different lengths and extrapolating the overall pressure drop to zero length and (2) experimental calibration with Newtonian fluids of known viscosity and density. Water and 50/50 glycerol/water mixture were used as calibrating liquids.

A computer controlled Brookfield HADV-II+ rotational viscometer was also used in the experimental program. This device measures the torque required to rotate a spindle immersed in a fluid. For a given viscosity, the viscous drag, or resistance to flow, is proportional to the spindle's speed of rotation and is related to the spindle's geometry. Measurements made using the same spindle at different speeds are used to detect and evaluate the rheological properties of the test material. Viscosity measurements were made at spindle angular velocities in the range of 1 to 100 rpm. The viscometer was calibrated by using 50/50 and 99/1 glycerol/water mixtures and 3.5% polyacrylamide solution. A round acrylic tube with internal diameter of 58 mm and 227 mm length was used as a fluidization chamber (Figure 3-13). Pressure taps were provided along the column. The pressures were measured using a computer controlled differential pressure sensor. The fluidization chamber was arranged for use with air as the operating fluid. Compressed, dried and pre-filtered air under pressure up to 840 kPa was supplied to the bottom of the fluidization chamber. Air pressure and flowrate were measured by a pressure gauge and rotameter, respectively. A polypropylene porous plate with 0.250 mm pore size and 3.175 mm thick was used as an air distributor. Capacitive and photometric methods for two-dimensional measurements of the bed void factor in fluidized silica sand were developed.

All measurements were made with sand that was supplied by Wexford Sand Company, Wexford, MI. The average particle density of sand used was 2.593 g/cc. The distributions of particle diameters used were as follows: less than 0.212 mm, from 0.212 mm to 0.425 mm, and from 0.425 mm to 0.710 mm. To prevent wall slippage effects, the surface of the spindle was adhesively coated by sand of the same particle diameter of sample to be tested. As a cold box binder system we used ISOCURE LF-305/904 G system produced by Ashland Chemical Company, Dublin, OH. According to the existing foundry procedures and following the manufacturer's instructions, in our experiments we used the composition at a 55/45 ratio of ISOCURE Part I binder to ISOCURE Part II binder components. The total binder level was

1.5% based on sand weight and the bulk density of the coated sand was 1.426 g/cm^3. Recently we experimentally investigated the rheological and thermal properties of a phenolic resin (ISOCURE Part I LF-305) and polymeric isocyanate (ISOCURE Part II 52-904 GR), and their blends and determined that although both binders are Newtonian liquids, their blends exhibit non-Newtonian shear thinning fluid flow behavior and elasticity.

The apparent shear strain rate γ_a and the apparent shear stress τ_a at the capillary wall are defined by:

$$\gamma_a = 4Q/\rho \pi r_o^3 = 4 \upsilon/r_o$$

and

$$\tau_a = \Delta P \, r_o /2 L,$$

where Q is the mass flow rate, u the threading speed, ΔP the pressure drop in the tube, r sand density, and r_o and L the radius and the length of capillary tube, respectively. The apparent viscosity η_a is: $\eta_a = \tau_a/\gamma_a$. In the case of sand flow, the capillary viscometer technique determines the apparent viscosity as the averaged value of all inner local viscosity. The value of the apparent viscosity is obviously a function of the shear strain rate γ_a. Apparent viscosity data of dry and coated sand particles ranging in diameter from 0.425 mm to 0.710 mm and obtained on both the rotational and the capillary viscometers as functions of the apparent shear rate are shown in Figures 3-14a and 3-14b, respectively. Regardless of the method of measurement, there is a general consistency in the data obtained with the Brookfield viscometer (low shear rates) and capillary viscometer (high shear rates). As seen from Figures 3-14a and 3-14, the apparent viscosity can be satisfactorily correlated with the apparent shear rate as following equation: $\eta_a = \kappa \gamma_a^{n-1}$, which is empirical functional relation known as the power law model.

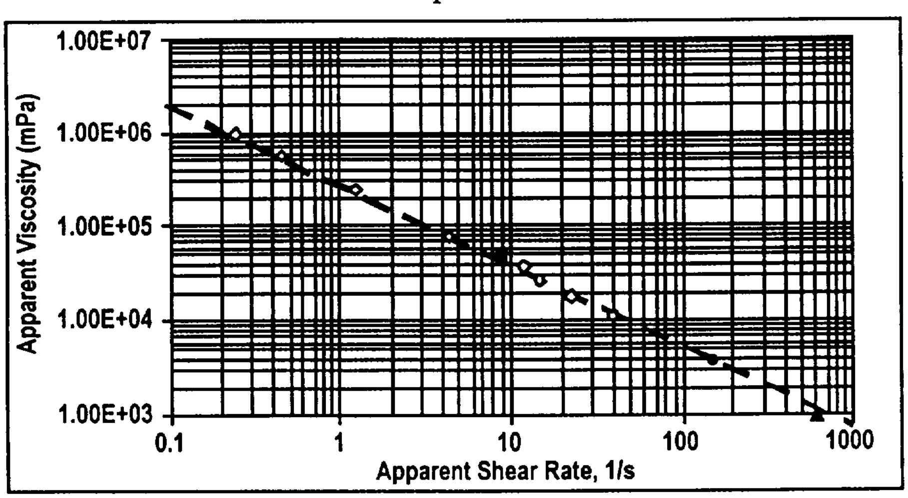

Figure 3-14a. Apparent Viscosity of Sand Bed as a Function of the Apparent Shear Rate

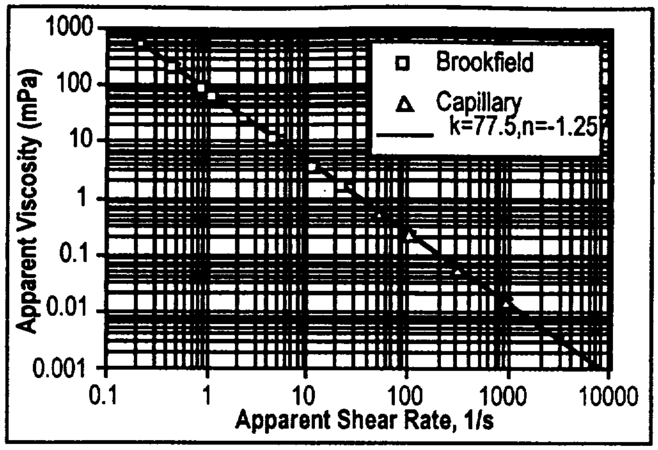

Figure 3-14b. Apparent Viscosity of Binded Sand as a Function of the Apparent Shear Rate

(◊ Brookfield; Capillary: ▲L/D=15.33, ● - L/D=30.67, □ - L/D=61.33,
O - L/D=122.67, ■ - L/D=245; — Power Law Correlation

Introducing two components of the apparent viscosity as apparent shear viscosity $\eta_{a.sh.}$ and apparent kinetic viscosity $\eta_{a.k.}$, which defined as: $\eta_{a.sh.} = 75\ E_p^2\ \mu\ D^2/16\ (1-E_p)^3\ (\phi d_p)^2$ and $\eta_{a.k.} = 7\ E_p\ \rho\ D^3\ \gamma_a/1024\ (1-E_p)^3\ \phi\ d_p$, lead to the following form of the rheological model: $\tau_a = [\eta_{a.sh.} + \eta_{a.k.}\ (\gamma_a)]\ \gamma_a$, where $\eta_{a.sh.} + \eta_{a.k.}\ (\gamma_a) = \eta_a$.This model predicts that the flow curves of gas-solid suspensions depend on the gas properties, particle diameter and sphericity, void factor and tube diameter. The experimental data obtained for Poiseuille flow of air-sand system gives a quantitative confirmation of the predictions over a wide range of shear rates.

Experimental instruments were designed and fabricated evaluating the apparent viscosity of dry and coated sand by both rotational and capillary viscometers. The apparent viscosity of the test systems can be correlated with the apparent shear strain rate as power law model. Regardless of measurement methods, there is a general consistency in viscosity data obtained at low shear rates (on rotational viscometer) and at high shear rates (capillary viscometer coated by sand of the same particle diameter). The apparent viscosity decreases as the bed voidage factor increases. The rate of decease of viscosity is greatest near incipient fluidization. Thereafter the rate of decrease lessens. The apparent viscosity is little affected by changes in particle diameter. A rheological model based on a semi-empirical correlation has been developed for the air-sand system over a wide range of shear rates.

3.1.2.4 Task 1.4 – Compressible Flow Model Development. The objective of this task was to explore micro/macro modeling. The Computational Materials Laboratory (CML) at NASA Lewis Research Center was responsible for assessing numerical models for the core filling process. Since the team at Ford was responsible for assessing numerical models for the core filling process. Since the team at Ford Casting Operations performed a complementary assessment of ProCast (see Task 1.5), NASA concentrated on several different approaches. In all cases, solutions which were either available off-the-shelf, or off-the-shelf with a little extra work, in order to provide realistic, significant results in the near term were evaluated. To this end, Fluent, a finite-volume flow solver, which had included multiphase flow modeling capability was investigated. This avenue was impractical due to the memory- and CPU-intensive nature of this approach, even for fairly simple geometries. Even if this were not an issue, this approach is best suited for dry granular media with empirically known momentum exchange coefficients. The possibility of developing a simplified numerical model based on physical insight was also explored. Unfortunately, experimental data became available too late in the process for us to make much progress in this area; however, this ought be explored in depth now that experimental evidence is available. The rest of this section is devoted to the results of the third approach, micro/macro modeling.

The basic concept of micro/macro modeling is to separate the extremely complex microstructural evolution from the overall fluid flow, but still allow information to flow from one scale to the other as appropriate. The flow behavior at the macroscale is modeled by an integrated single-phase flow, while the microstructural evolution of the fluid at the microscale is modeled by numerous micromodels or constitutive models. This separation is very significant in that it indicates that the global behavior of the multiphase flow is similar to that of single-phase flow, but the local phenomena of the flow can be as complex as nature. The micromodels can be easily made functions of local density and shear stress, the shape of the particles, their arrangement, size and size distribution, binder properties, binder percentage, and agglomeration of the solid particles. This versatility is extremely attractive considering the range of processing conditions which might be considered by any generic sandcasting process.

Information from the macromodel flows down to the micromodels by providing the pressure and average velocity fields and their gradients. The micromodel calculates local stress, which is fed back up to the macromodel. This exchange of information occurs at every iteration. For this case, the CPU time required for the simulation is increased by a factor of 1.5 to 3 relative to the single-phase power-law fluid case.

Comparison of Numerical Model with Experimental Results. Micro/macro simulations were performed for: (a) Ford's experiments #1 and #2 with dry sand; (b) Auburn University's (Overfelt, et al.) simplified core box with wet sand in 2D and 3D; and (c) Ford's 3-chamber prototype core box (Beckwith) with wet sand in 2D. Below some results from the simulation of Auburn's experiments are shown.

Constant pressure boundary conditions were applied at the inlet nozzle and at the vents. The normal velocity at the vent was a function of a specified resistance (to mimic the effect of the vent screen), and the tangential velocity was zero. Volume fractions were also prescribed at these locations for the use of the micro-model. It was assumed that the air/sand/binder mixture did not wet the walls, and simply used a zero velocity boundary condition at the wall. Finally, a symmetry boundary condition was applied at the centerline of the geometry, for simplicity.

From the simulation of Auburn University's core box, the 2D model was found to underpredict the retarding influence of the bounding walls in the third dimension. Logically enough, the filling patterns differed. Specifically, the 2D simulation tended to fill the entire core box with some sand and then increased density throughout, whereas the 3D simulation filled the entire core box more slowly but more uniformly. The locations of the last-to-fill regions differed as well as the extent of those regions. Although no experimental evidence was available at that time, the 3D simulation was more true-to-life, particularly near the condition of nominal filling. This was subsequently validated by comparing the filling patterns with the experimental results of Overfelt et al., and Beckwith (see Task 1.3).

In Figure 3-15, filling patterns are shown as calculated by the micro/macro model at four times in the core filling procedure. The filling pattern in Figure 3-15(a) shows that the sand flow has reached its first obstruction, a wall, and must turn to accommodate its presence. The bulk of the core box is still empty, but when the sand flow hits the first wall, the local density reaches close to its maximum density. Later in the simulation, the flow impinges on a second wall, Figure 3-15(b), and splits into two streams. The mass flow in both streams appear roughly comparable, at least until the upper stream interacts with the vent at the top of the core box. At that time, the pressure gradient near the vent acts to pull more of the air/sand mixture into the top part of the core box relative to the lower part. Also note the bending of the main fluid stream as it approaches the second wall, which is expected to be a function of inlet and outlet pressures, vent placement, and the mold curvature.

Still later in the cycle (Figure 3-15(c)), the mold is incompletely filled, but the sand/air/binder mixture has impacted the walls. Sand density is most concentrated at the left wall of the downstream end of the core box. In fact, the right wall is almost sand-free, in agreement with Auburn's filling patterns. Wall pressure contours at this time (not shown) show a characteristic increase at the location of flow impact, corresponding to momentum loss as the flow slows and changes direction. At this time, there is marked similarity between the density and the pressure fields. Near the point of nominal filling (Figure 3-15(d)), the simulation shows that the last region to fill occurs at the right wall of the downstream end of the core box, in agreement with Auburn's subsequent results. When the whole core box is nominally filled, the local density continues to evolve until a quasi-steady state is reached. The model is not faithful to Auburn's last-to-fill results in the upstream end of the core box, but the exact behavior in this area was not anticipated due to the simplification of blowtube geometry.

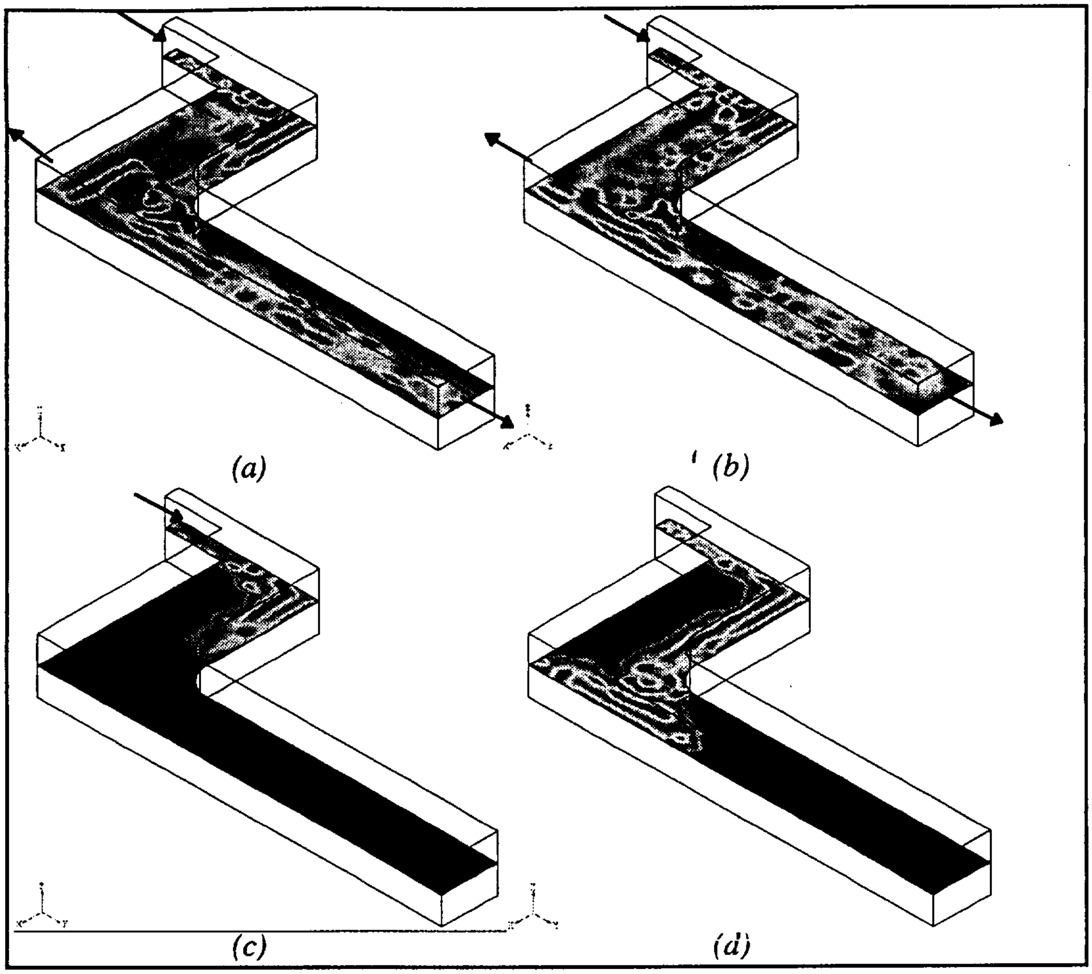

Figure 3-15. Filling Pattern at Four Successive Times in the Filling Process, as Calculated by the Micro/Macro Model (3D Results). Arrows Indicate Air/Sand Flow Entering or Air Flow Leaving the Mold

For this process, the density at the surface of the sand form is of most interest. Thus, the density and pressure at the walls near the end of the simulation are shown in Figure 3-16. The complexity of the relationship between density and pressure in these processes is illuminated here. If only pressure were relied on (Figure 3-16(a)) to predict density, the upper part of the core box would be at high pressure and so, high density, and the lower portion would have lower density and perhaps be prone to defects. Note the high densities near the points of wall impact in Figure 3-16(b), as indicated by the arrows. Pressure and density are both high-valued in these regions. Two arrows point to regions of disorganized, but moderate, density. The corresponding pressure contours in these regions are vastly different. Recall that the local density can be affected by both the pressure gradient and the shear rate. When the pressure is the dominant factor of the flow, proportionality between these two variables is observed. However, when the shearing dominates flow behavior, this similarity disappears because the shearing direction is normal to that of the pressure. When a region of the mold is nearly filled, the pressure becomes quite uniform, and

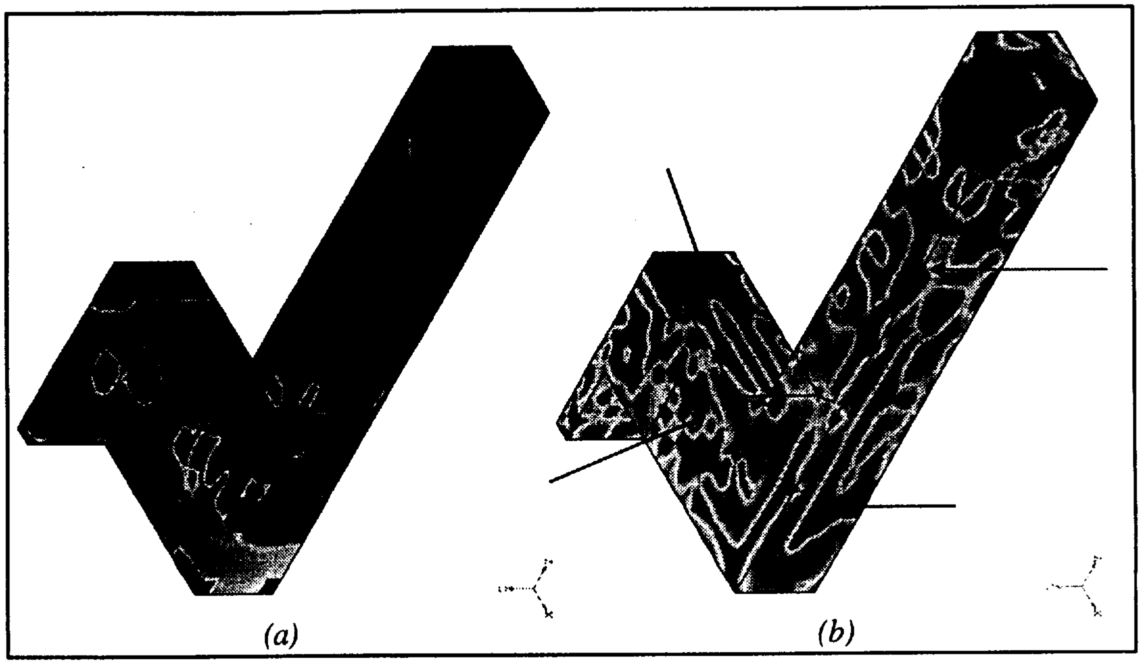

Figure 3-16. Pressure and Density at the Walls Near the End of the Core Filling Process

shear can become very important. This is precisely the point at which the model must be the most accurate, since it is the final density distribution which predicts the quality of the core. Thus, it is insufficient to use the pressure field alone to predict the success of the process.

The micro/macro modeling approach was applied successfully to a mixture of air, sand and binder filling an initially evacuated core box. The stability, convergence and CPU time required was reasonable for design diagnostics.

The filling patterns shown here were obtained prior to the experimental results, but did show extremely good qualitative agreement with Overfelt et al.'s and Beckwith's subsequent experimental data. The nonuniform density distribution at the conclusion of the process showed regions of high density at locations at which the flowing mixture impacts the walls. For many simple flows, the density distribution is proportional to that of the pressure. Although a direct correlation between the density and pressure at early times in the filling process was observed, they lose this similarity in the later stages of core filling.

Further improvement in the micro-model could be made by incorporating the effects of particle shape (spherical particles were assumed), slip boundary condition at the walls, and including particle stickiness. The insight gained from the experimental results of Beckwith and Overfelt could now be exploited to develop simpler models which could perhaps be used in a production environment.

3.1.2.5 Task 1.5 – Core Box Fill (One Phase) Model Development. The goal of this task was to develop and validate a single-phase, core-box die fill flow model.

A series of sand flow tests were conducted at Ford Research Laboratory to provide some initial insight into the flow behavior of blown sand. In the tests, a straight Plexiglas tube, with a funnel attached at the bottom, was filled with resin coated sand. And various tube pressures were used and the time for the sand level to drop through the measurement section was recorded. The sand draining times versus various funnel exit diameters and exit tube lengths were also tested and recorded.

In a parallel study (see Task 1.3), the Auburn University developed a design of experiment, using both standard and non-standard rotational- and tube-type rheometric instruments, to investigate the flow characteristics of coated sand during blowing process. Figure 3-17 is the test apparatus used. Numerical representation of the apparent viscosity of fluidized resin coated sand was derived and used in computer model development to improve the modeling accuracy.

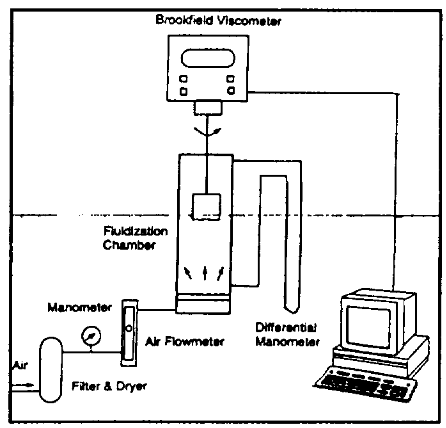

Figure 3-17. Sand Flow Property Test

The University of Alabama (see Task 1.2) designed an experimental apparatus, as illustrated in Figure 3-18, to measure the packed sand physical properties, such as absolute permeability and effective diffusivity, that affect transportation and reaction of catalyst gas (TEA) in a resin coated sand core. In the tests, pressure gradients across the packed sand were measured by pushing nitrogen through the core at various inlet pressure ranges. The permeability of the core sample was derived from the measured flow rate and pressure difference within the core. Using a similar test setup, diffusivity of the sand core was obtained by applying a small impulse of helium and measuring the time it took to diffuse from the inlet to the outlet.

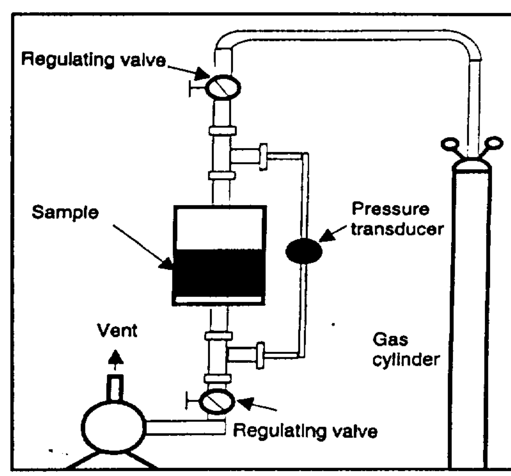

Figure 3-18. Sand Permeability Test

In order to simulate the chemical reactions in curing process, a curing kinetics model was derived from the measured transport properties, which were collected under different sand and process conditions to represent its generality. These transport properties are essential inputs for the curing model. The experimental data indicate that curing reaction rate depends on the exposure area of the resins to the TEA catalyst and the presence time of TEA catalyst.

A benchmark result of a variety of commercially available modeling packages suggests that ProCast was a feasible and capable tool, with further enhancement and modification, to model the sand blowing process assuming it is an incompressible, single phase flow. ProCast then was customized for modeling sand core blowing process. The first sand blowing simulation was performed on the 2.3L Ranger slab core. The advancing front and velocity field of sand flow were calculated. The velocity field shows a consistent pattern with the CT scanned density result. Based on this correlation, core density distribution was predicted by converting the calculated flow velocities using a mapping formula derived from CT scanned data. And the formula is numerically expressed as

$$\text{Density} = a + b * \text{Velocity}^2$$

a and b were obtained by least square fitting of the velocity field with the CT scan density. The density predicted by ProCast shows good correlation with the CT scan density data.

Methods for modeling curing process were developed by FDI, Inc. using their software package, FIDAP. An interface program was developed by UES, Inc. to transfer the density prediction result from ProCast to FIDAP for the cure model input.

The curing simulation consists of two phases. In the first phase, velocity field of the gas (nitrogen) flow was calculated considering the sand core as a porous media and the inlet pressure as a boundary condition. With the velocity predictions from the first phase, the second phase was carried out to compute the TEA flow front and the concentration throughout the sand core. With the curing kinetics model of the University of Alabama, it was assumed that the sand core is cured instantaneously while the TEA is in presence. Therefore, the TEA flow front can be a good indicator for the curing state of a sand core.

This modeling method is capable of predicting the catalyst (TEA) flow advancing front, its concentration and cycle time for the curing process. And the curing model has been successfully integrated with the blowing model into a software system which can simulate the complete core making process. Figure 3-19 illustrates the methods and procedures of the modeling software system.

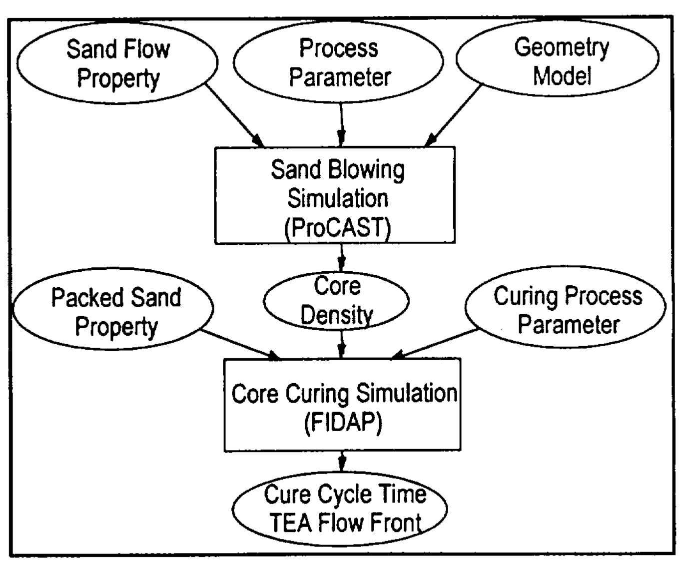

Figure 3-19. Simulation Software System

In support of the software validation, several testing techniques/methods were developed and applied in the designs of experiment.

A high speed video was made of the blowing process using a 2.3L prototype core box with two Plexiglas windows, to verify the computer model on the flow front and the cycle time. Two Non-Destructive Test (NDT) techniques were investigated and used to measure the real core density. They are in use of IR thermal image technique and CT scan process. Study showed that the CT scan is superior to the IR thermal image, because it provides 3-dimensional density information, and it is not sensitive to the scanning object orientation. The CT scan data for the 2.3L Ranger slab core was obtained through the service of ARACOR, and was used to validate the computer modeling results. A translator program was developed to convert the CT scan data into spatial density distribution that can be imported to ProCast post-processor for display.

A pH indicator (Bromocresol Green solution) was added and blown in the sand/resin mixture to detect the TEA catalyst flow advancement in the core curing process. A curing process can be divided into two stages, gassing and purging. In the gassing stage, this pH indicator mixed in the resin coated sand turned color from yellow to blue when the TEA is in presence. And a yellowish line was formed as a clear interface between the gassing and purging stages.

Two verification experiments were performed to validate the simulation software system. The first verification is done with a single chamber transparent core box. This transparent core box has a simple geometry, and was designed to reflect the momentum loss of a turning flow and the sand density variation of different venting configurations. This core was blown and cured in Ford FRL Sand Core Manufacturing Lab. Figure 3-20 illustrates the apparatus for the verification test.

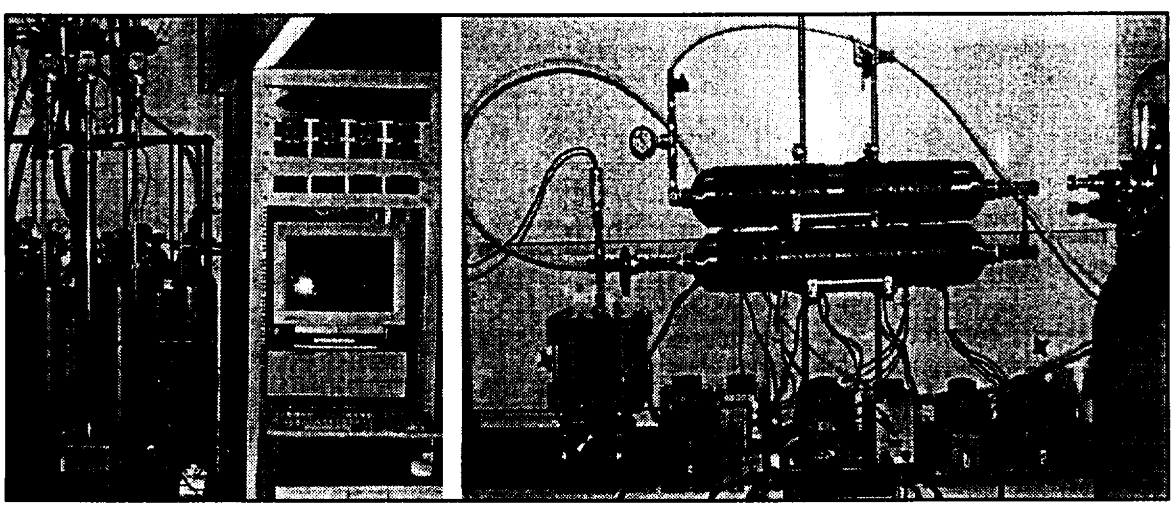

Figure 3-20. Single Chamber Core Box Verification Test Setup

The blowing pressure was recorded by a data acquisition system. A video photography was made to record the filling sequence, pattern and time to validate blowing model. A CT scan density data was obtained to verify the model predicted density distribution. For the curing model validation, the TEA tracing technique was employed to monitor the TEA flow front.

About computer simulation, a solid model and the finite element model of the test core box were created at Ford. Sand flow properties and sand core transport properties from Auburn University and the University of Alabama were incorporated into the blowing and curing models. Simulations were performed with ProCast and FIDAP respectively. Figure 3-21 is a comparison of the CT scan density and the model predicted result, which shows reasonable correlation with each other. In Figure 3-22, the FIDAP calculated TEA flow front showed the consistent pattern with test data.

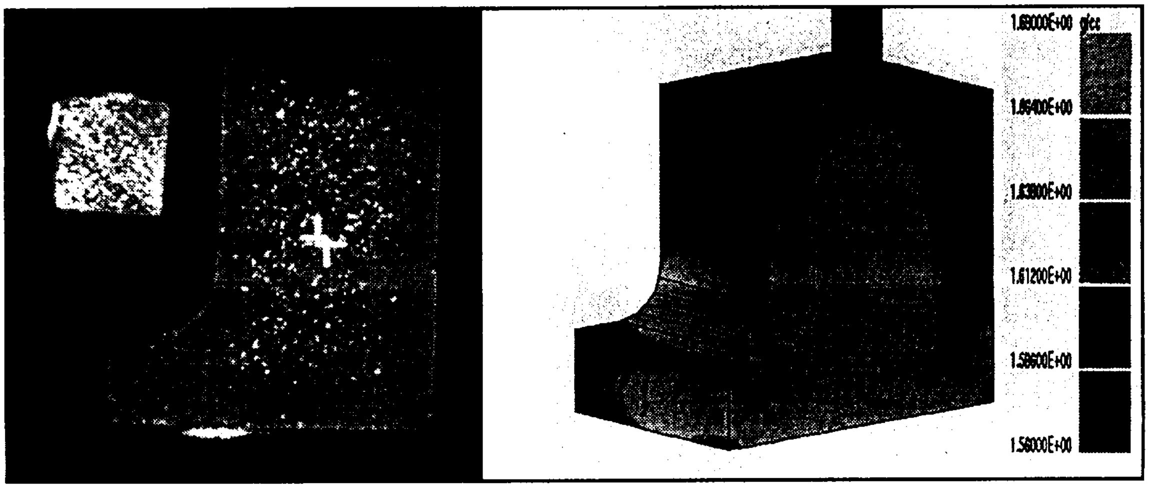

CT Scan Density *Model Prediction*

Figure 3-21. Density Pattern Comparison

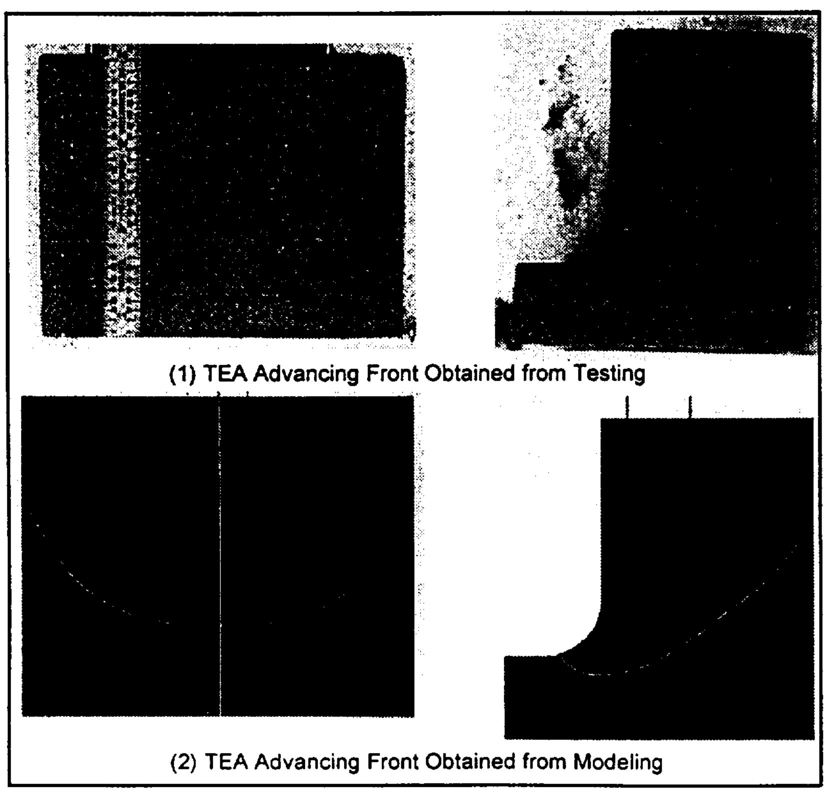

Figure 3-22. TEA Moving Front Result Comparison

To further validate the modeling system for a real and complicated geometry core, the 2.3L Ranger slab core was chosen in the second verification. Figure 3-23 is a sand core made during this test.

The experiments were performed on the modified prototype core box with two Plexiglas windows, using the state-of-the-art core making machine in Ford AMTD. The high speed photography, CT scan and TEA tracing techniques were employed to monitor and measure the sand blow sequence, density distribution and TEA catalyst flow advancement flow front. In order

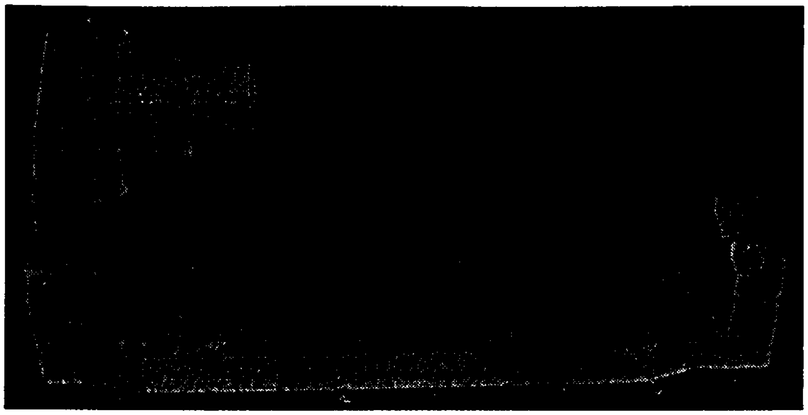

Figure 3-23. 2.3L Ranger Slab Core

to correlate curing model for various intermediate phases in a complete cure process, the gassing process was done in 4 cycles. Correlation of the sand filling pattern and density between testing results and model predictions is consistent and with good agreement. Figure 3-24 is the comparison of CT scan density vs ProCast model predicted density.

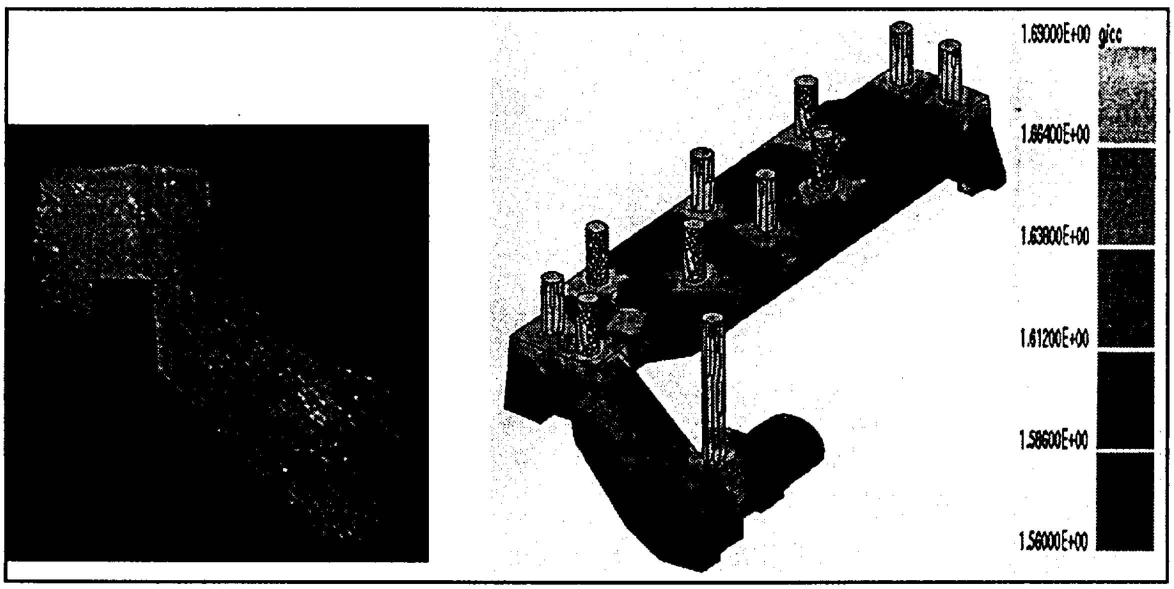

CT Scan Density *Model Prediction*

Figure 3-24. 2.3L Ranger Slab Core Density Comparison

Regarding cure model verification, because the slab core geometry is relatively complicated to generate a finite element model with all hexahedron elements, FDI, Inc. decided to build a high order tetrahedron mesh, instead, for the cure model. That approach is believed to be more practical and time effective for engineering application; however, some difficulties were encountered in the FIDAP curing simulation with this new approach. This tetrahedron finite element model tends to be more unstable in the numerical calculation that easily diverges the solution, comparing to a hexahedron finite element model. Figure 3-25 is a comparison of the TEA moving front at the end of each gassing cycle. The TEA moving front predicted in the modeling shows consistent pattern with the test results. Although the FIDAP curing model was verified and validated with the 2.3L Slab core, Ford and FDI Inc. will further improve the accuracy and robustness of the tool.

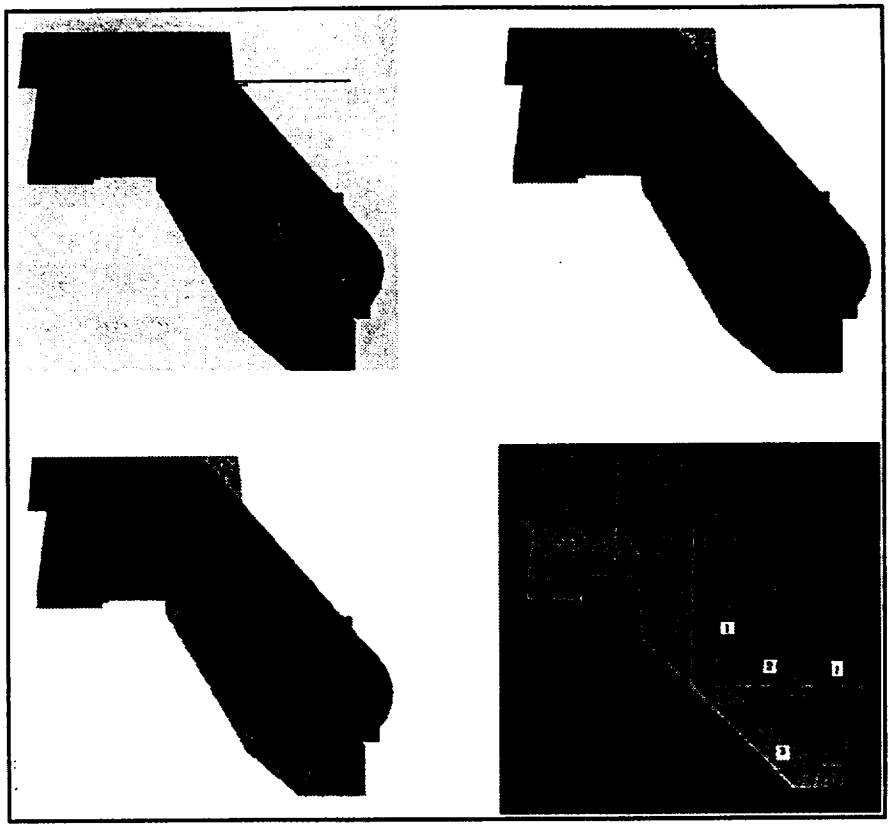

(1) TEA Front After 1st Cycle (Upper Left - Simulation)
(2) TEA Front After 2nd Cycle (Upper Right - Simulation)
(3) TEA Front After 3rd Cycle (Lower Left - Simulation)
(4) TEA Front Recorded In Test (Lower Right - Actual Core)

Figure 3-25. Gassing TEA Moving Front Comparison

Conclusions. Based on the analysis of the test data, it is concluded that the sand/air mixture can be modeled as a single phase, incompressible, non-Newtonian flow. An equivalent viscosity relationship was then derived and used for sand blowing model development. Computer simulations of the experiments were also performed with ProCast to confirm the feasibility of experimentally determined "equivalent sand flow properties."

3.2 TASK 2.0 – SIMULATION AND CONTROL OF INJECTION MOLDED CORES

3.2.1 Introduction and Summary

Injection molded and sintered cores form the inside surfaces and passageways and typically include some of the most critical dimensions in complex investment castings. Core related defects are a major source for rejecting airfoil investment castings. Study of the manufacturing process lists the primary problems as: 1) Distortion of the cores during the core manufacturing process; 2) Inaccuracies in placement of the finished cores in the part wax injection die; and 3) Distortion of the cores during subsequent casting process operations (Dewax and Alloy pour).

Cores must be manufactured out of refractory materials since they are completely surrounded by molten alloy during casting pouring and solidification. They must be strong enough to survive handling, wax pattern injection, molten metal temperatures, pressures, impingement loads and thermal shock, yet compliant enough to allow (1) the solidifying metal to contract normally and (2) easy removal after the casting cools.

The injection molding of cores is a complex process that is utilized by a large part of the U.S. investment casting industry. Figure 3-26 displays a flow diagram of the overall core injection molding process. Injection molding involves injecting a mixture of refractory powder and proprietary carrier material into a metal mold under high pressure. Vents in the mold allow air to escape during the injection process. The extremely fragile "green" cores are then debinded from their carrier material and finally sintered at temperatures in excess of 1200°C to obtain cores ready for insertion into wax patterns for later investment casting. Many core defects (overall dimensional accuracy and stability, low surface density, voids, breakage, non-fill, etc.) produced in these core fabrication steps can translate directly into defects and lead to higher scrap in the investment castings themselves.

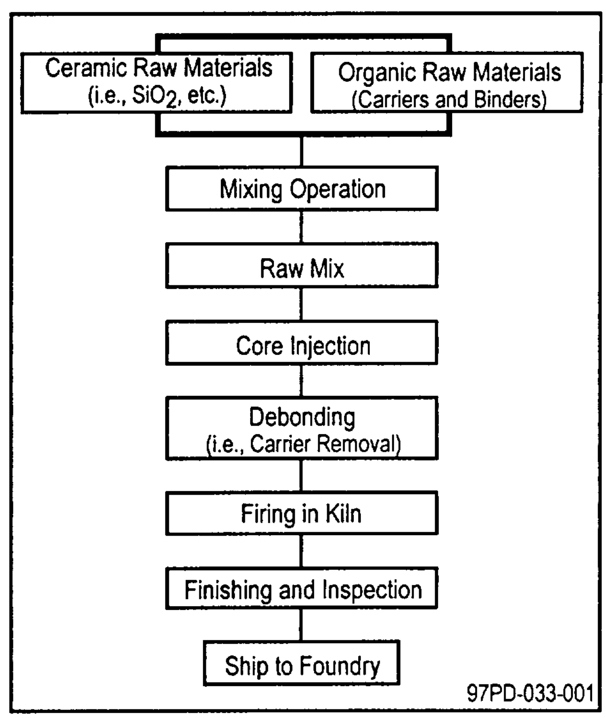

Figure 3-26. Typical Injection Molded Core Fabrication Process Steps

Part of the Task 2.0 effort of this AITP program included both experimental and analytical thrusts to better understand core injection molding and sintering processes. Howmet Corporation (HC) and PCC Airfoils independently completed initial experimental efforts to develop a better understanding of the core injection process from primarily an empirical standpoint. The primary focus of these experimental efforts was to characterize the process parameters that have a strong impact on dimensional control issues of injected cores during their fabrication. Findings from the experimental efforts completed at these two companies as a part of this program were transitioned into the production core making facilities with favorable results.

Also within this task, UES was chartered to evaluate and develop analysis methods and tools within ProCast that can be used to analytically predict the core injection molding process, and provide insight into coupled fluid flow and heat transfer effects such as particle segregation (density variations), core porosity, and non-fill problems. These modified tools are available for core injection molding process modeling and die design. During the conduct of the program, it was found that the ceramic particle density variations within injection molded cores could not be adequately correlated to basic flowfield results. In order to accurately predict particle density variations a multiphase flow model would be required.

Auburn University during the program developed an empirical data base to evaluate dimensional changes occurring in ceramic core materials during the sintering stage of core processing.

At the start of the program there did not exist a methodology to examine cores, patterns and castings for flaws or dimensional errors in a rapid or near real time environment throughout the casting production cycle. Part of the current effort was directed to develop both software and hardware to enable the use of 2.5D X-Ray techniques to enable near, real-time, three-dimensional evaluation of cores and/or castings. These 2.5D methods allow direct comparison of part geometric data to known reference or CAD solid models and can be used to eliminate out of specification parts earlier in the casting production cycle. GE developed the 2.5D X-Ray software tools while ARACOR and Howmet provided radiographic scan services and engineering data base support for this development effort. The focus of this work was to develop a representation for describing deformations of cast parts in order to permit accurate quantification, monitoring, and control of part geometry.

A deformation representation is useful for accurately describing a wide variety of castings and their possible deformations. It allows actual deformations to be computed readily from measurements of a part, such as measurements obtained from X-Ray images or coordinate measuring machines. Finally, it yields information that is useful both for understanding deformations and for correcting them.

To meet these requirements, GE developed a parameterized model for characterizing various deformations in investment castings. The model was derived from experience in casting precision aircraft engine parts, but it is expected to be applicable to a wide range of other castings. Note that only distortions in shape are addressed -- not, for example, defects of material composition or of grain structure. GE also developed algorithms to process digital X-Ray images for the purpose of generating a deformation description of actual part geometries.

3.2.2 Procedures and Results

3.2.2.1 Task 2.1 – Analysis of Core Injection Molding Defects (Howmet). Although a wide variety of core defects reduce yields and increase costs of investment cast airfoils, poor dimensional quality was chosen as most important. Dimensional quality was chosen since wide tolerance bands for key core dimensions and difficulties in accurately measuring airfoil shapes can contribute to the production of scrap castings from in-specification cores. Improvements in core dimensional consistency will improve casting yields, even if overall core yields are not greatly improved.

The approach chosen to improve dimensional consistency of cores was to evaluate the steps of core manufacture and attempt to develop a more fundamental understanding of how process variations cause dimensional variations. Earlier internally funded work at Howmet had concentrated on developing techniques for producing filler with consistent surface area and particle size distribution. This work had also shown that considerable dimensional inconsistency was caused by process variations prior to core firing. Possible causes for core distortion include local variations in solids content, local variations in filler size distribution, surface area, or chemistry, and the relief of residual stresses during binder/carrier removal.

A special test core geometry was chosen for the study to avoid some of the practical problems associated with measuring production cores in laser or guillotine gauges and the statistical problems associated with analyzing dimensional yield data. The test core contains a series of measurement pads which define radial, chordal, pitch and combination dimensions in the die cavity and the cores. Each series of cores is compared to the ideal dimensions of the die, and a dynamic S/N is calculated which expresses the overall group deviation from this ideal. This single quality characteristic can be used in statistically designed experiments to evaluate the effects of process variable changes on dimensional consistency. As with other S/N characteristics, the results are expressed in decibels (dB), and an increase of three decibels is approximately a 50% reduction in variation.

The core material chosen for evaluation was an injection molded silica-base core with zircon as a major secondary phase. The initial experimentation was split into two phases: an internally funded effort to examine effects of binder chemistry and solids content and a follow-on effort to evaluate the effects of core injection parameters.

Initial, internally funded, evaluations showed strong correlation between dimensional consistency of the test core and the degree of separation between the filler and the binder which occurred in an internally developed rheology test. These preliminary tests which evaluated different binders, fillers and compound solids contents showed a decrease in dimensional consistency (dynamic signal-to-noise ratio, S/N) with increased separation between binder and filler. These results indicated that at some dimensional inconsistency may be due to separation of the binder and filler during injection, with resultant local variations in solids content or filler character.

After determining that local variations in as-injected (green) cores might be responsible for at least a portion of the dimensional inconsistency of fired cores, experiments were run to evaluate the effects of injection parameters on local variations in green cores and then on dimensional consistency. The experiment variables were chosen to affect local variations in solids content or filler character, as well as residual stresses. Solids content was measured in seven core locations and a nominal-the-best S/N for each injection condition was calculated as a measure of solids content uniformity.

An analysis of the initial D-optimal 19 run experiment (which was successfully confirmed) is shown in Figure 3-27. The most significant variable on each quality factor shown in bold type. Generally the injection speed just prior to die fill, the die and material temperature and the cycle time before removing the green core from the die had the greatest effects on measured quality factors. In contrast to initial expectations, the correlation between solids content uniformity and fired core dimensional consistency was very small (coefficient of -0.1). In addition, those conditions which increased dimensional consistency were exactly those which increased visual defect counts in fired cores.

Figure 3-27. Effects of Injection Parameter Variations on Core Quality Measures

Variable	Increased Dimensional Consistency	Increased Solids Uniformity	Reduced Visual Defects
Temperature	Cold		Hot
Acceleration			
Initial Speed		Slow	
Deceleration			
Final Speed	Fast	**Slow**	Slow
Pressure			
Dwell Time	Long	Short	**Short**

Additional experiments of the same design were performed with two additional batches of core compound: one that contained 1.5 volume % less solids loading than standard, and another that contained 1.0 volume % more solids than standard. These experiments were performed to determine if the dimensional and solids content consistency measures were sensitive to nominal solids content.

The results of the analysis of effects of injection conditions on these two materials are shown in Figure 3-28. In general, the materials responded similarly to variations in injection parameters, except for some increased sensitivity to parameter change for the low solids material. The correlation between

Figure 3-28. Effects of Injection Parameters with Different Compound Solids Levels

Variable	Increased Dimensional Consistency		Increased Solids Uniformity		Reduced Visual Defects	
	-1.5%	+1%	-1.5%	+1%	-1.5%	+1%
Temperature	Cold	Cold		Cold		
Acceleration	High					
Initial Speed		Slow	Slow			
Deceleration	Low			High		
Final Speed	Fast	Fast	**Slow**	**Slow**	Slow	
Pressure			Low			
Dwell Time	**Long**	**Long**	Short		**Short**	

dimensional consistency and solids uniformity was still very low, with correlation coefficients less than 0.2.

The lack of uniformity in solids content of the cores was driven by two areas of the core: the trailing edge core print which had higher than nominal solids and a convergent/divergent flow area (conical) between the root and the cooling passages that had lower than nominal solids (Figure 3-36 shows the results of a FEM that simulated these results). The bulk properties of fired cores (porosity and apparent density) of these two areas and two core areas that had nearly nominal solids loading in green cores were measured. Figure 3-29 compares average green core binder contents (100% minus solids) to the percent porosity in fired cores from the same four core sections. The extremely good correlation may explain the lack of dependence of fired core dimensional consistency on uniformity of solids in the green core. Excess or reduced binder in a

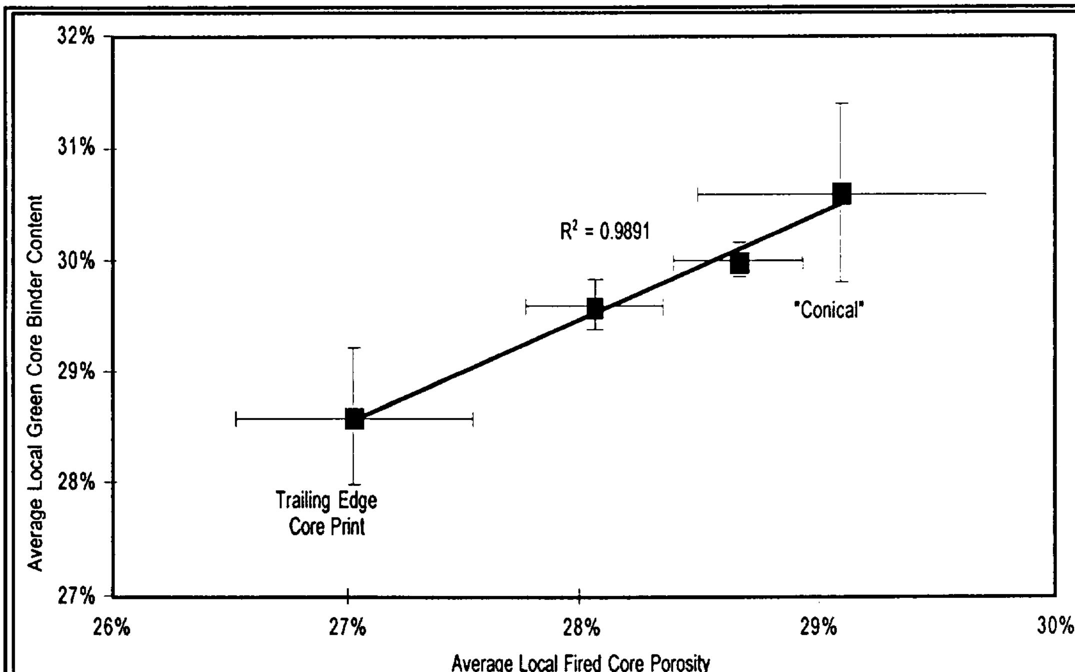

Figure 3-29. Relationship Between Local Measure of Green Core Binder Content and Fired Core Porosity

local area directly resulted in excess or reduced porosity in the fired core, which means that the amount of volume shrinkage must have been independent of green core solids loading. Thus varying solids content in the green cores did not result in differential shrinkage.

In addition to variations in local porosity of fired cores, local variations were noted in fired core apparent density (actual density of ceramic material). The average apparent density in the trailing edge core print (which had low porosity) was 1.5% lower than other areas of the core. This was most likely due to lower than nominal zircon levels, although they were not measured. Apparent density consistency was most strongly affected by material and die temperature, with cold temperature improving consistency. Slower speed and longer cycle times also improved consistency of apparent density.

The results of these experiments indicate first that there are significant effects of injection parameters on fired core dimensional consistency and second that these effects are not mainly due to variations in filler content in the green cores. Local variations in solids content and local chemistry were present, but did not correlate with the measure of dimensional consistency. The relative importance of cycle dwell time on dimensional consistency indicates that any modeling efforts should include not only the injection portion of the process, but also the pressure hold and solidification portion of the process.

3.2.2.2 Task 2.2 – Analysis of Core Injection Molding Defects (PCC). The PCC Airfoils approach under this task was to identify, study and minimize a number of core defects that are important to the core and investment casting manufacturing process. These include dimensional control (e.g., bow, twist, lift, etc.) of a core. In addition there are other factors such as core breakage, either on a large scale or very localized areas. This project selected dimensional control as the most significant problem. The general approach taken was to analyze each step of the core making process, optimize the parameters and evaluate the results by measuring critical dimensions in the cores and/or castings. The primary variables selected for study in the program were:

- Core injection compound mixing parameters and methods
- Injection of the Core into the Die (Injection timing, weight of the material injected, pressures during the injection process)
- Interactions of the above process variables

The first step in the PCC program effort was to run tests on the mixing of the core injection slurry raw materials. Parameters involved included temperature, time and speed. A series of runs were conducted to obtain parameters that produced a consistent product. Next, cores from four different mixing configurations were injected and processed under standard process conditions. These core samples were evaluated dimensionally at the end of core processing. The key dimensions are not the thickness of the

Figure 3-30. Dimensional Comparison of Two PCC Core Compound Types

FR 2198	Length		Length	
	921P	741	921P	741
Average	5.2748	5.2654	0.0491	0.0499
Standard Deviation	0.0012	0.0026	0.0002	0.0002
Maximum	5.2760	5.2700	0.0500	0.0500
Minimum	5.2720	5.2600	0.0490	0.0490

FR 4061	O/A Length		TE Length		T-Bar Length	
	921P	921	921P	921	921P	921
Average	3.266	3.263	2.573	2.568	0.074	0.073
Standard Deviation	0.001	0.001	0.002	0.004	0.000	0.000

97PD-033-002

core but distortions of the cores as measured in critical areas. Figure 3-30 presents the data for two core configurations with standard and optimized processing. The standard core materials are designated 741 or 921 and the optimized material is listed as 921P. These were characterized by the size of the core. On configuration FR 2198 the overall length varied by 0.010 inch with the standard material and only 0.004 inch with the improved material. On the smaller physical dimension of T-bar pitch (thickness) there was no measurable difference between the two materials. This is fairly typical of core behavior. On the second part (FR 4061), there was negligible difference in overall length and T-bar pitch. However the trailing edge (TE) length had a smaller standard deviation of 0.002 inch for the 921P material as compared to 0.004 inch for the baseline 921 material.

The other key dimensional characterization is not the size of the core, but the shape of the core. This is a more complex measurement that is sensitive to how the core is positioned for measurement. In order to get a comparison, the cores were measured in either a laser gage or the older block type gage. Typical distortions measured by this method are bow, twist and trailing edge lift. The results are tabulated as yield (i.e., the number of parts which are acceptable). In all cases the improved mix (921P) was equal to or better than the standard materials.

In a second set of experiments, the mixing parameters were optimized for a SiO_2 based core system. Again, the parameters included timing temperature and energy input. The evaluation criteria was both visual yield and gage yield. Visual yield detects surface imperfections while gage yield is sensitive to

Figure 3-31. Gage Yield Comparison by PCC Part Number and Mix Type

FR 2198	Mix Type	Gage Type	Gage Yield
4061	921 921P	Laser Laser	97% 98%
9177	741 921P	Laser Laser	84% 85%
2198	741 921P	Block Block	96% 97%
1229	921P	Laser	100%
1229	741 921P	Block Block	96% 96%
1229	921 921P	Block Block	67% 76%

97PD-033-003

distortions. Figure 3-31 shows the results for the second optimization on a traditionally difficult core configuration. For both criteria, there were improvements in the yields.

Figure 3-32. Typical Process Yields with Different Controls on Injection Cycle

Cycle	Yield
1	85%
2	56%
3	76%

97PD-033-004

The next step of the process to be experimentally studied is the injection of the core material into the die. Process parameters selected were concerned with the timing of the injection cycle for a difficult part (FR 1166C17). The yield results are shown in Figure 3-32. Cycle 1 was optimized for final core yield with 85% of the product acceptable. Cycle 2 was deliberately run outside of acceptable limits resulting in a low yield of 56%. Cycle 3 was the baseline process with a 76% yield. These data show the importance of accurately controlling the injection cycle in order to improve the quality of the final product.

The effect of optimized 921P composition and injection parameters on core yield compared to the standard core is given:

Contour Yield on High Pressure Blade	
Standard Core	65.0% First Time
	80.0% with Refire
921P	99.7% First Time

This shows a significant improvement in core quality to the foundry.

3.2.2.3 Task 2.3 – Core Injection Molding Model Development (UES). This task was focused on developing numerical methods and models that will be useful for aiding the design and evaluation of core injection molding dies and tooling, and the "virtual" development of acceptable core injection molding processes. The approach was to use single-phase, non-Newtonian, incompressible Navier-Stokes flow modeling to capture the bulk macro fluid flow behavior during the core injection molding process. The macro model results compared favorably to qualitative macro events present during core injection (fill times, fill shapes, solidification times, etc.).

An attempt was made to correlate the particle density variation data of experimentally formed cores with measurable quantities in the numerical models, such as, shear rate history, velocity history and geometrical features. This "micromodeling" effort used a CT derived density database on several different core body shapes. No significant correlation was obtained with measurable quantities in the numerical models and the experimental density data. In order to accurately predict particle segregation effects (agglomeration, inertial packing, etc.) in injection molded cores it will be necessary to adopt a multiphase flow solution method. An efficient algorithm for this multiphase flow calculation has been formulated and could be incorporated in ProCast.

Core injection molding modeling development thermophysical databases and geometries were provided by Howmet in support of the UES Task 2.3 modeling efforts: 1) The Howmet selected core injection slurry material was experimentally tested by FMI in order to determine its temperature dependent thermal conductivity and specific heat. 2) Howmet made Differential Scanning Calorimetry (DSC) measurements of the core injection material as well as measurements of compound thermal expansion and Non-Newtonian viscosity as a function of temperature and shear rate. 3) A core geometry was chosen for the Task 2.3 modeling efforts which was also used for Task 2.1, Task 2.5 and Task 2.6 dimensional study efforts.

The simplified finite element model for the Process Improvement Team (PIT) core model is shown in Figure 3-33. The model was simplified by eliminating some of the smaller features found in the actual core from the FE model geometry. The simplification is justified because the smaller features have a negligible effect on the bulk fluid behavior, and the inclusion of such small features would create a finite element mesh with too many elements. 4) A core die was also produced with Howmet internal funds that contains two simplified features for model verification. The core die contains a zigzag arrangement to amplify inertial separation of the filler from the binder and a second feature with convergent/divergent flow to evaluate the effects that flow pattern will have on filler/binder distribution. 5) Initial injection trials were made with the simplified geometry die to provide thermocouple and flow data to help verify the process models.

A core injection molding machine at Howmet was studied in action and important process parameters were quantified. Howmet supplied core injection molding process information (velocities, pressures, temperatures, etc.) in support of UES and HC core injection molding modeling efforts.

A parameter estimation program was written at UES to determine the input data required for the non-Newtonian flow model in ProCast, based upon the experimental viscosity results at different temperatures and shear rates. The C program source code and a technical description of the program were delivered to Howmet.

A CAD model of the generic core to be studied was received from Howmet. A finite element tetrahedral mesh of the part was created with MeshCast (see Figure 3-33). However, since the original

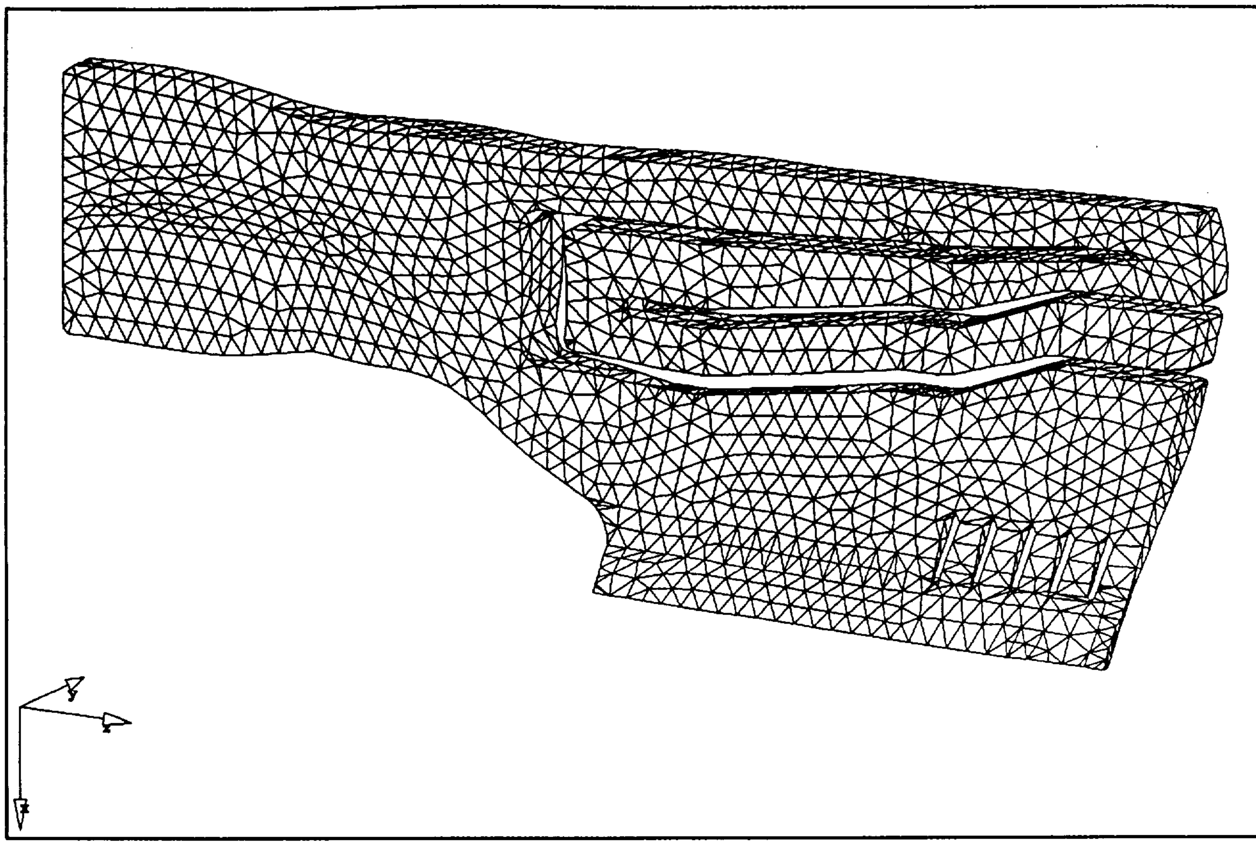

Figure 3-33. Generic PIT Turbine Blade Core Finite Element Mesh

CAD part file did not include the gating and die, additional effort was required to complete the injection molding model. The core geometry was rebuilt and meshed at Howmet as part of a subcontract from UES. The ProCast analysis files were set up and run to acquire results for core injection molding conditions.

Figure 3-34 shows the temperature contours on the PIT blade model during the baseline core injection process. While this figure displays results during the filling sequence, some of the gating and thinner sections near the core trailing edge are starting to solidify. Figure 3-35 displays the non-Newtonian shear rate fringe plot at the same time in the fill sequence as the temperature contour plot shown previously. The shear rate value is reflective of the velocity gradients present in the flow field. High values are seen where the flow is accelerating, decelerating and rapidly changing directions. Figure 3-36 depicts the fraction solid contours of the injected core while the part is solidifying after completion of the core injection cycle. Information such as this can be used to locate porosity formation in injected molded cores. Porosity initially will be assumed to be a last-to-freeze type defect, analogous to macro porosity formation in solidifying metals.

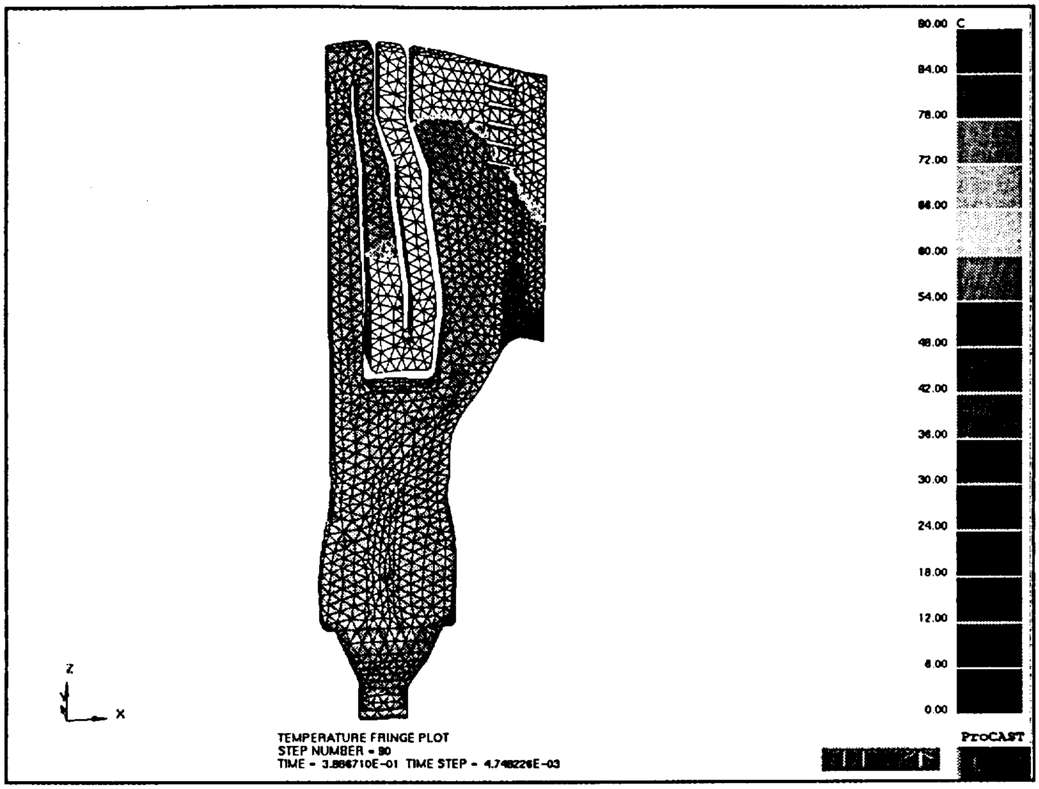

Figure 3-34. PIT Core Temperature Contours During Filling

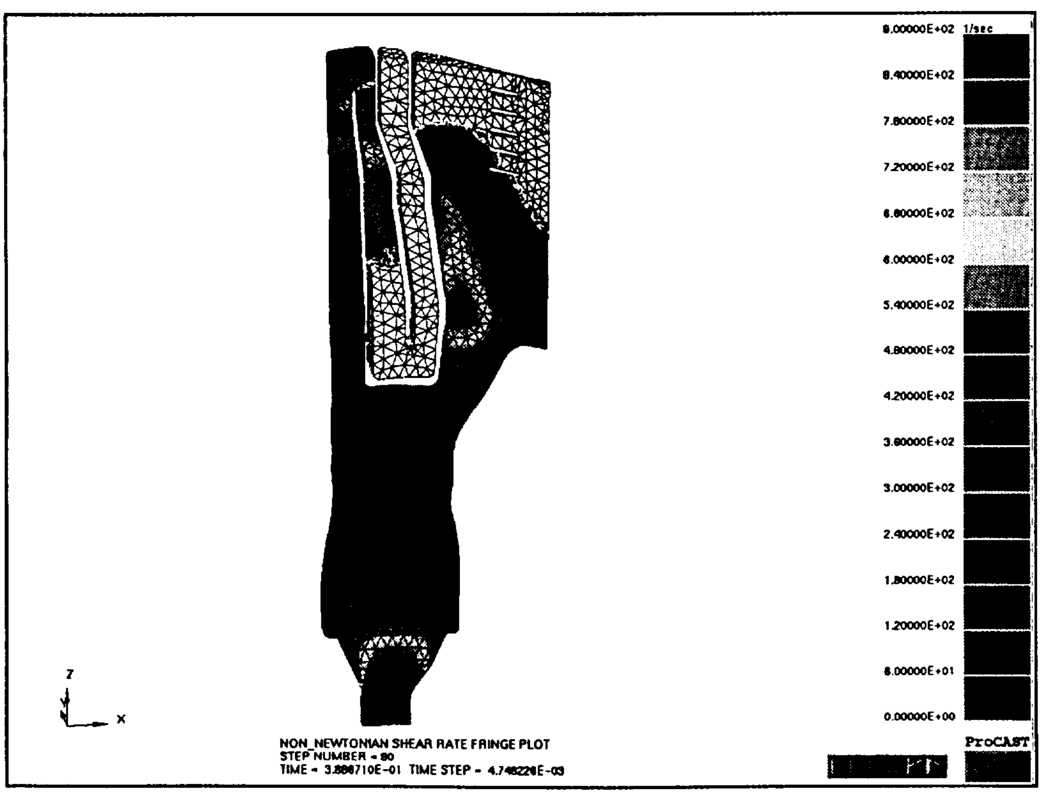

Figure 3-35. PIT Core Shear Rate Contours During Filling

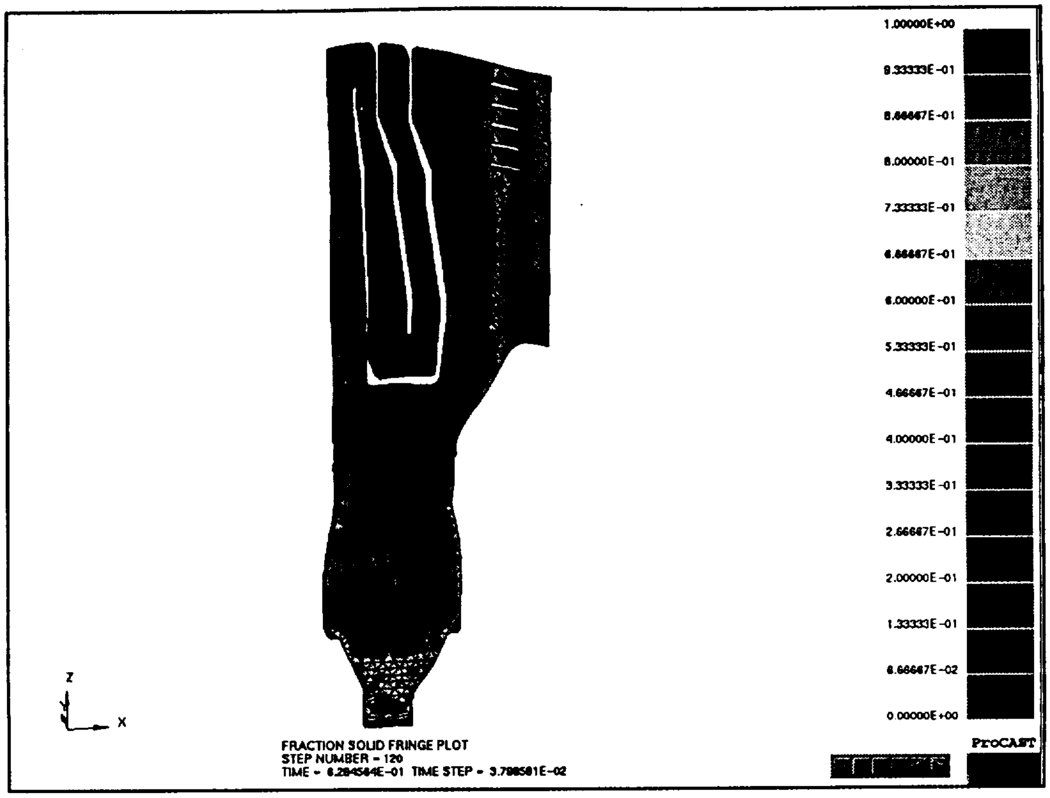

Figure 3-36. PIT Core Fraction Solid Contours Just After Filling

The simplified venturi and zigzag die model has also been meshed from the Unigraphics CAD file provided by Howmet. The finite element mesh for the die containing the venturi and zigzag components is shown in Figure 3-37. This was the geometry primarily used for the micro density variation correlation efforts.

An attempt was made to correlate the particle density variation data of the experimentally formed zigzag cores with measurable quantities in the numerical models, such as, shear rate history, velocity history and geometrical features. This "micro modeling" effort used a CT derived density database in an effort to find correlation between the flowfield properties and the particle distributions. No significant correlation was obtained with measurable quantities in the numerical models and the experimental density data. In order to accurately predict particle segregation effects (agglomeration, inertial packing, etc.) in injection molded cores it will therefore be necessary to adopt a multiphase flow solution method.

A literature review of colloidal suspensions was undertaken to determine the state-of-the-art in multiphase particle flow modeling. Injection molding, particle packing, and particle fluidization literature was reviewed. The literature suggest that segregation is due to differences in particle size, shape, and density. An injected wax/ceramic slurry will probably segregate due to bridging and agglomeration

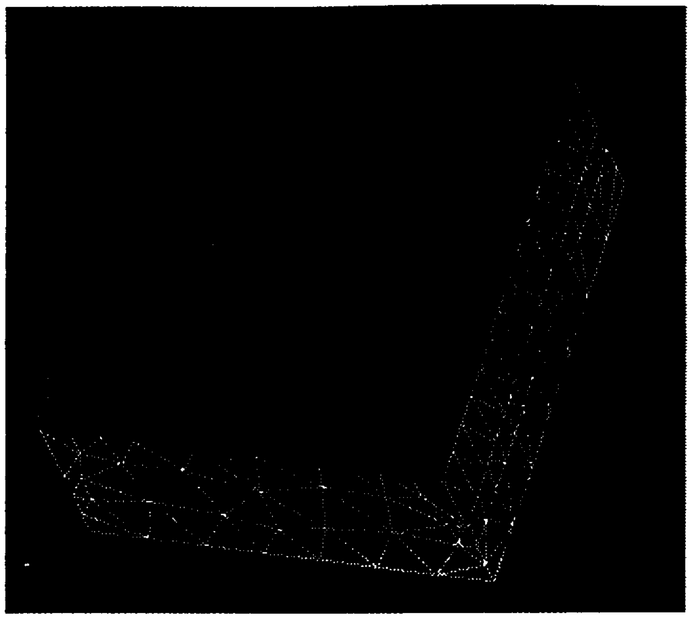

Figure 3-37. Zigzag and Expansion Die Finite Element Mesh

patterns in tight places in the airfoil core geometry. A numerical multiphase model was reviewed which can more completely model the effects of particle size, shape, and density. The details and solution algorithm of the proposed multiphase flow model are shown in Appendix A.

3.2.2.4 Task 2.4 – Sintering Model Development (Auburn). The objective of this research was to characterize the densification and deformation of sintered core materials from Howmet Corporation. In the first year of this project, a reliable experimental facility was developed and tests on core materials from Howmet Corporation were initiated. In the second phase, a detailed study of the sintering behavior of the Howmet core materials was performed. Particular attention was devoted to understanding the influences of particle size variation, wax carrier mixes, and injection molding pressures.

In order to in-situ measure the diameter changes of the sintering sample, a special high temperature dilatometer was designed. Instead of using traditional contact dilatometry measurement, this device utilized a laser micrometer to remotely measure the dimensional changes of the coupons without contact to avoid any enhanced deformations due to contact pressures. The laser micrometer has a resolution of 0.0005 mm and can record diameter changes of samples in real time during sintering in the small-bore furnace. A furnace atmosphere control device was also fabricated for modifying humidity, maintaining inert atmospheres and simulating the environment in gas-fired kilns. A programmable temperature controller was utilized to ensure that the desired thermal cycles were obtained. In addition, a computer data acquisition system was developed to concurrently record the temperature from a thermocouple adjacent to the sintering sample as well as the dimensional data from the laser micrometer. A schematic of the system is shown in Figure 3-38.

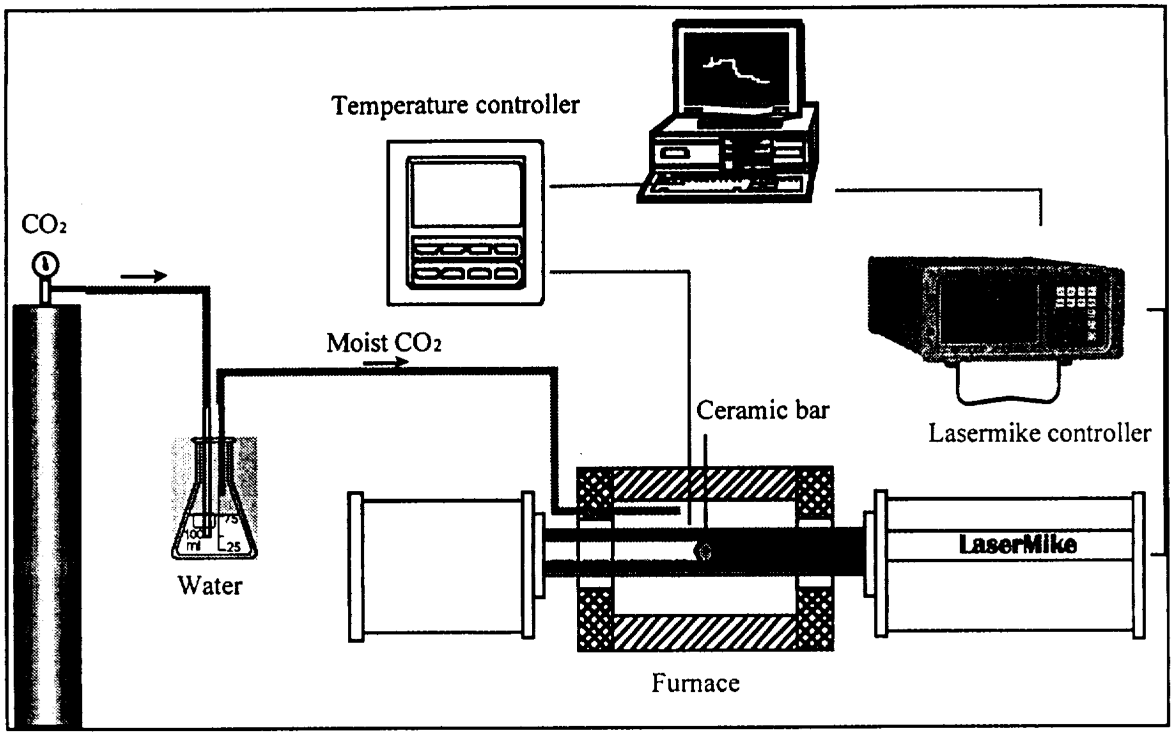

Figure 3-38. Auburn Sintering Furnace and Experimental Setup Schematic

Auburn University and Howmet Corporation jointly designed an experimental protocol to study dimensional changes during sintering of injection molded silica aggregates. Howmet utilized existing tooling to produce green cores from a range of particles sizes, carrier mixes, and injection pressures. Auburn University was provided with information and materials necessary to simulate normal production binder removal and core firing processes.

Howmet Corporation provided two groups of core samples to Auburn University for investigation. In the first group, samples were produced with two distinctly different injection pressures referred to in this report as simply "high" and "low". In the second group, in addition to the injection pressure differences, samples were injection molded with different solid carrier loading which is referred to in this report as simply "high" and "low" solid loads. It should be mentioned that in this report the absolute values of the injection pressures, carrier mixes, sintering temperatures, sintering times, and thermal expansion (contraction) coefficients obtained are not shown on any of the results to protect the intrinsic proprietary nature of these data. All samples received from Howmet Corporation were "debinded" from their carrier materials at Auburn University using the standard Howmet Corporation technique. Then, the coupons were sintered at various temperatures (referred relative to the standard temperature T_0) and times (referred relative to standard sintering time t_0).

Investigations on the temperature and time effects on the sintering behavior were conducted on the first group of samples. Figure 3-39 shows a summary of the results of shrinkage of the first group of core samples relative to various sintering temperatures. The results show that there is a critical sintering temperature at about 40°C below the standard sintering temperature T_0. Sintering processes conducted below this temperature result in almost zero size changes. This indicates that the sintering reaction will not occur at temperatures below the critical temperature and the samples will not sinter to full density to provide mechanical properties required in reasonable amounts of time. The data also suggests that the sintering response was significantly more uncertain for the coupons molded using low injection pressures.

Figure 3-40 shows the results of shrinkage of the same group of samples sintered at various temperatures with three times of the standard sintering time. The results show that with longer sintering time, the critical sintering temperature was relatively lower than that with the standard sintering time. However, extension of sintering time has very limited influence on the percentage of shrinkage of samples processed at the standard sintering temperature. Furthermore, at higher sintering temperatures, the sintering behavior shows little difference between samples molded with high or low injection pressures.

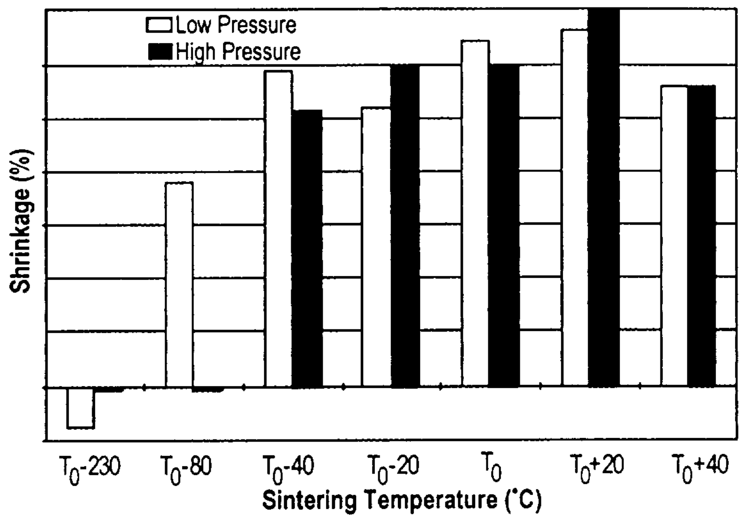

Figure 3-39. Core Sample Shrinkage Relative to Sintering Temperature with Time t_0

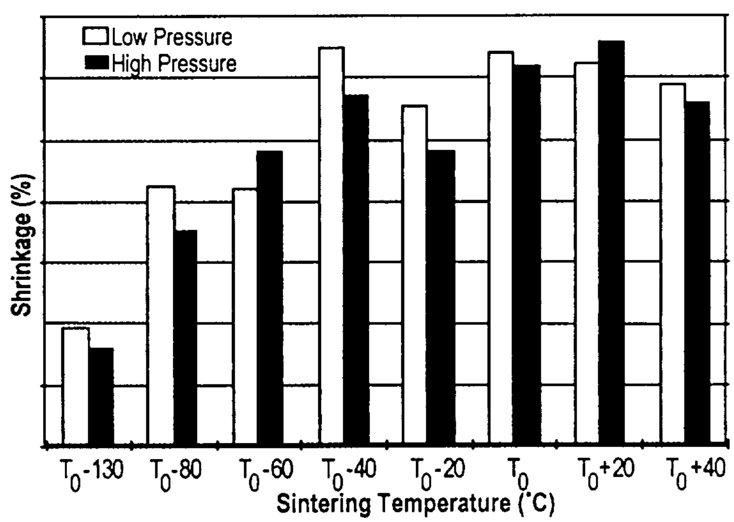

Figure 3-40. Core Sample Shrinkage Relative to Sintering Temperature with Time $3t_0$

The purpose of tests on the second group of samples was to determine the atmospheric effect on core sintering. Sintering experiments were conducted in an air environment and moisturized CO_2 atmosphere which simulates the environment of factory gas-fired kilns. The summarized results are shown in Figure 3-41. In the chart LSLP represents low solid/low injection pressure samples, LSHP represents low solid/high pressure samples, HSLP represents high solid/low pressure samples

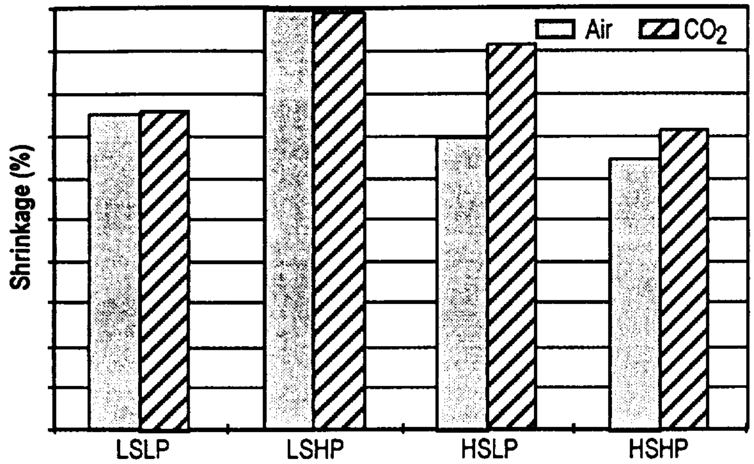

Figure 3-41. Summary Chart of Sample Shrinkage in Air and Moist CO_2

and HSHP represents high solid/high pressure samples. The results show that moisturized CO_2 atmosphere has a tendency to increase the rate of sintering. This tendency is more visible in LSHP and HSLP samples than LSLP and HSHP samples. LSHP samples has the highest sintering rate while HSHP samples the lowest. There is also a tendency that higher solids content and injection pressures decrease the rate of sintering. However, for low injection pressure samples, the difference of sintering behavior between high and low solid contents appears to be less significant.

Samples after sintering were sent back to Howmet Corporation for microstructure analysis. The result shows that samples sintered in an air environment produced 53 to 95% of the standard cristobalite content of the sample fired in gas-fired kilns with the typical sintering process utilized at Howmet Corporation. However, samples sintered in a moist CO_2 atmosphere produced 147 to 163% of the standard cristobalite content. This indicates that moist CO_2 atmosphere has a strong tendency to increase the rate of sintering.

Tests were also conducted on identical samples with the same solid load mixture and injection pressure to determine the systematic errors and uncertainties of the data. The result shows an uncertainty of about 6% with the sample group of four. This indicates the experimental error was an acceptable level.

In summary, the current sintering process practiced by Howmet Corporation is a well chosen process to obtain optimum results in a minimum time. However, the results produced by this investigation indicate that temperature uniformity in sintering furnaces should be minimal to produce a uniform sintering response. In addition, the chemistry of the sintering furnace atmosphere should be closely controlled and monitored.

3.2.2.5 Task 2.5 – 2.5D X-Ray Measurement Software (GE). The approach for this task was to develop a geometric representation, a data exchange standard, and tools to compute structural deformations in casting in order to track dimensional control information between casting process steps. Experiments were aimed at finding and quantifying core shifts in the PIT part using the developed software tools.

Discussions with investment casting experts reveal that only a limited variety of deformations occur commonly, despite a proliferation of terminology. These common deformations are not arbitrarily complex, but rather each can be characterized by a small number of simple, intuitive parameters such as: rigid body transformation, uniform or orthogonal scaling, twist and unwrapping, bend and shell bulging; versus: core-shift and sag.

The approach taken by GE in this task was to identify this extensive repertoire of these simple deformations, called deformation modes, and to model a part's overall deformation by a series of consecutive applications of deformation modes. Each mode is controlled by parameters whose values are estimated from measurements of features on the part. GE defined this deformation modeling scheme and an initial repertoire of deformation modes, in precise mathematical terms.

Deformation modes are classified as core defects, which affect only a part's interior surfaces, and part-body defects, which may affect both exterior and interior surfaces.

Core defects include:

- Rigid-body displacement of the core with respect to the overall part
- Rigid-body displacement of one section of the core with respect to the overall core.

Each rigid-body displacement is characterized by six parameters: three for rotation and three for translation. The remaining deformation modes summarized below are each parameterized in a similar fashion.

Part-body defects include:

- Rigid-body displacement of a section of the part with respect to the overall part
- Shrinkage or expansion of a part section, either uniformly in all directions or by differing amounts along each of three principle axes
- Twist of a part section, defined as rotation about some axis with the degree of rotation varying (uniformly or otherwise) with position along the axis
- Unwrapping of a part section, defined similarly to twist but allowing portions of the part to rotate in opposite directions
- Bending of a section of the part, defined as shift of the part in a direction perpendicular to some axis, by an amount that varies (uniformly or otherwise) with position along that axis
- Shell bulging, defined as a displacement of a local region of surface, in a direction normal to the surface, by an amount characterized by a functional form such as a Gaussian.

Deformation of a typical turbine airfoil part would be described by a combination of several modes; these would include for example: twist, unwrapping, and bending deformations defined with respect to the part's stacking axis, plus displacement of core sections and shrinkage.

To validate and demonstrate the deformation modeling scheme, GE developed software tools for specifying deformation models, for computing deformation parameters from X-Ray and CMM data, and for visualizing and analyzing deformations.

Experiments were performed using PIT data from ARACOR and Howmet to measure core shifts. From X-Ray images, lines and point features on the core are reconstructed in 3D using the epipolar constraints and the push-broom camera geometry. Deformation parameters are then solved from least-square-error fitting of 3D line and point features, on the CAD model and on the PIT part image. The PIT part is held in a fixture with tooling balls to provide in-situ calibration of the outside surface with the CAD reference frame.

A file format for representing deformation models and their parameters was developed in consultation with AITP consortium members. This format, based on DEX and STEP, is intended to serve as a basis for an industry-wide data exchange standard that will facilitate communication about casting deformations.

A suite of C++ tools: DefSolve, DefApply, PartDiff, and an accompanying software guide (Appendix B) were developed to solve for a deformation mode from 3D point and line features and correspondences; to apply deformation to CAD model points and lines; and then compute and visualize the differences between the CAD model and the actual casting. These tools have been made available to consortium members. A flow chart depicting the dataflow and the use of the developed software tools is shown in Figure 3-42.

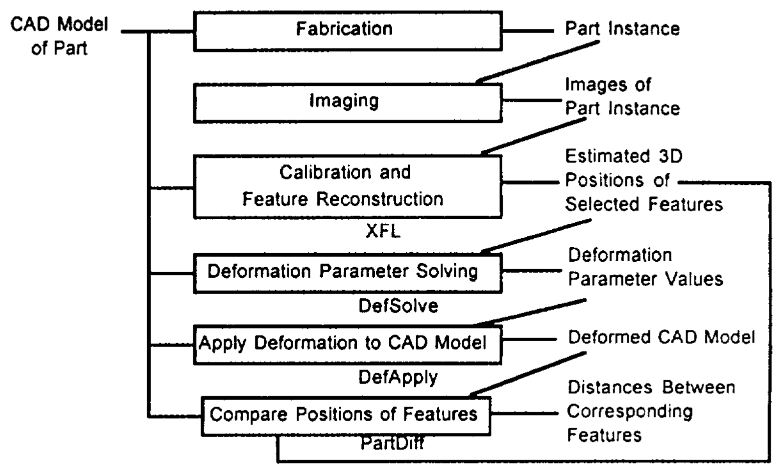

Figure 3-42. Recovery and Application of Deformation Parameters

Today, the 2.5D X-Ray Hole and Feature Layout systems are being used regularly on the shop floor at GE Aircraft Engines in Madisonville, Albuquerque, and Evendale, saving millions of dollar every year, and reducing design and manufacturing cycle times from weeks to hours. From this success and partnership in the NASA AITP, GE Corporate Research and Development is now working with ARACOR and Howmet on ARPA and DOE funded projects to measure shape deformation and wall thickness on larger and more difficult castings. There are plans to speed up the system by a factor of 20x, increase accuracy by a factor of 10X, and especially to use low curvature occluding surfaces in solving for core shifts and higher degree deformations. The current system is limited by the detectability, accuracy, number, and location of the high curvature features such as the corners and thin strips on the PIT part.

3.2.2.6 Task 2.6 – 2.5D X-Ray Measurement Hardware (ARACOR/Howmet). Howmet interfaced with GE and ARACOR on this task for the development and verification issues associated with the 2.5D X-Ray method. Howmet developed and supplied the nominal Unigraphics CAD solid model of the PIT blade to GE, and completed a CMM data base on 24 PIT castings to aid development of the deformation model.

Howmet, GE and ARACOR worked together to design and ARACOR fabricated a X-Ray transparent fixture capable of holding the PIT blade in the proper part coordinate system for scanning at the ARACOR ARNIS facility.

ARACOR was under subcontract to Howmet to provide 2.5D-CT scan services for the AITP program. Early in Year 1, a Test Plan Document was developed. According to this plan, ARACOR would scan a maximum of twenty parts.

The Sacramento-based ARACOR ARNIS CT/DR testbed produced exceptional images. The measured resolution was about 3 lp/mm (pixels/millimeter). This level of performance represented another important radiographic milestone – the development of a high-resolution high-energy scanner. Both CT and DR images were successfully acquired. Test images were successfully sent electronically to GE.

The part selected by Howmet for study was referred to as the Process Improvement Team (PIT) part. The fixture for the PIT is a six-point nest designed and fabricated by ARACOR with help from GE and Howmet. It accommodated both the wax and metal PIT parts. The fixture also incorporated tooling-ball fiducials needed by the 2.5D-CT algorithm. Figure 3-43 shows a radiographic image of a PIT blade being held in the ARACOR fixture. The core passage details and the tooling balls are evident in the image. ARACOR radiographed all of the Howmet supplied parts at the 2.5D-CT testbed facility after coordination with GE for obtaining the necessary image angles necessary for 2.5D reconstruction.

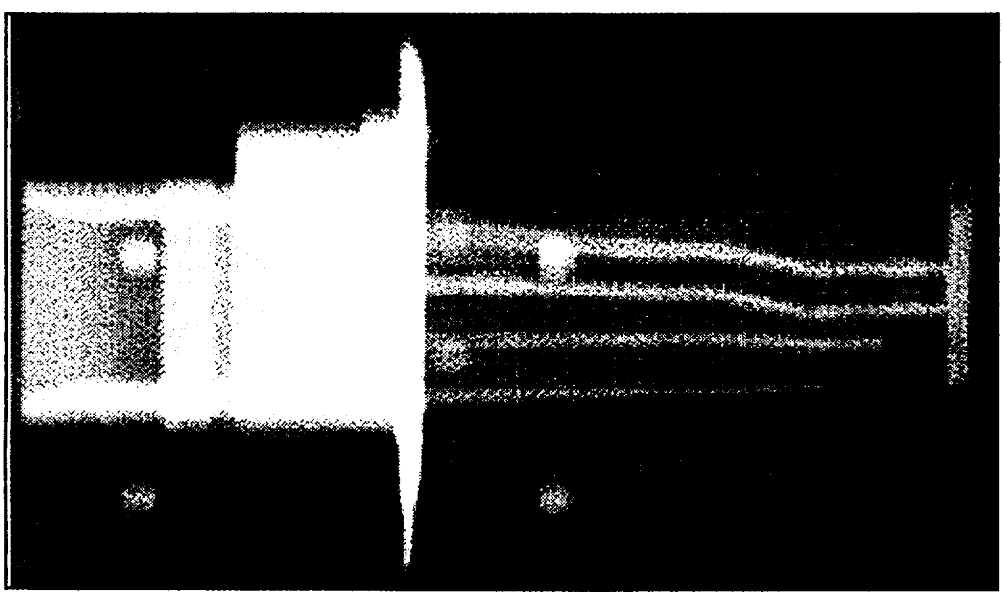

Figure 3-43. PIT Blade Radiographic Image Showing Core Passage Details

3.3 TASK 3.0 – RAPID, NEAR-NET SHAPE CASTING

3.3.1 Introduction and Summary

The overall objective of this task was to apply advanced technologies for the rapid fabrication of low-cost, high-quality aerospace grade castings.

Various innovative technologies were integrated into a process referred to as Rapid, Near-Net Shape Casting and demonstrated as a low cost manufacturing approach for producing components (Figure 3-44). Labor intensive, conventionally fabricated parts were converted into cost effective, single piece investment castings in a shortened development cycle. Following redesign, advanced casting simulation software was used to analyze the simultaneous mold fill and solidification of the components. Casting process parameters (e.g., design of the riser, runner and gating system, prediction of the chill, insulator and vent locations, pouring speed and temperature, etc.) were analyzed, varied, and optimized before a significant nonrecurring expenditure was made at the foundry.

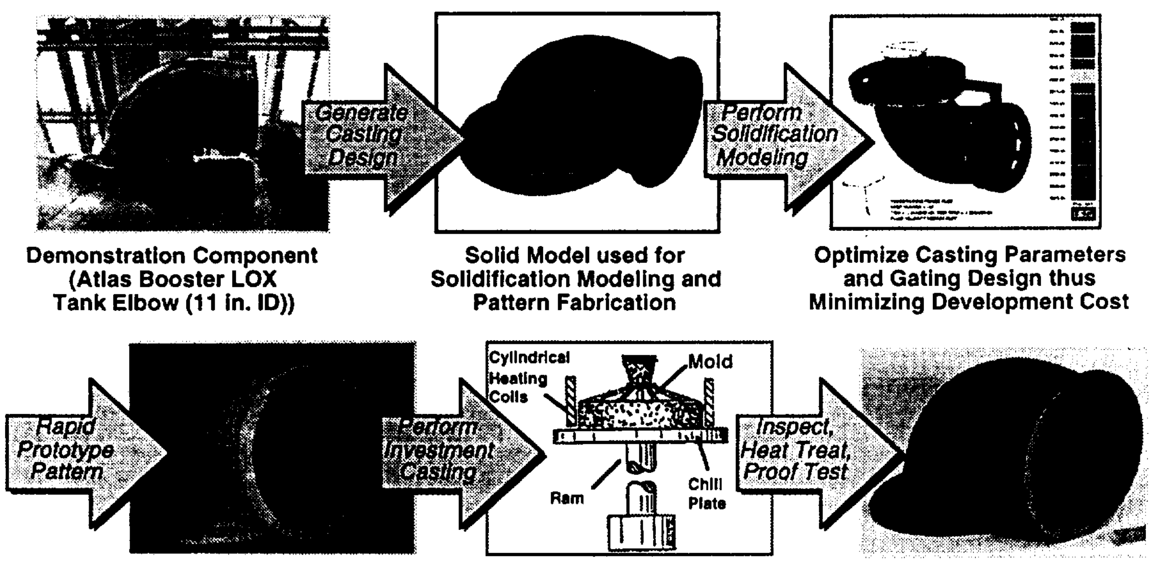

Figure 3-44. Low Cost Manufacturing Approach Via the Rapid, Near-Net Shape Casting Process

It should be noted that two approaches were used to generate CAD files:

1) CAD files were created by using computed tomography (CT) to reverse engineer a part
2) CAD files were generated by conventional design.

Next, investment casting patterns were fabricated via rapid prototyping. Rapid prototyping (e.g., Stereolithography, Selective Laser Sintering, Laminated Object Manufacturing, etc.) has revolutionized pattern fabrication in that three-dimensional CAD data is converted directly into a solid, physical model, which is then either used as a consumable heat disposable pattern or as master pattern for fabrication of "soft tooling" for producing wax patterns. Following the attachment of gating to the pattern and investment of the shell material around the gated pattern, the investment shell is put into an autoclave to burnout the gated pattern, thus creating the subsequent casting mold.

Two different casting processes were used for production of demonstration components; 1) the static or conventional investment casting process, and 2) the Thermally Controlled Solidification (TCS) process. Both processes allow the means of producing highly complex metallic structures, offering the engineer almost unlimited design freedom. The recently developed TCS process allows the controlled advancement of the solidification front in the mold minimizing the occurrence of casting defects (e.g., cold shuts, shrinkage porosity, etc.) that result from premature solidification thin-walled sections. Thus, the TCS process permits the casting of ultra thin-walled, light weight structures not readily produced with the conventional investment casting process.

Rocketdyne also investigated SLS to produce metal dies and components directly. The objective of this effort was to evaluate the feasibility of using rapid prototyping as a means of forming a green part which could be subsequently sintered to high density and near-net shape. Figure 3-45 shows an overview of the fabrication process: Metallic powders are blended with a plastic binder; the binder is fused together during the SLS process, and then the binder is removed. The green part is then sintered to a near-net shape.

SLS of metals was demonstrated to be a potential method to form parts and dies, but much work is still needed to refine the process as a viable production tool.

3.3.2 Procedures and Results

3.3.2.1 CT Scan of Rocket Engine Parts (Rocketdyne). The objective of this task was to develop the methodology to reverse engineer a rocket component. The overall approach to reverse engineer a part using CT is shown in Figure 3-46. The following steps were followed to reverse engineer a component:

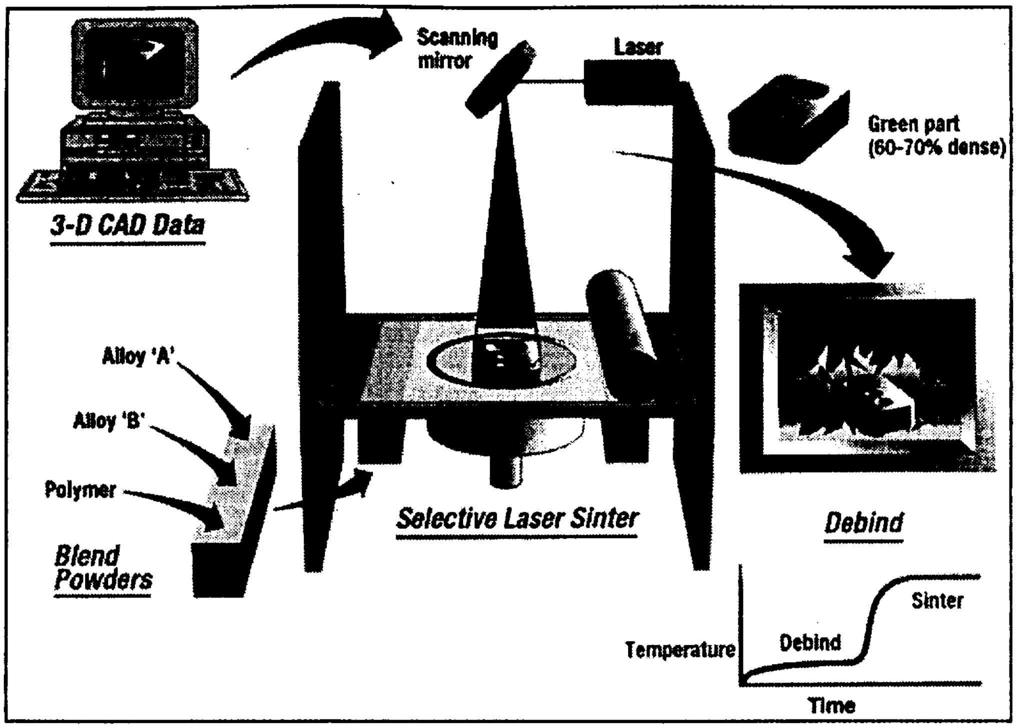

Figure 3-45. Selective Laser Sintering (SLS) Process

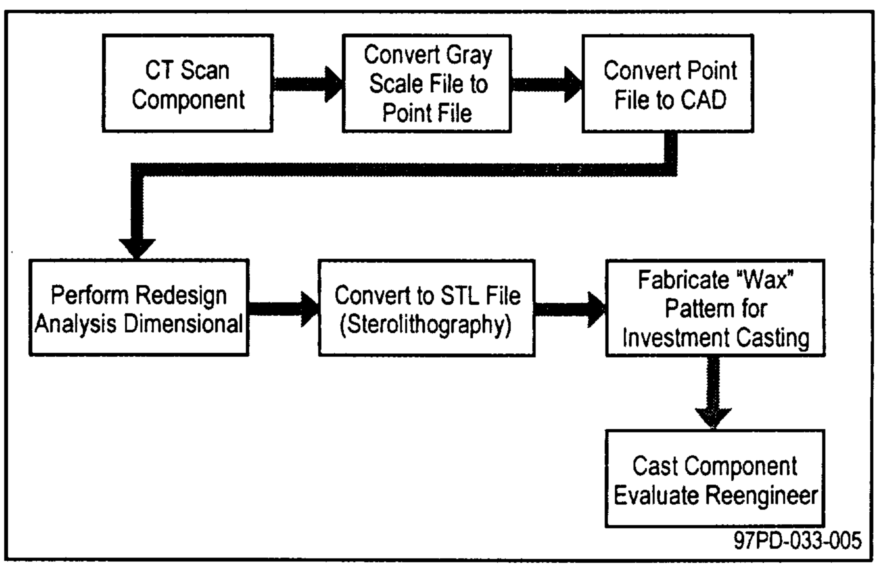

Figure 3-46. Approach to Reverse Engineer a Component Using CT

Selection criteria were established for downselecting an existing rocket engine component which is normally fabricated from a machined and welded assembly; an electronic file was generated by using CT to scan the existing part; software was applied to produce an IGES file from the scan data. The electronic file was converted into an engineering CAD database which allows for reengineering of the part into a "castable" design. Once the castable design was developed, then an STL file was generated and rapid prototyping patterns produced.

Criteria were established by which a machined, welded and fabricated component from a rocket engine would be selected for fabrication by reverse engineering. The selection criteria included hardware availability, future Rocketdyne applications, cost savings potential, complexity, and redesign performance. Component selection was performed by evaluating recommendations from key Rocketdyne programs to these criteria. Using the selected component, a CT image database was generated and translated into an IGES file which was, in turn, used to generate a CAD file.

Project team leaders from several programs, such as, the Expendable Launch Vehicle (ELV) and Evolutionary Expendable Launch Vehicle (EELV) teams were surveyed. A candidate engine component was downselected using the selection criteria on Figure 3-47. A gas generator housing was chosen over the other candidates. Figures 3-48a and 3-48b shows a copy of the drawing as well as a photo of the hardware. The component selected consisted of approximately thirteen details. Manufacturing operations ranged from drop hammer die forging, to machining and welding, for each detail. This process was labor intensive and required multiple "form to fit" operations that resulted in hardware variability and high costs.

CRITERIA / CANDIDATE COMPONENTS	Availability	Future Application Potential	Cost Savings Potential	Complexity	Performance
NK 33 Injector	○	●	●	●	◉
J-2 S Injector	○	●	●	●	◉
MK 3H Impeller	●	●	○	○	●
MK 3H Inducer	●	●	◉	◉	◉
GG Duct / Elbow	●	●	●	◉	●
MK 3H Turbine Manifold / Nozzle	●	●	●	●	◉
RS27 Combustor	●	●	●	●	●

● High ◉ Medium ○ Low

Figure 3-47. Selection Criteria Used to Evaluate Candidate Hardware

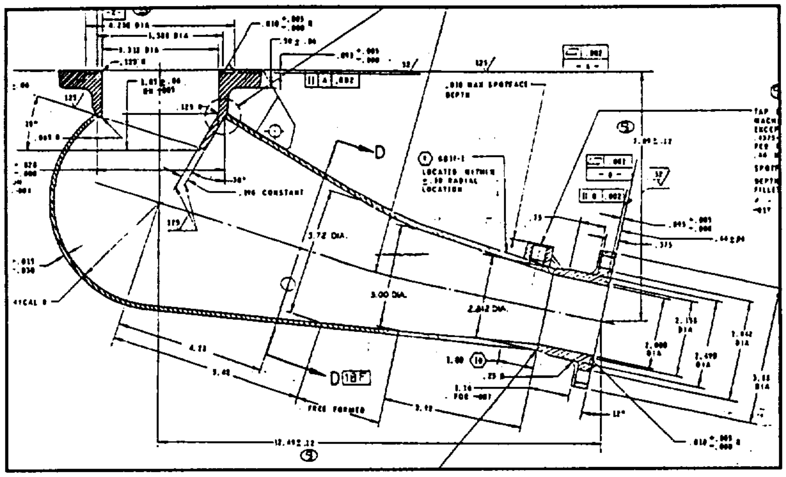

Figure 3-48a. Gas Generator Housing Design

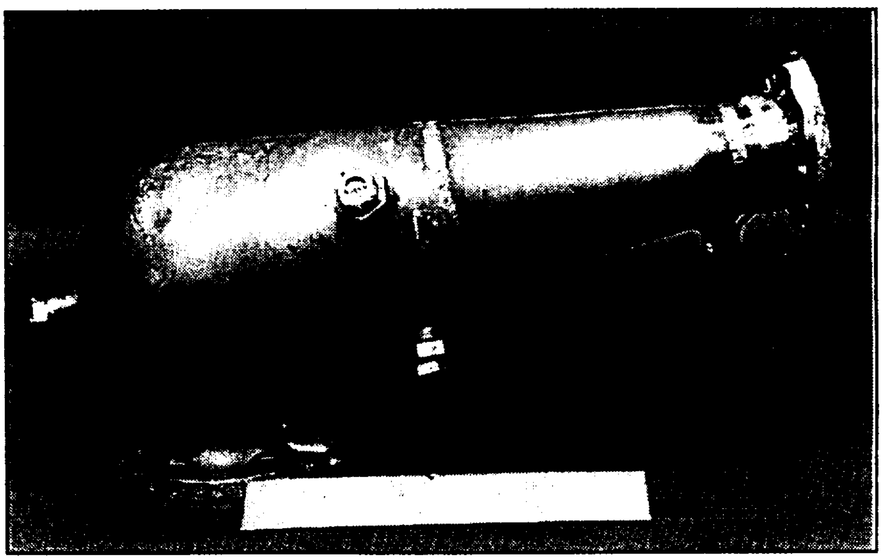

Figure 3-48b. Gas Generator Housing

After selecting the gas generator housing, an existing part was removed from a test engine and delivered to the CT Lab at Rocketdyne's Santa Susana Field labs. The component was CT scanned using the SMS (2.5 MEV) machine at 0.005 inch increments. The scanned images were then converted into a point data file that was ready to be translated into a CAD format.

Prior to translating the point data file, it was necessary to chose a conversion software package. A detailed review of software packages was performed to evaluate ease of translation and file manipulation. Software system evaluation criteria were established to evaluate and rate software manufacturers. The following criteria were considered during reverse engineering software system evaluation:

- Interface between the SMS CT equipment, located at Rocketdyne's Santa Susana Field Lab, and the reverse engineering system

- Functionality of the reverse engineering system
- Interface between reverse engineering system and popular CAD systems, such as, CATIA, Pro-E, UG, etc.

Based on these criteria, Imageware's Surfacer software was chosen for performing the conversion.

The collection of data from the CT scan consisted of over 400 files, approximately 36 megabytes of memory; it was prepared for file conversion using Imageware's file conversion software. It took Imageware personnel about 20 hours to create a surface model based on the given data. An IGES file was created from Surfacer; then, it was successfully read into CATIA, STL, and Pro-E to create various CAD model formats. Figure 3-49 shows a Pro-E CAD image of the reverse engineered part.

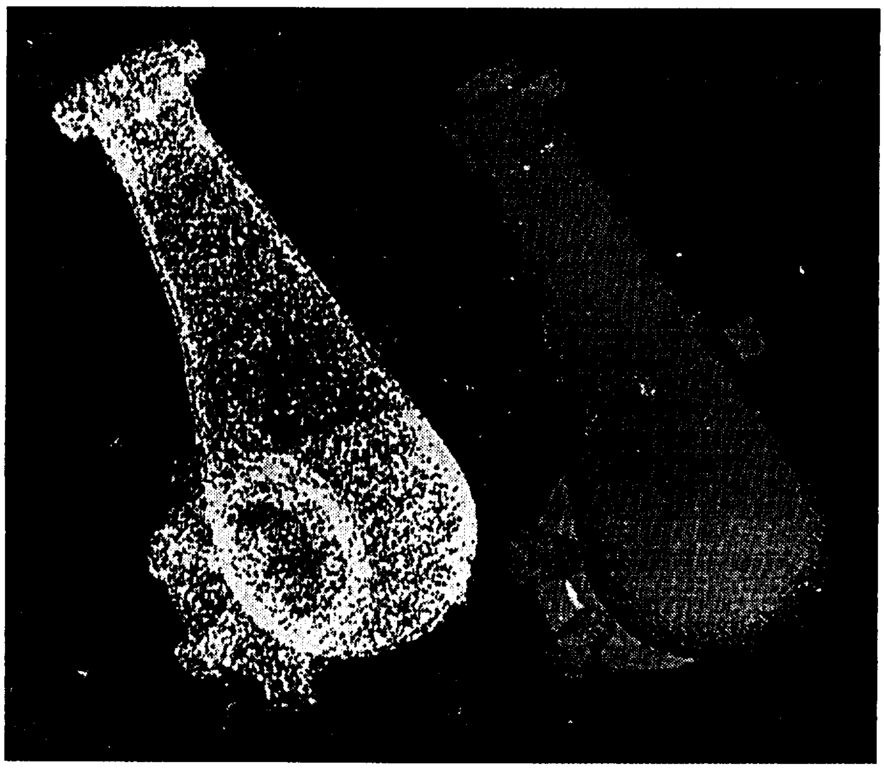

Figure 3-49. Pro-E CAD Image of the Gas Generator Housing

In Imageware, the CAD file, that is imported to Pro-E using the IGES translator, results in an exact rendition of the scanned part. The part can be zoomed and rotated; however, modifying the part proved to be very difficult. This was due to the fact that all of the parametric data used to build designs in Pro-E was not there; the image is considered as one big shape as opposed to a number of parametric surfaces.

To change the shape or size of the object, one can either recreate the geometry over the top of the digitized data, which is time consuming and difficult, or make the modifications using software that is specifically set up to make the modifications. Imageware allows the capability to make some file modifications; however, the ease of manipulation is an issue that was further evaluated in the Technology Implementation phase of this program (see Section IV).

Another approach is to use CAD software that does not require a parametric database to generate a file. One such possibility is to use CATIA, which does not require a parametric database. This effort was also evaluated in the Technology Implementation phase of this program (Section IV).

The STL file generated by Imageware was sent electronically directly to the rapid prototype laboratory located at Rocketdyne where two polycarbonate patterns were produced (see Figure 3-50). One of the patterns was shipped to PCC and Howmet for cost estimates. Howmet was chosen to produce the castings and perform solidification modeling as part of the casting effort.

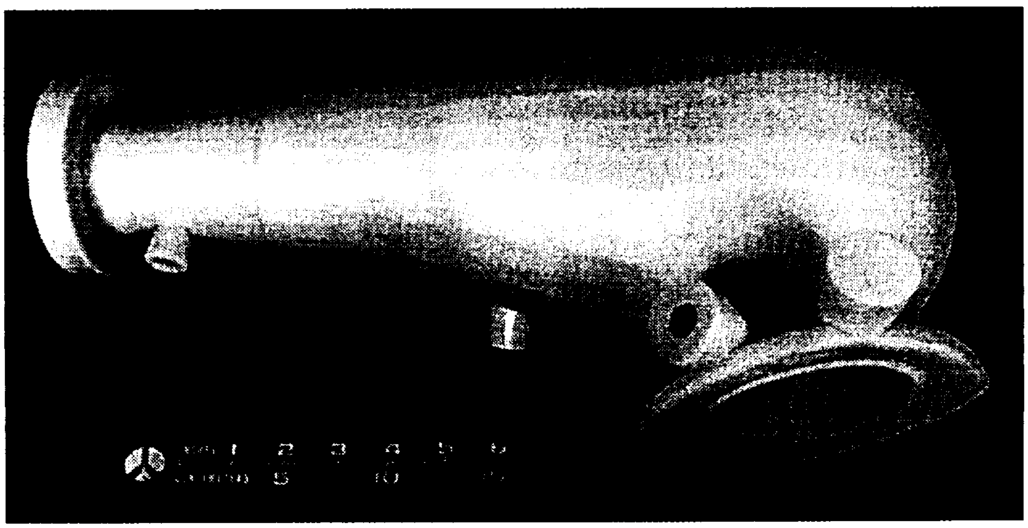

Figure 3-50. SLS Polycarbonate Rapid Prototype Pattern

All three file formats were delivered to Howmet for initial evaluation for file application to Solidification Modeling Analysis. Howmet initiated file type evaluation and initial results indicated that the STL file has greater compatibility with their Unigraphics CAD modeling needs.

3.3.2.2 Rapid Prototype Design and Process (Rocketdyne). The fabrication of metals directly using selective laser sintering has been recently established by the Rockwell Science Center. The methodology to produce near net shape components directly from the CAD using selective laser sintering is shown in Figure 3-45. The approach used for this program was to adapt that basic technology and to produce metallic, prototype shapes. Alloys, such as, nickel-base superalloys and steels, were used for initial evaluation. The task objective was to evaluate new SLS materials for metal sintering technology and sintering parameter development.

Conventional methods for prototype fabrication have relied on generation of drawings, hard tooling, numeric control programming, complex machining, and/or extensive hand work. These approaches are typically characterized by long lead-time, high cost, and multiple iterations to achieve desired results. Implementation of rapid prototyping using selective laser sintering (SLS) has enabled Rocketdyne to produce hard prototypes quickly and cost-effectively without machining part-specific tooling from drawings.

Rapid prototyping is defined as fabrication of hardware directly from a computer aided design (CAD) database. The SLS process, shown schematically in Figure 3-45, produces 3-dimensional parts from plastic and metal powders using the heat generated by a CO_2 laser. The CAD database is used to control the scanning path of the laser beam as it hits the powder bed, selective melting or fusing thin layers of powder to form a solid object. The 3-dimensional part is formed, one thin layer at a time, with each consecutive layer bonded to the layer below it.

The SLS process allows easy check out of configuration, fit up, and flow testing so design limitations can be identified early in the design process. Because SLS is so fast and relatively inexpensive, engineers are given more latitude to enhance their designs prior to reaching the manufacturing floor. By ensuring optimum designs before involving manufacturing, we can better align our shop resources to do the "right part right" the first time.

The availability of rapidly produced, inexpensive casting patterns has proven an order of magnitude reduction in investment casting development time and cost at Rocketdyne. Production of near-net shape castings provides an alternative to long-lead, expensive machining of complex shapes from wrought billets.

To date, rapid prototyping has been used mainly to make plastic models to verify designs and show proof of concept and produce patterns for investment casting. Fabrication of metal components directly for functional prototypes has not been successfully demonstrated for high-strength, large-scale parts. This effort has met with some success in demonstrating the feasibility to fabricate functional metal rapid prototype parts, using a DTM Sinterstation 2000 (see Figure 3-51). In addition to making functional, rapid-prototype parts, this process may also be used to make metal tooling for the sheet metal stamping industry, the plastic injection molding industry and for wax injection tooling for the casting industry.

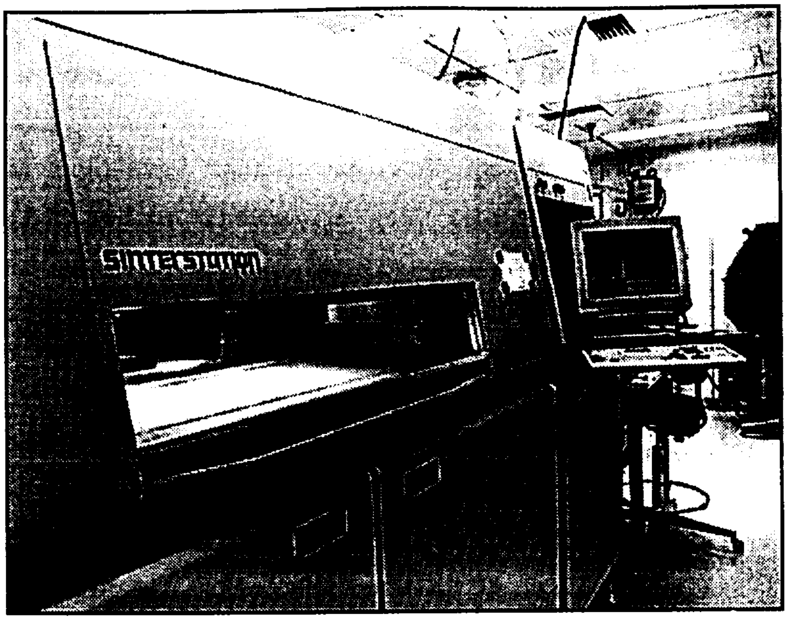

Figure 3-51. Photograph of DTM Sinterstation 2000 Used to Produce Metallic Components Directly

Rapid prototyping technology at Rocketdyne has quickly progressed in the direction of laser sintering metal powder to produce net-shape parts. The Rockwell Science Center, in cooperation with Rocketdyne, has developed a proprietary process depicted in Figure 3-45. Implementation of SLS metal processing will simplify the fabrication of complex designs by eliminating difficult machining operations and many of the weld and braze joints normally required. Rapid free form fabrication of fully functional metal components is an enabling technology for significantly reducing both cost and time in developing new hardware. In a business like Rocketdyne's where a limited number of parts are often required, rapid prototyping of metal hardware could easily be integrated as a manufacturing technique on the shop floor. Fabrication of net-shape metal dies for plastic injection molding and sheet metal forming has the potential to revolutionize the tooling industry.

SLS Metal Development. A two-stage method has been developed for free form fabrication of nickel- and iron-based alloy parts. The first stage uses the SLS process to build layer-by-layer a green-state part from a blend of metal and polymer powders using CAD data to define the part. In the "green" state the metal powder is simply held in shape by the polymer binder. No metal sintering has occurred in the SLS process. The second stage is an ambient pressure, high-temperature heat treat cycle for binder removal and liquid phase sintering of the metal powder to achieve fully-dense, net-shape parts. A major advantage of this metal free form fabrication method is the ability to utilize a commercially available SLS system (Sinterstation by DTM for Corp.) with no modifications from its standard configuration. The heat treat cycle can also be conducted in readily available commercial furnaces.

The SLS metal approach allows complex, high strength metal components to be fabricated as homogeneous metal alloys rather than a low melting matrix in a higher temperature preform. The process is adaptable to nearly any nickel or iron based alloy and has even shown promise for copper alloys.

As part of the AITP project, Rocketdyne focused efforts on fabricating demonstration hardware from the SLS metal process using a low carbon steel system. The powder is an off-the-shelf product produced by Hoeganous (product no. ANCR-ATW-230, Lot #: 27). It is 99+% iron and has been classified to -325 mesh (44 micron). For the SLS process, it is blended with a small percentage of Ni-Si-B (melting point suppressant for liquid phase sintering) and a small volume percentage of a polymer binder. Approximately 600 pounds of metal powder is required to load the DTM Sinterstation to achieve a full build of 12 inch diameter x 15 inch tall. The low carbon steel/Ni-Si-B system is not metallurgically an ideal alloy system for powder metal processing to achieve optimum strengths or ductility; however, this powder was readily available at Rocketdyne in the large quantity required for this development program and processing parameters developed for both the SLS and liquid phase sintering are applicable to more useful alloy systems like Inconel 718 and Haynes 230.

The objective of the SLS metal development effort on the AITP program was to:

(1) establish SLS parameters for green part fabrication, (2) establish furnace parameters for binder burn off and densification, and (3) fabricate demonstration hardware for an injection molding die.

A total of nine SLS runs were completed to develop SLS parameters and fabricate injection mold dies as shown in Figure 3-52. Sinterstation parameters for green part fabrication were established as follows:

Figure 3-52. Processing Parameters

Title	Title
Fill Laser Power	15.5 watts
Fill Scan Size (speed)	70
Fill Scan Spacing	0.003 in.
Part Bed Temperature	342°F (172°C)
Powder Feed Temperature	194°F (90°C)
Powder Layer Thickness	0.006 in.

Because the metal powder is much more conductive than plastic powders, parts with cross-sections greater than 5x5 in. tend to overheat and a poorly defined edge will form. This issue was eliminated by adding a powder layer delay of 20 sec before a new powder layer was added and the laser scanned the next cross-section. Heat management in the Sinterstation is somewhat more of an issue with metal powder than with plastic. However, fabrication of the green parts proved relatively trouble free.

In the green state, net shape parts are handled with care to remove the loose powder from the surfaces and internal cavities. Some minor surface preparation can be done in the green state such as light sanding to remove the stepping effects of the layers, addition of drilled holes, etc. The green parts are strong enough to handle during clean up and preparation for heat treat but can be easily chipped or broken. Green parts would be very difficult to ship via conventional carrier so it is essential to have heat treat facilities in the general local of the SLS fabrication.

Green parts are placed in a furnace retort and subjected to the following furnace cycle:

- Ambient pressure argon
- Hour at 600°F (315°C)

- Hour at 1950°F (1065°C)
- Held at 2240°F (1227°C) for various times depending on the part geometry.

Ramp rates are very slow to reduce thermal gradients in the part as it goes through the densification process. If temperatures are not well controlled, the green part will distort and/or crack during the liquid phase sintering process. If oxygen is introduced into the furnace environment, the part will not densify.

The average linear shrinkage in a part from the green state to the fully dense state is 15%. Because parts are shrinking significantly, accurate modeling will play a significant role in achieving tight tolerances for complex SLS metal hardware. Fortunately, the metal sintering process yields very repeatable results from part-to-part and the basic guidelines for net-shape powder metallurgy processing applies. Tolerances and surface finishes expected from SLS metal parts are comparable to castings.

Figure 3-53 shows examples of a metal die and rocket engine rotor that were produced using this process.

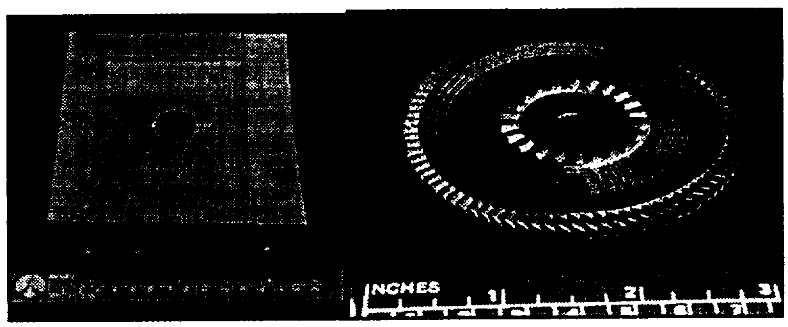

Figure 3-53. Photograph Metallic Parts Produced Directly with SLS

3.3.2.3 Rapid Prototype Design and Process.

Component Selection and Casting Design. Lockheed Martin evaluated various propellant feedline components from the Atlas Booster for conversion to single piece castings. Generally, most of the components which were analyzed utilized designs and fabrication techniques originally developed in the 1950s for the first Atlas Booster, i.e., multiple pieces of sheet material are cut into complex geometries, hammer formed into duct halves, and gas tungsten arc or seam welded to machined flanges or adjoining subassemblies. Using a developed selection criteria, eight (8) components were evaluated, of which, the LO_2 Tank Elbow (Figure 3-54) was selected as the best candidate for demonstration of the Rapid, Near-Net Shape Casting process.

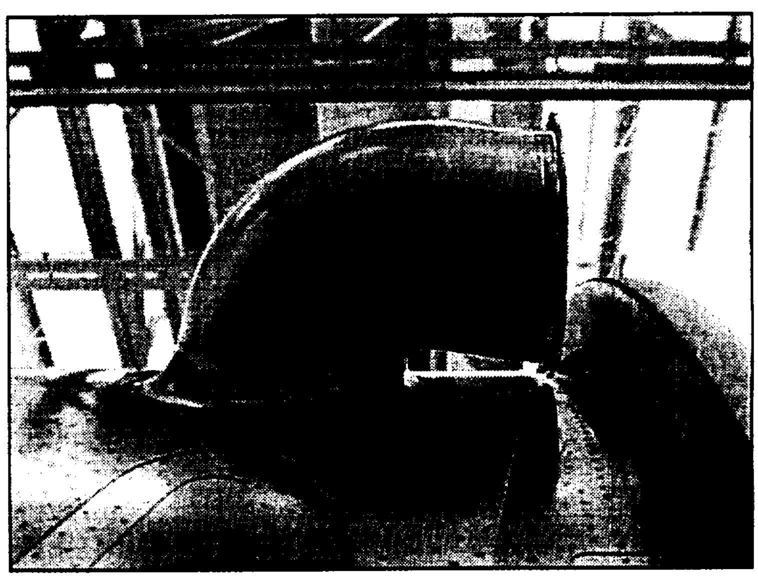

Figure 3-54. Photograph of the 321 Stainless Steel LO_2 Tank Elbow (11 in. ID) Joined to the Wall of the Atlas IIAS Booster

The design of the conventionally fabricated LO_2 Tank Elbow was studied to obtain an understanding of the functional requirements and critical dimensions required for the design of the single piece casting. The component's cost, weight, materials, environment, etc. were examined. Assembly of parts at the next higher level, in particular joining/welding were also considered. SDRC IDEAS Master Series software Version 2.1 was used to generate the design. Precision Castparts Corp. and Howmet both provided recommendations with regards to improving the producibility of the component, and these recommendations were incorporated into the initial design. Several casting design guides were also referenced.[1,2,3]

Casting alloy CF-8C (similar to 347 wrought stainless steel) was selected to replace the 321 CRES sheet material and forged ring. Minimum mechanical property allowables (e.g., 70 ksi UTS, 30 ksi YS, and 30% Elong.) for the CF-8C were taken from AMS 5362G.[4] Classical stress analysis was used to calculate the minimum thickness required for sustaining the internal pressure loads. The casting design incorporated slightly greater internal pressures to simulate those proposed for the Atlas IIAR. Also, design factors of safety of 1.5 for proof pressure and 2.5 for burst pressure were used per ESMCR 127-1 (required for the design of new equipment).[5] Casting factors were not used. Given the new design pressures, factors of safety, and material properties, the minimum wall thickness required for the LO_2 Tank Elbow Casting was calculated as 0.055 in. The 0.055 in. wall thickness provided a slightly positive margin of safety at a proof pressure of 127.5 psi. A summary of the casting design versus the conventionally fabricated component is given in Figure 3-55.

Figure 3-55. Summary of the Conventional Design Compared to the Casting Design of the LO_2 Tank Elbow

	Conventional Design	Casting Design
Material	321 CRES	CF-8C
Number of Detail Parts	6	1
Factors of Safety		
Operating	1.0	1.0
Proof	1.5	1.5
Burst	1.88	2.5
Design Pressures (psi)		
P_{op}	77.5	85
P_{pr}	105	127.5
P_b	146	212.5
Wall Thickness, min. (in.)	0.032	0.055
Weight (lb.)	11.06	TBD

[1] Casting and Machining Design and Manufacturing Standard, 100-09, Engineering Process Improvement, Martin Marietta. Sept. 1 1993.

[2] AGARD Handbook on Advanced Casting, NATO, Advisory Group for Aerospace Research and Development, AGARD-AG-299, March 1991.

[3] Rocketdyne Casting Design Manual, Publication 572-K-081 New 8-89, Rockwell International

[4] Per AMS 5362G, Steel Castings, Investment, Corrosion and Heat Resistant, 19 Cr-12 Ni-1.0 (Cb+Ta), Solution Heat Treated, Revised 1 Jul 85, Solution heat treated condition, pg. 3.

[5] Atlas II Final Stress Report (No. GDSS-A/II-89-013 Rev A), Feb. 1991, Vol. 1, pg. 1.4.5. Note that per ESMCR 127-1 that the design factors of safety for new equipment (i.e., Main Propellant Supply and Vent Components) are set at 1.50 for Proof and 2.50 for Burst (D>1.5 inches)

Solidification Modeling of the LO_2 Tank Elbow for the AITP. UES, Inc. of Annapolis, MD, was contracted to perform solidification modeling for the static (or conventional) investment casting of the LO_2 Tank Elbow. Note that two investment casting processes, i.e., static and Thermally Controlled Solidification, were utilized during this study, but only the static investment casting process was modeled. Casting process parameters for the static process and material properties were provided by PCC Airfoils Inc. Additional solidification modeling support was also provided by PCC Airfoils. Modeling was performed on two thickness variations of the LO_2 Tank Elbow Casting: 1) a 0.200 in. nominal wall thickness, and 2) a 0.100 in. nominal wall thickness. During the preliminary design of the casting, PCC Airfoils recommended that the wall thickness of the component be tapered from 0.200 in. at the ends of the casting to 0.100 in. near the middle to facilitate complete mold fill. The 0.100 in. wall thickness was thought by the foundry to be the minimum achievable wall thickness using conventional investment casting. PCC also stated that as a general rule the ratio of the feed distance to wall thickness should not exceed a maximum of 20.[6] The first model (0.200 in. wall thickness) was performed to analyze the characteristics of the fluid flow through thin-walled sections over extensive feed distances. Note that with a nominal wall thickness of 0.200 in., the ratio of feed distance to wall thickness was approximately 120. The approach was to modify gating designs, alter the casting parameters, and most importantly, employ differential wraps of insulation to extend the feeding distance.

The 0.200 in. thick wall LO_2 Tank Elbow casting design was provided to the UES, Inc. via the Internet. The gating system (designed by PCC Airfoils) was joined to the LO_2 Tank Elbow Casting using IDEAS. Feed stock was added to the ends of the casting to allow for final machining. The entire finite element mesh of the casting model, i.e., gating and casting, was created in MeshCast using tetrahedral elements. The shell was created in PreCast (preprocessor for ProCast™) using the automatic shell generation technique. Since the model was symmetric, a half symmetry was assumed while creating the finite element mesh (Figure 3-56), thus decreasing the total number of elements required. The total number of elements and nodes in the model were approximately 78,135 and 27,246, respectively.

The physical and thermodynamic material properties used for the CF-8C stainless and investment shell were either provided by PCC Airfoils or researched by UES, Inc. for analysis. The required data included solid vs temperature, liquid vs temperature, density, heat transfer coefficients, viscosity, latent heat, specific heat as function of temperature, conductivity as function of temperature, etc. The initial temperature of the shell was selected to be 1800°F and the pouring temperature of the alloy was selected to be 2900°F. Differential wrap using Kaowool was used to insulate various portions of the mold and gating

[6] L.D. Graham, "Lockheed Martin LO_2 Tank Elbow Casting", Precision Castparts Corp., Feb. 9, 1996.

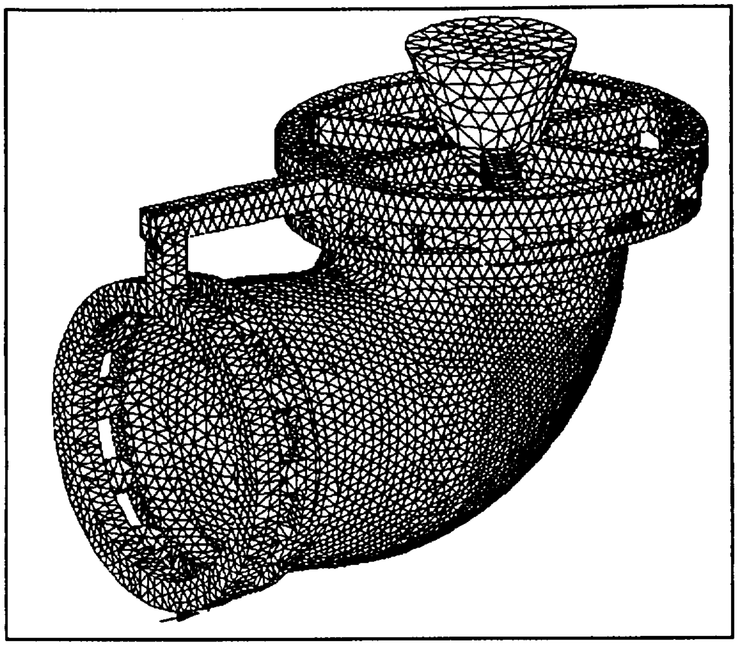

Figure 3-56. Schematic of Meshed Gating System and Casting for the LO_2 Tank Elbow

system. The inlet velocity was calculated from the volume of the casting, the inlet area, and the time to fill. Thus for a fill time of 3 sec, the inlet velocity was calculated to be 2 m/sec.

Several iterations of the solidification model were performed by both UES and PCC Airfoils. Preliminary results from UES showed that with the initial process parameters, the casting was more or less completely filled by the top gates, with the side gates acting as risers to feed the casting as it solidified. In an attempt to get more fluid flow through the side runners, the pour velocity was increased and the gating design was modified. Little or no effect was gained by increasing the pour velocity. Modifying the gating design, however, resulted in improved fluid flow. Additionally, PCC Airfoils found that the use of wrap removal to increase the thermal gradient during solidification was beneficial, however the timing of the removal was very important. Both UES, Inc. and PCC Airfoils concluded that from the analyses and modifications carried out, a sound casting having a nominal wall thickness of 0.200 in. could be readily produced.

Next, solidification modeling was performed on a LO_2 Tank Elbow Casting having a nominal wall thickness of 0.100 in. The modifications employed on the first model were again used on the thinner walled casting model. UES concluded that the reduction in wall thickness had little effect on the flow pattern and solidification as shown in Figure 3-57. The occurrence of shrink porosity or improper filling was not observed. These results were verified by PCC Airfoils. Again, both UES and PCC Airfoils concurred that the solidification modeling results indicated that a sound casting could be produced. The optimized gating system design (with dimensions) is shown in Figure 3-58.

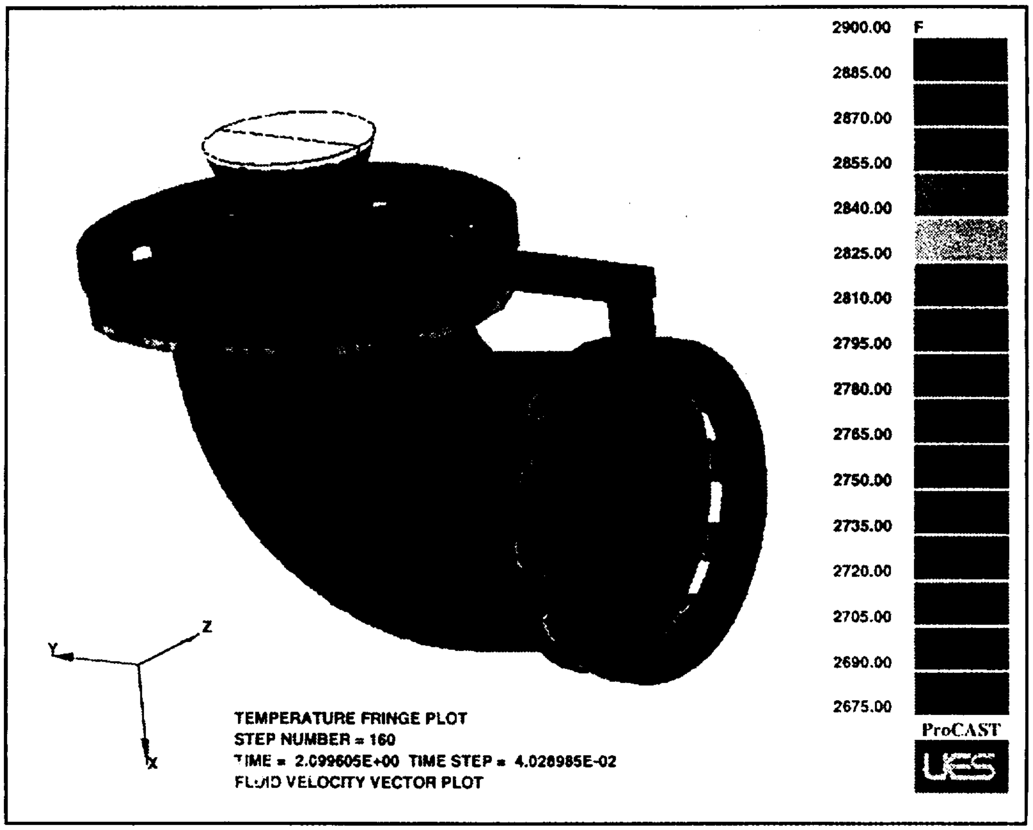

Figure 3-57. An Example of a Temperature Fringe Plot of the Static LO_2 Tank Elbow Casting (0.100 in. Thick Wall) Solidification Model (at 2 sec After Start of Pour Using a Fill Time of 2 sec (Pour Velocity of 3 m/s))

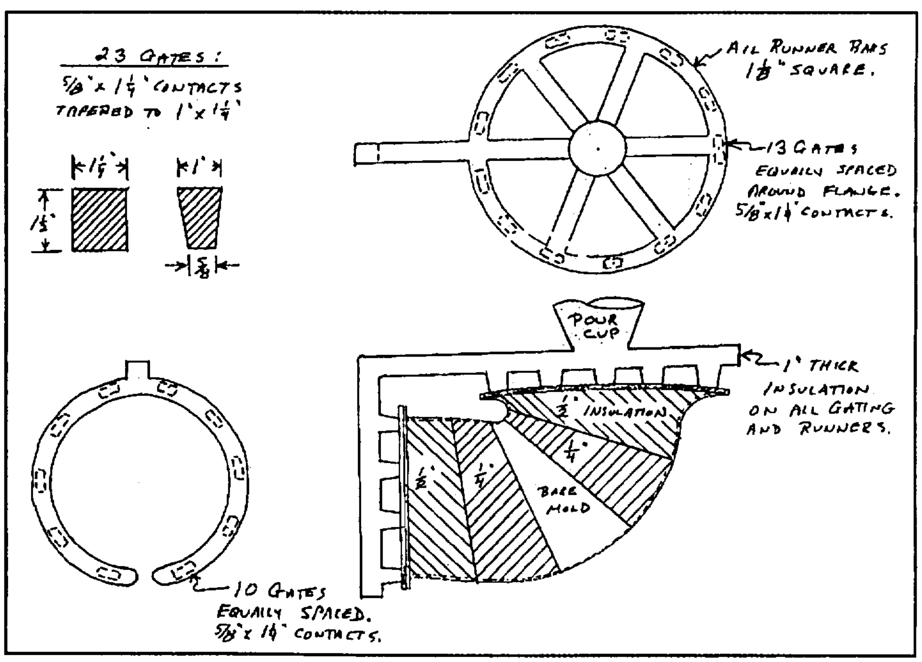

Figure 3-58. Gating Design for 0.100 in. Thick Walled LO_2 Tank Elbow Static Investment Casting. Schematic Also Shows the Differential Wrap of Insulation Used to Extend Feed Distances

Rapid Prototyping of Static LO_2 Tank Elbow Casting Pattern. Preliminary technical discussions with several investment casting foundries indicated that stereolithography, using the QuickCast™ technique, is the preferred rapid prototyping process for directly producing consumable heat disposable patterns. QuickCast™ utilizes a unique build style which results in an open lattice internal structure. During burnout of the pattern from the investment shell, the quasi-hollow pattern permits the pattern to collapse inward, which greatly reduces the probability of breakage of the shell due to the differences in thermal expansion.

Accelerated Technologies, Inc. of Austin, TX was contracted to produce the patterns for the LO_2 Tank Elbow Casting. Shrink factors, i.e., factors which compensate for the shrinkage of the metal during solidification, were incorporated into the "STL" file of the casting design. A 3D Systems' SLA-500 machine was used to fabricate the patterns with a Ciba-Geigy 5170 resin system. The build rate for each 0.100 in. thick walled pattern was 105 hours with cleanup times of 8 to 10 hours per pattern (Figure 3-59). Three patterns were fabricated for $3K each and delivered in approximately 10 days. Each pattern was dimensionally inspected using a coordinate measuring machine.

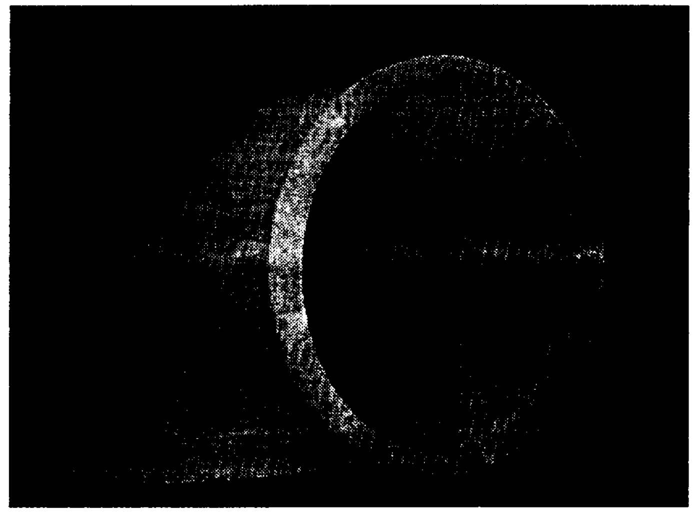

Figure 3-59. Photograph of a Stereolithography (QuickCast™) Pattern of the LO_2 Tank Elbow Casting (11 in. ID, 0.100 in. Wall Thickness)

3.3.2.4 Cast Rocket Engine Parts (Rocketdyne). Howmet Casting Corporation was selected to develop a casting process for the Gas Generator Housing Component, using an iterative process modeling/casting trial methodology. Solidification Modeling analysis and two Inconel 718 casting iterations of the reverse engineered design were performed. The following are the steps that were followed:

1. Establish an electronic path by which an IGES file can be electronically converted into a format, that is, readily readable by Procast's solidification modeling software.
2. Perform solidification modeling analysis on the gated design.
3. Apply the gating recommendations resulting from the electronic analysis
4. Cast and evaluate the results to cross-check analytical predictions.
5. Re-analyze the electronic model and apply the lessons learned from the first pour.
6. Cast and analyze the second casting.
7. Deliver the castings to Rocketdyne

An IGES file geometry of the reverse engineered Gas Generator model was delivered to Howmet. The file consisted of surface information as a baseline to construct a solid Unigraphics CAD model. Unigraphics is the primary CAD tool used by Howmet and is universal to the ProCast reverse engineering software. Unigraphics software was used to apply gating and risers to the design. Then, these designs were analyzed using ProCast software

The first casting trial yielded a sound part with minimal shrinkage that was initially associated with incomplete Kaowool wrapping. This resulted from an unwrapped zone that cooled off too quickly during solidification and did not adequately feed the solidifying metal. Non-destructive results validated the presence of shrinkage in the combustion mixing bowl zone of the casting. A second casting was processed using the same gating technique employed on the first pour; however, efforts to properly wrap and process the casting were employed. The casting resulted in shrinkage in very much the same location as previously observed, but the casting was easily weld repaired.

Although some shrink was observed in each casting, the solidification model provided a sound basis for determining where the gates and risers should be. It should be noted that the casting selected was considered an extremely difficult shape to cast.

3.3.2.5 Cast Launch Vehicle Component (Lockheed Martin). Two different casting processes were used for production of demonstration components; 1) the static or conventional investment casting process, and 2) the Thermally Controlled Solidification (TCS) process. Both processes allow the means of producing highly complex metallic structures, offering the engineer almost unlimited design freedom. The recently developed TCS process allows the controlled advancement of the solidification front in the mold, therefore minimizing the occurrence of casting defects (e.g., cold shunts, shrinkage porosity, etc.) resulting from reduced fluid flow through thin-walled sections. Thus, the TCS process permits the casting of ultra thin-walled, lightweight structures not readily produced with the conventional investment casting process. Note that solidification modeling was not performed for the TCS process (due to its proprietary nature according to Precision Castparts Corp.) The following provides a description for the development of each process:

Static Investment Casting of the 0.100 in. Thick Wall LO_2 Tank Elbow

Gating of the SLA Pattern. Lockheed Martin Astronautics provided PCC Airfoils' Prototype Foundry with the solidification modeling results (e.g., casting parameters, gating design, etc.) and several investment casting patterns of the 0.100 in. wall thickness LO_2 Tank Elbow. The gating system, as previously shown in Figure 58, was composed of thirteen gates equally spaced around the circumference of the larger diameter flange (or bell mouth) and ten similar gates around the smaller diameter flange. The contact size of the gates was 0.625 in. x 1.250 in. The ring runners and spokes of the gating were

1.125 in. x 1.125 in. square. Figure 3-60 shows the gating system (wax) joined to the epoxy resin SLA pattern.

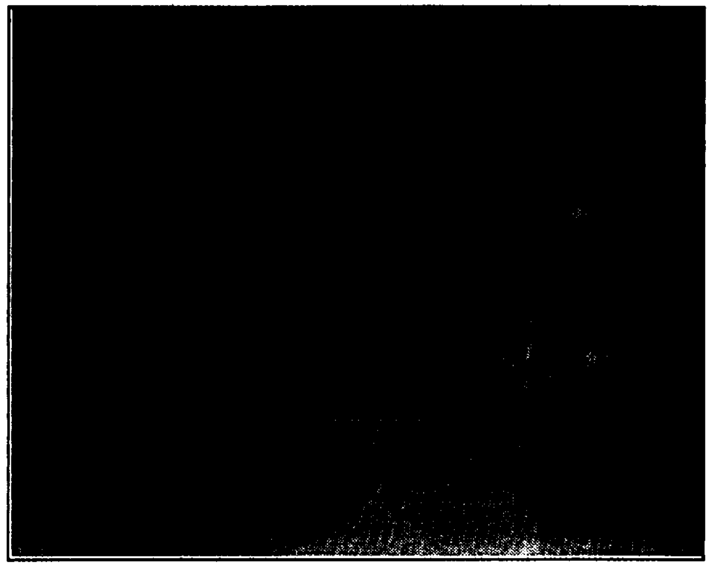

Figure 3-60. Photo Showing the Gating of the First 0.100 in. Thick Walled LO_2 Tank Elbow

Shell Fabrication. The gated pattern was given a total of ten dipcoats during the fabrication of the investment casting shell. The ceramic materials used for each dip are provided in Figure 3-61. The slurry binder for each coat was colloidal silica and each dip was tunnel dried. The cobalt aluminate used in the first coat serves as a nucleating agent for grain refinement. After the final dip coat and dry, the numerous melt tips are opened up to allow for wax and pattern expansion during burnout. The shell was successfully deplasticized and dewaxed during burnout, and no shell cracking occurred.

Figure 3-61. Fabrication Process and Materials Used for Production of the Investment Casting Shell for the 0.100 in. Thick Walled LO_2 Tank Elbow

Dip No.	Slurry Solids	Stucco
1	Zircon + 10% Cobalt Aluminate	Zircon
2	Zircon	Kyanite, Fused Silica
3-9	Zircon, Kyanite, Fused Silica	Kyanite, Fused Silica
10	Zircon, Kyanite, Fused Silica	None (Seal Dip)

Differential Insulation Wrap. As performed in the solidification modeling, the mold was insulated with various amounts or thicknesses of insulation (i.e., Kaowool fiber) to establish temperature gradients in the casting in order to promote directional solidification. As previously shown in Figure 3-57, the center section of the mold was uninsulated, i.e., left bare, with increasing thicknesses of Kaowool towards the flanges. The intention was that upon pouring, the molten metal in the uninsulated area of the mold would cool the fastest and solidify first, and then solidify towards the direction of the flanges.

Foundry Practice and Casting Results for Casting Lot #1. The mold was preheated overnight at 1800°F in a gas fired furnace. A 127 lb charge of CF-8C stainless steel was melted in the Prototype Foundry's batch type vacuum furnace. The chamber was evacuated and then backfilled with 500 mm Hg pressure of argon prior to melting. The charge was melted and the temperature stabilized at 2900°F. The mold was then removed from the 1800°F preheat furnace and taken to the melting furnace. The melting chamber was vented with argon, the preheated mold was set in place and poured under atmospheric conditions.

During the pour, the mold was somewhat out of position, therefore causing the pour rate to be reduced somewhat. This resulted in a slower pour speed, estimated to be about 4 sec vs the 2 sec predicted in the solidification model. After pouring, the liquid metal in the pour cup was hot topped with an exothermic material.

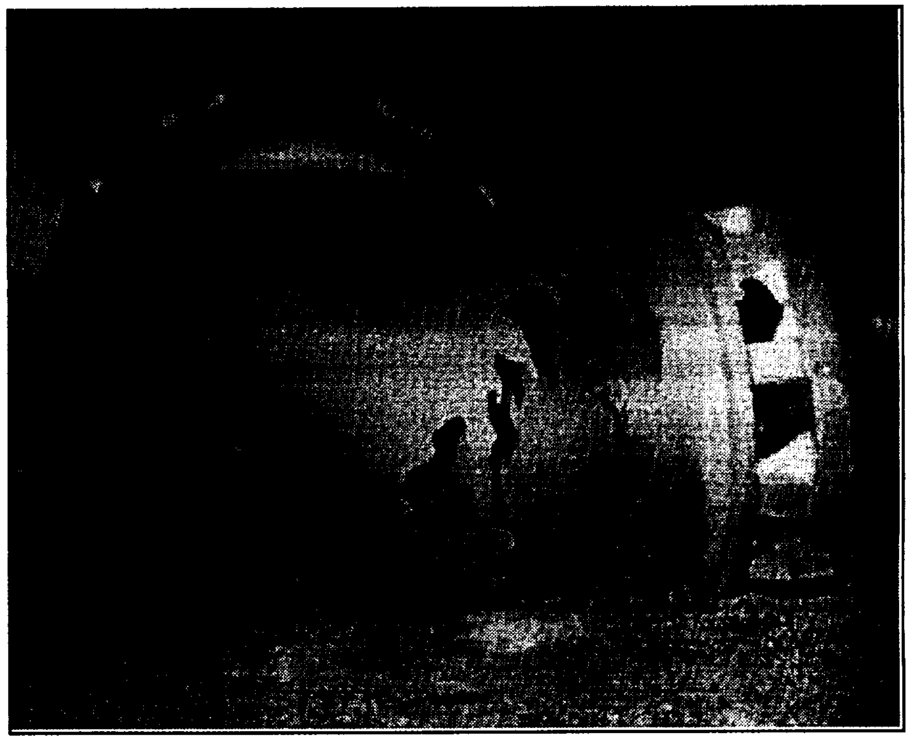

Figure 3-62. Photos of First Elbow Casting (Lot #1) After Ceramic Removal and Shot Blasting, Showing Extensive Area of Nonfill

Figure 3-62 shows the resulting casting after ceramic removal and shot blasting. The part had extensive nonfill on the bottom portion of the elbow near the smaller flange. The misrun was initially thought to have been caused by the slow pour velocity which may have changed the head pressure, thus altering the fluid flow. Portions of the casting that did fill out had good surface finishes and closely duplicated the surface of the SLA pattern. X-rays taken of representative areas of the 0.100 in. walls showed scattered shrinkage, which could have been healed via hot isostatic pressing. X-rays taken of the flanges showed no shrinkage.

Modifications of Gating and Mold Design for Casting Lot #2. The results of the first casting attempt (i.e., Lot #1) showed potential, therefore PCC Airfoils prepared a second investment mold for casting Lot #2. The gating system for Lot #2 was similar to that of Lot #1, except that runner bar connecting the two ring runners was enlarged and the pour cup was also enlarged. The runner bar connecting the ring runners was increased from 1.125 in. x 1.125 in. to 1.125 in. x 3 in. This was an attempt to deliver metal faster to the smaller flange to lessen the misrun tendency in that area. The pour cup was substantially enlarged, both to provide a larger target for faster pouring and to increase its volume to prevent any possibility of metal overflowing the cup. The pour cup bottom opening was kept at 3.2 in. diameter, but the height was increased from 4.5 in. to 6.5 in. and the top diameter was increased from 6.5 in. to 8.0 in. The mold making procedure for Lot #2 was identical to Lot #1.

Additionally, the insulation scheme of the mold for Lot #2 was modified to lessen the amount of mold cooling after removal from preheat and to reduce the tendency for misrun. Instead of using differential wrap as in Lot #1, whereby a portion of the mold was uninsulated, a constant thickness of 0.500 in. thick Kaowool was used to wrap the entire mold.

Description of Foundry Practice and Casting Results for Lot #2. The same mold preheat and pour temperatures, 1800°F and 2900°F respectively, and metal charge weight (127 lb) were used for casting Lot #2. The pouring operation was reported to have gone very well. The mold transfer time from preheat to pouring was 3 minutes (vs about 4 minutes for Lot #1) and the pour time was 2.1 sec, similar to that used in the solidification model and half of that for Lot #2. As shown in Figure 3-63, the Lot #2 casting also had substantial misrun towards the flange. The misrun for Lot #2 was approximately 50 to 60% of that for Lot #1.

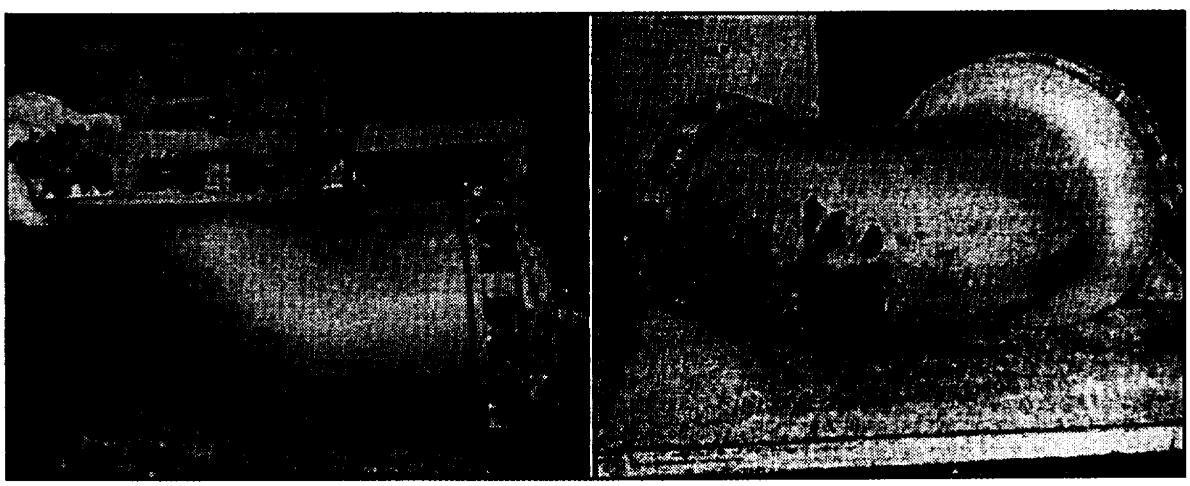

Figure 3-63. Photos of Second Elbow Casting (Lot #2) After Ceramic Removal and Shot Blasting, Showing Extensive Area of Nonfill

Discussion of Results. The solidification model provided by UES, Inc. showed that the 0.100 in. thick wall LOX Tank Elbow was readily cast using the preliminary casting parameters provided by PCC Airfoils. These results were verified by PCC Airfoils using their "in-house" solidification modeling capabilities. After the pour of Lot #1, the extensive misrun was thought to have been caused by the reduction in pour speed due to the misalignment of the pouring crucible with the pour cup. Following the implementation of a number of modifications to improve the producibility of the 0.100 in. thick wall LO_2 Tank Elbow, the casting of Lot #2 also resulted in significant misrun.

Both UES, Inc. and PCC Airfoils were asked by Lockheed Martin to determine the probable cause of failure of the solidification model to predict accurate results. UES, Inc. reevaluated and confirmed the input parameters provided by PCC Airfoils. PCC Airfoils, concerned with the amount of heat loss that resulted in the premature "freezing off" of the molten metal, reran the solidification model with various heat transfer coefficients to determine if they could simulate the actual casting results (i.e., size and location of misrun). Successive plots of the temperature of the leading edge of the metal flow as a function of time were produced (as shown in Figure 3-64) in order to "reverse engineer" the heat transfer coefficient. PCC Airfoils determined that heat transfer coefficient should have been 5.6 times the value that was used in the original model, i.e., 0.050 cal/cm·°Cs vs 0.009 cal/cm·°Cs.

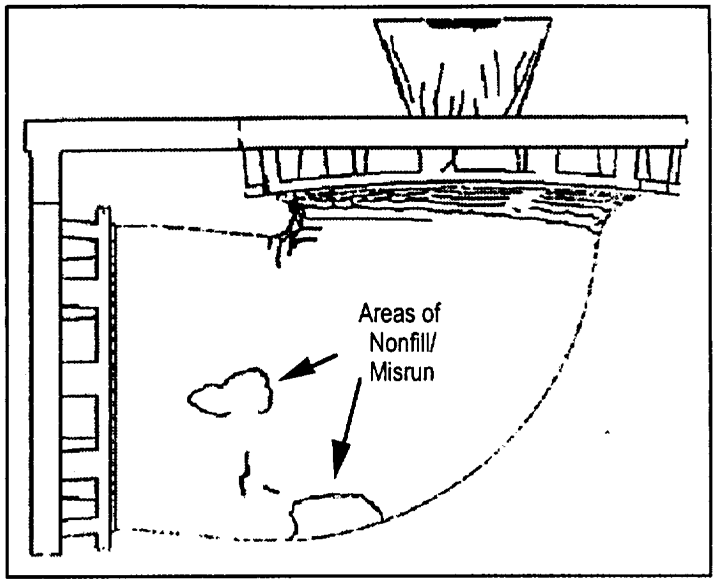

Figure 3-64. Schematic Showing Results of PCC Airfoils' Reverse Engineering of the Heat Transfer Coefficient for the 0.100 in. Thick Wall LO_2 Tank Elbow. Areas of Nonfill/Misrun Predicted by the Solidification Model are Similar to Those Observed in the Casting

An important element in the heat flow equations used to characterize heat loss, such as used in the solidification modeling software, is in the determination of an accurate heat transfer coefficient, K, between the metal and the mold. In large structural castings, where the foundry can use high mold preheats and pour temperatures, the heat transfer coefficients used in the heat flow equations and solidification models are well established. In the case of thin-walled structural castings, there is considerable mixing of the metal and impingement of the metal on new surfaces of the mold which can result in significantly higher heat transfer, and therefore make the determination of accurate heat transfer coefficients more difficult.

There are several methods that can be employed to determine the interface heat transfer coefficient. The first method is via experimentation using thermocouples attached to representative sections and/or thicknesses of a casting. The second method, such as performed by PCC Airfoils, is by reverse engineering the heat transfer coefficient after viewing the size and location of the misrun.

As a result of the error in the assumed interface heat transfer coefficient, the solidification model inaccurately predicted complete mold fill. It was later determined that the coefficient was the only unknown variable in the solidification model. PCC Airfoils reported that the coefficient that they provided UES, Inc.

was empirically determined for metal that was not flowing, or in other words, a "static" heat transfer coefficient. The larger value was considered a "dynamic" heat transfer coefficient that accounted for the mixing and impingement of the molten metal on new surfaces.

Upon discussing these results with the Precision Casting Consortium at an AITP Milestone Review Meeting held at Rocketdyne in Conoga Park, CA on October 11, 1996, it was recommended that the corrected solidification model be used to determine if the casting parameters (e.g., pour temperature, pour velocity, etc.) could be modified such that the component could be produced. PCC Airfoils re-ran the model and concluded that there was not sufficient margin within the casting parameters and thus recommended that a completely different gating system ("bottom" gating approach) would have to be used. At that time, because of the lack of funds, schedule, and success with the TCS process development (as discussed below), the work at PCC Airfoils was discontinued.

Casting of the 0.055 in. Thick Wall LO_2 Tank Elbow using the Thermally Controlled Solidification Process

Introduction to the TCS Process. As previously discussed, the typical wall thicknesses for the Atlas Booster's propellant feedline components, fabricated of formed and welded stainless or Inconel sheet, are approximately 0.030 in. thick. For castings having complex geometries and extended feed distances, the minimum achievable wall thickness using conventional investment casting is approximately 0.100 in. The increase in thickness due to the limitation of the casting process results in a substantial increase in component weight. The potential recurring cost savings gained in the manufacture of a propellant feedline component via conventional investment casting wanes in comparison to the cost of a significant weight increase.

The Large Structurals Division of Precision Castparts Corp. in Portland, OR has been developing a proprietary casting process, referred to as Thermally Controlled Solidification (TCS), for producing cost effective, complex, thin-walled (0.030 in.) castings. The TCS process, as shown in Figure 3-65, allows the controlled advancement of the solidification front in the mold, therefore minimizing the occurrence of casting defects (e.g., cold shuts, shrinkage porosity, etc.) resulting from reduced fluid flow through thin-walled

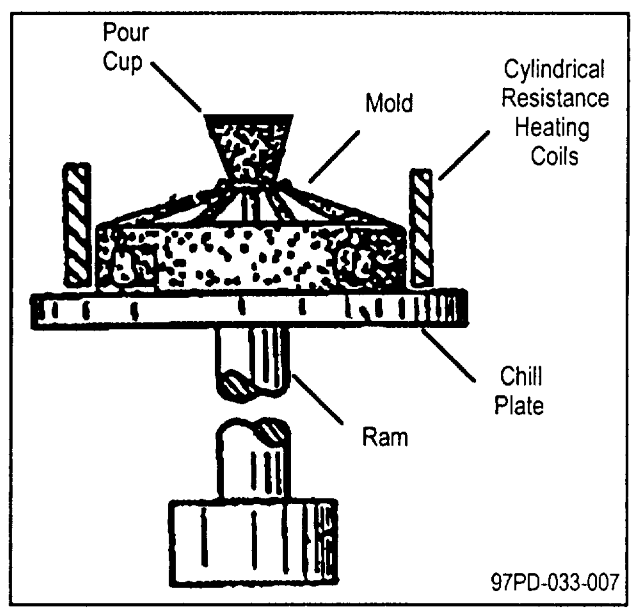

Figure 3-65. Schematic Representation of Precision Castparts Corporation's Thermally Controlled Solidification Furnace

sections. Cylindrical resistance heating coils are used to provide a differential thermal profile (up to 110°C) to the mold prior to pouring. Following the vacuum-induction melting of the alloy into a crucible and a temperature stabilization step, the molten metal is poured into mold's pour cup. At that time, the heating coils are slowly withdrawn from the mold. Solidification first occurs in the mold nearest the chill plate, and then proceeds at a slow, stable rate controlled by the rate of heating coil withdrawal.

Preliminary development by PCC of the TCS process was performed using a laboratory scale TCS furnace with a capability of pour weights up to 120 lb and molds measuring up to 20 in. OD x 20 in. height. A TCS investment casting shell system was developed and proven compatible with consumable, heat disposable patterns produced via stereolithography (having similar coefficients of thermal expansions). However, this furnace will not accommodate many of Lockheed Martin Astronautics applications because of its limited size. In August of 1995, PCC completed construction of a larger TCS furnace with a capacity of pour weights up to 900 lb and molds measuring up to 43 in. OD x 40 in. height. A different TCS shell was developed for the larger furnace, and at the time, had not been used with investment casting patterns produced by stereolithography.

In a parallel effort with the Aerospace Industry Technology Program, Lockheed Martin Astronautics began a program with PCC Large Structurals Division to developed the TCS process for casting ultra thin-walled, low cost propellant feedline components. The 11 in. ID LO_2 Tank Elbow was again selected as the demonstration component for the development of the process. The geometry of this component is such that the results of this study will be applicable to other propellant feedline components, i.e., thin-walled, extended feed distances, etc. [Note that in order to incorporate a greater operating pressure and factor of safety for burst to simulate conditions for the Atlas IIAR, the wall thickness of the casting is greater (0.055 in. vs 0.030 in.) than that of the conventionally formed and welded manufacturing process (see Figure 3-55)]

The scope of the program included the evaluation of a suitable shell system for the large furnace which was compatible with SLA patterns (Phase I) , optimization of the TCS process parameters (Phase II), and the casting of three "production-like" components (Phase III) for characterization by Lockheed Martin. An overview of the development path is provided in Figure 3-66. The steps used for producing each TCS process development casting are shown in Figure 3-67. The general requirements for the casting were per AMS 5362 (except the composition per ASTM A743) and inspection requirements per MIL-STD-2175 Class 1, Grade B.

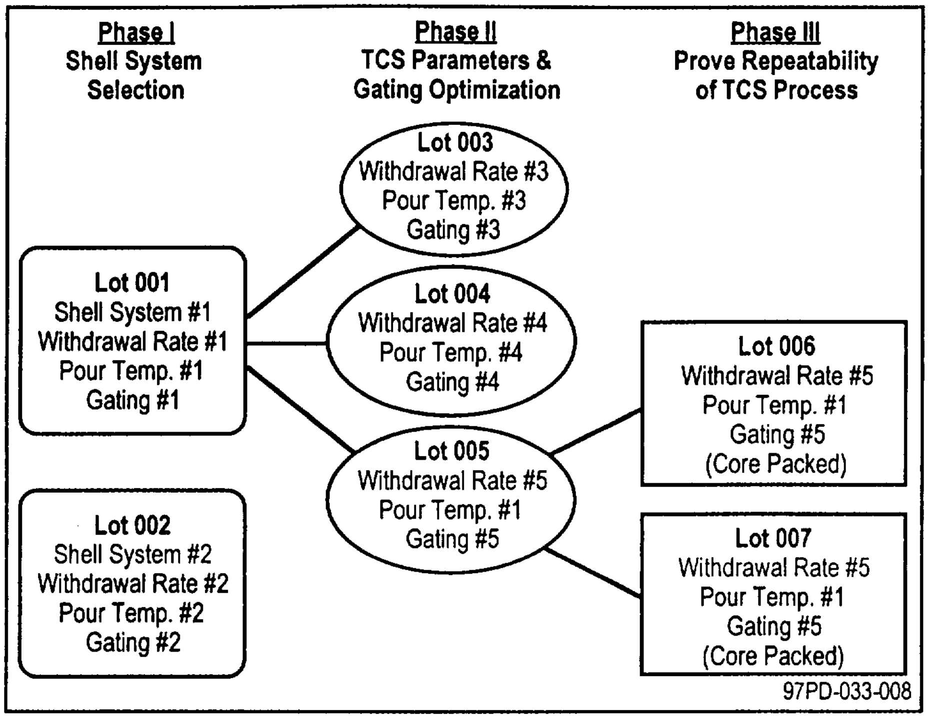

Figure 3-66. Overview of the TCS Process Development Study

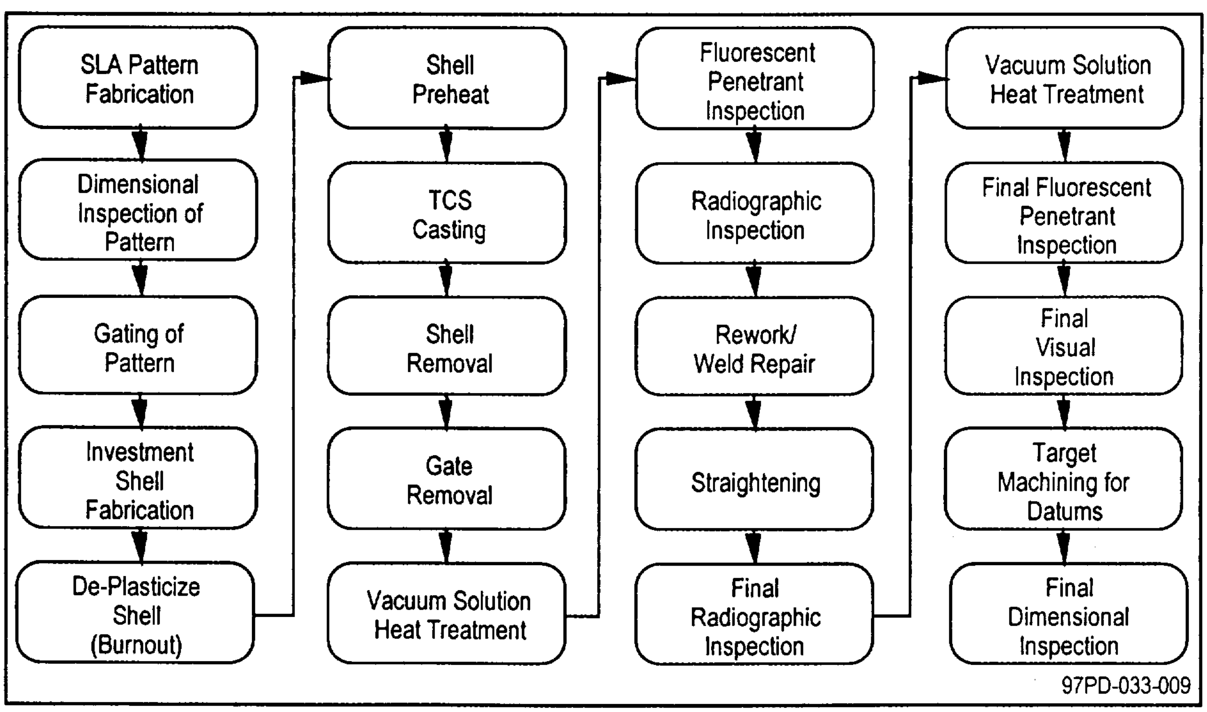

Figure 3-67. Steps Used for Producing TCS Process Development Castings. Note that Castings were Procured to Meet the General Requirements of AMS 5362 and Inspection Requirements of MIL-STD-2175 Class 1, Grade B

Rapid Prototyping of the Thin-Walled LO_2 Tank Elbow Pattern. The SLA QuickCast™ patterns for the TCS development were fabricated by Accelerated Technologies, Inc. (ATI) of Austin, TX. Before starting the fabrication of the patterns, ATI stated that some portions of the patterns may be solid because of the QuickCast™ software's inability to formulate an open lattice internal structure build style between the thickness range of 0.040 to 0.090 in. As previously stated, the open lattice structure reduces the probability of breakage of the shell during pattern burnout. At this time, according to 3D Systems, the producer of QuickCast™, no changes were being made to the software to accommodate thin-walled investment castings patterns in the 0.040 to 0.090 in. thickness range.

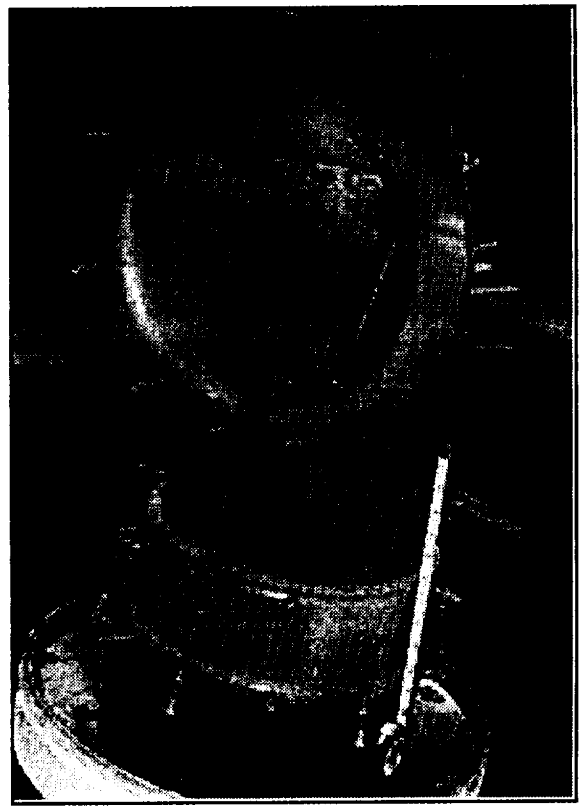

Figure 3-68. SLA QuickCast™ Pattern for the 0.055 in. Thick Wall LO_2 Tank Elbow Casting Used in the TCS Process Development. Note that Some Portions of the Gating Design are Also Shown

The 0.055 in. pattern (Figure 3-68) included some of the gating near the flange and also a pattern base at the bell mouth to add stability to the pattern and to better facilitate the TCS process. A 3D Systems' SLA-500 machine was used to fabricate the patterns with a Ciba-Geigy 5170 resin system. Because of the additional material for the gating and pattern base, the pattern was fabricated in two pieces, and then joined together. The build rate for the 0.055 in. thick walled stereolithography pattern for the TCS process development was 64 hours. Following the build, the part was allowed to drain for 24 hours and then cured for 12 hours under UV lights. Each pattern required between 18 to 20 hours additional hand work (e.g., support removal, cleanup, etc.).

Summary of the TCS Process Development. The objective of Phase I of the TCS process development study was to determine a suitable shell system which would be compatible with the thin-walled SLA QuickCast™ patterns and PCC's large TCS furnace. Two shell systems were evaluated: 1) a new low-expansion shell system [referred to as the LX shell system (Shell System #1)], and 2) a standard shell system (Shell System #2). Note that Shell System #1 was originally designed for use with PCC's wax patterns in the large TCS furnace and previously had not been used with epoxy resin patterns.

The thin-walled LO_2 Tank Elbow castings (i.e., Lots 001 and 002) for Phase I were fabricated using the preliminary steps in Figure 3-67 and with the general parameters shown in Figure 3-66.

Thermocouples were attached to various locations on the mold at different distances from the chill plate to record the temperature as a function of time. Both molds filled out completely with virtually no visual flaws. There was no evidence of shell failure on the parts prior to casting or after shell removal. Lot 001, the first thin-walled LO_2 Tank Elbow casting produced via the TCS process, is shown in Figure 3-69.

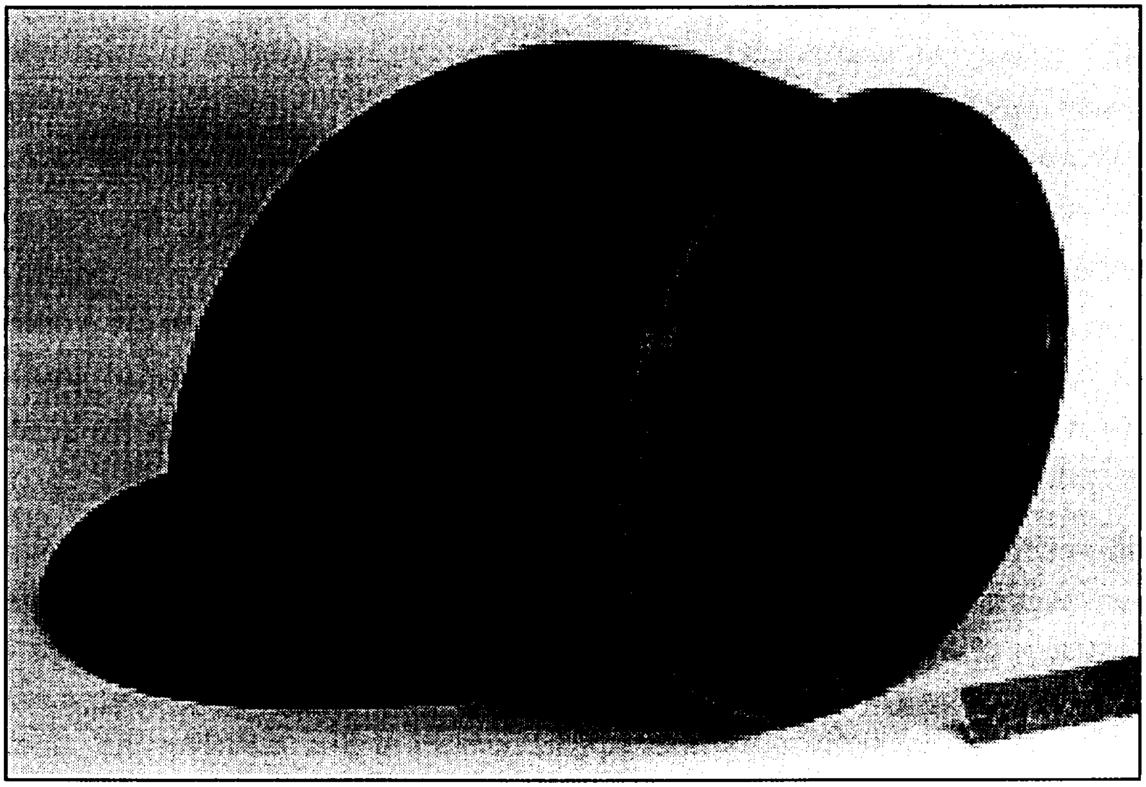

Figure 3-69. Lot 001 of the Thin-Walled (0.055 in.) 11 in. ID LO_2 Tank Elbow Casting (Alloy CF-8C SHT) Produced Via the TCS Process

Given the relative quality levels (e.g., visual, fluorescent penetrant inspection, and radiographic inspection) for Lots 001 and 002 of Phase I, it was concluded that the low expansion, LX shell system would be used for development work for Phase II. The objective of Phase II was to further develop and optimize the TCS process for casting the thin-walled LO_2 Tank Elbow. Various withdrawal rates, pour temperatures and gating designs were evaluated for casting Lots 003, 004, and 005 (as previously shown in Figure 3-66). From this work, the process and parameters used to produce Lot 005 were selected for casting several additional "production-like" thin-walled LO_2 Tank Elbows (Lots 006 and 007) to be used for the Technology Validation and Transfer portion of Aerospace Industry Technology Program (see Task 4.0).

3.4 TASK 4.0 – TECHNOLOGY VALIDATION AND TRANSFER

3.4.1 INTRODUCTION AND SUMMARY

Technology commercialization of the processes developed in this Aerospace Industry Technology Program was a critical aspect to the success of this program. An integrated process development team was assembled to develop and commercially implement selected casting manufacturing technologies that will:

- Enable significant reductions in the costs of castings,
- Increase the complexity and dimensional accuracy of castings, and
- Reduce the development times for delivery of high quality castings.

3.4.2 Procedures and Results

3.4.2.1 Implementation (Ford). The core box wear system, developed in Task 1.1, will be installed at Ford's Cleveland Casting Plant, during the summer of 1997. The automated core evaluation system is being transferred to Ford's Process Development Center. Various sensor technologies are being presented to plants for incorporation into existing production processes.

3.4.2.2 Injection Molded Cores (Howmet). The approach taken for this task was to provide guidance and insight into the physics involved with the core injection molding process. In addition, work was initiated on the correlation of defects in the injected parts to process parameters. Although no final answers were established, several key defects were identified for investigation: particle segregation, porosity due to shrinkage events and relaxation of residual stresses induced during debinding and sintering. For segregation, a single-phase, non-Newtonian flow model was used for initial investigations. Porosity was initially assumed to be a last-to-cure type defect, analogous to porosity in solidifying metal. Residual stresses can be calculated with the stress analysis capabilities in ProCast or other FEM solvers.

Sufficient process information was gathered to carry out initial finite element simulations: injection material thermophysical property data were experimentally determined, core injection molding process parameters were characterized, part and part/die geometries were created or obtained from 3D solid CAD models, and die specifications were obtained.

Several parts were selected for validation of the core injection: a zigzag and a venturi combined configuration (Figure 3-70), and a generic turbine blade core with features similar to production geometry (Figure 3-71). The latter, tet-meshed with MeshCast (as shown in Figure 3-33), has realistic trailing edge exit slots and turnarounds. The other two simpler geometries were selected to provide simple test geometries to enable the study of flow induced segregation and density field variations that can occur during the core injection molding process.

Zigzag/Expansion Die Tooling

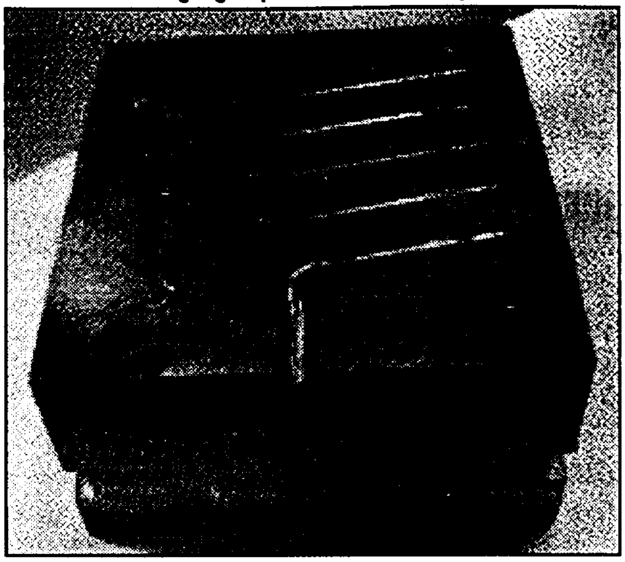

Zigzag/Expansion Die Unigraphics Model

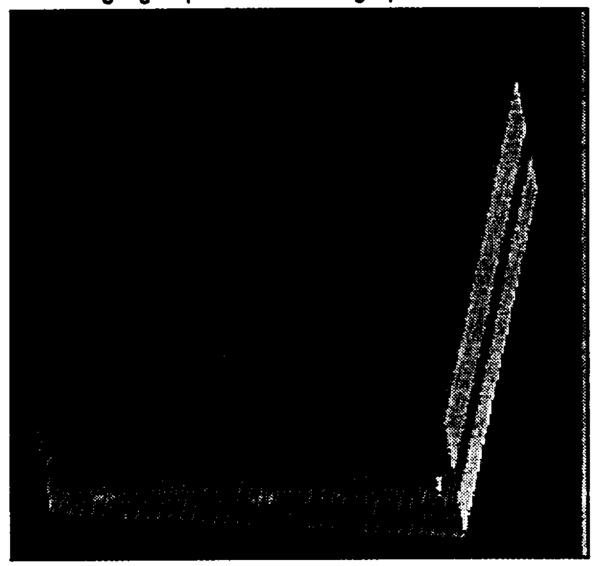

Figure 3-70. Zigzag and Expansion Die Tooling and CAD Models

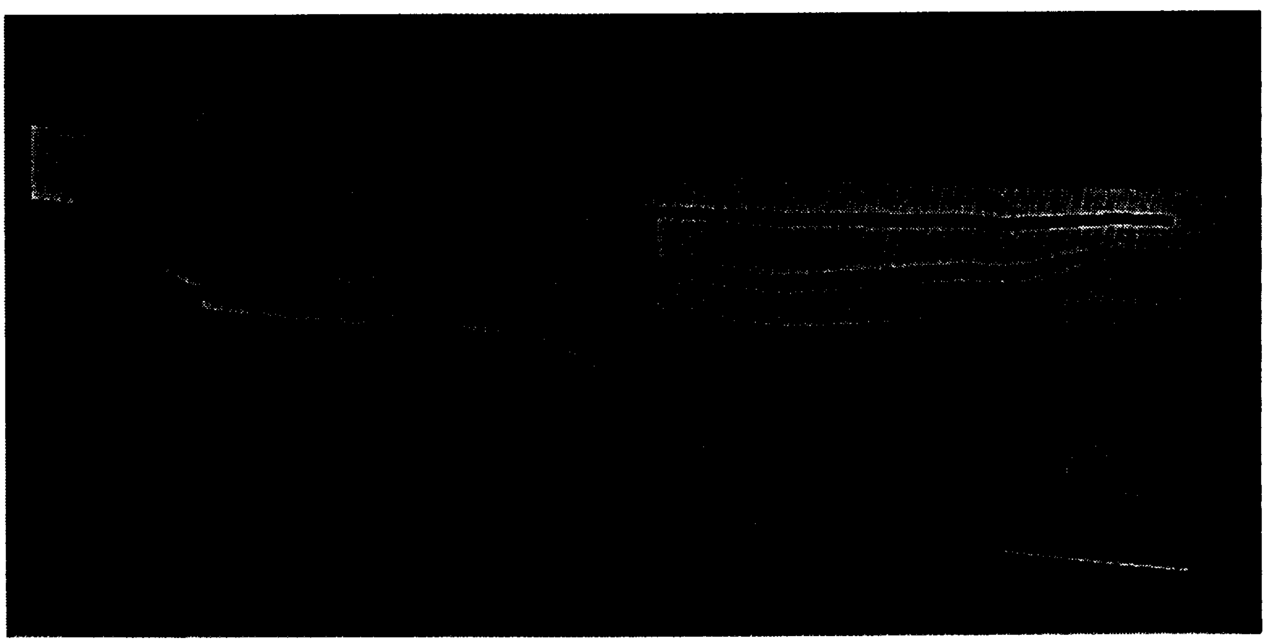

Figure 3-71. PIT Core Simplified Unigraphics CAD Model

Additionally, a turbine blade was also chosen for internal verification studies. It was selected because two pre-existing hexahedral meshes of differing element size were available. The results from these can be compared against a tetrahedral mesh. This will yield information on the non-Newtonian flow calculation's sensitivity to mesh type and mesh density in a complex geometry.

A software program was written by UES to determine the non-Newtonian coefficients, given the experimental viscosity as a function of temperatures and shear rate. The non-Newtonian simulations solved much slower than a standard mold filling solution. However, convergence and stability were excellent with very small time steps and the results appear physical. This showed that the equations for fluid motion seem to be solving correctly. However, more efficient solving routines need to be developed to improve performance for this class of problem.

Various boundary condition types were tested to determine those most appropriate for the injection process. Input solution control parameters were adjusted to better understand their effects on simulating mold filling and cooling processes. A partial list of these parameters includes time step sizes, convergence tolerances, free surface algorithms, and solution matrix solver schemes.

In order to validate actual injection runs, injection dies were instrumented.

Thermocouples were used to determine die temperatures, and pressure sensors were incorporated into the airfoil geometry die. Since the dies are under pressure, is it difficult to insert probes directly into the injection stream. Filling flow profiles will be determined by "short shooting" – that is the intentional incomplete filling of the die after beginning a normal injection run.

3.4.2.3 Injection Molded Cores (PCC). The approach was to determine the effect of each processing step on the product yield and dimensional tolerance. Because these problems are typically configuration dependent, multiple part numbers had to be evaluated with the new core system. When a satisfactory result was achieved on a part, then a production trial was conducted and, if this was successful then the core was placed into production. During the second year of this program, many part numbers were successfully transferred to the new core system and brought into full production with enhanced yield.

During the course of the program, the new core process was introduced on 40 parts/numbers. These were typically complex airfoil cores with tight dimensional requirements. Approximately 375,000 cores were produced and more than 100,000 castings shipped. The primary benefits of the new core process are higher yields on core production and better core dimensional control. The particular dimensional characteristic that is most improved is contour. This improvement is in turn reflected in enhanced wall control in the resulting castings. All of these effects lead to better overall casting yields.

3.4.2.4 Rapid Casting (Rocketdyne). The goal of this task for Rocketdyne was to validate the technology that had been developed in the previous tasks and help provide a means to transfer it into production. Two specific efforts were undertaken:

- The first effort performed validation tests on reverse engineering using computed tomography and appropriate conversion software, and

- The second included dimensional and metallurgical evaluation of the castings and the manufacture of additional castings representative of Rocketdyne's future product lines.

Software Evaluation for Reverse Engineering. Early efforts to apply reverse engineering to existing hardware, a gas generator housing, were labor intensive requiring significant edge smoothing and point manipulation. Further evaluation of software to speed up the data conversion process was required to facilitate the data file generation process.

In this final phase of the program, an industry review of the available software was made and comparison study performed. A Minuteman III Pressure Relief Valve component (that was to be used for a customer review) was selected as the candidate part for evaluating the software. The end product required for the customer review was a rapid prototype model of the existing valve.

Rather than creating surface models of each of the valve components, a more direct method of creating an STL model from existing hardware was selected. This enabled the reverse engineering methodology to be validated. Two software products, Materialise's CT-Modeller System Software Suite and ARACOR's Archimedes, were evaluated. Since the goal of the demonstration was to generate a rapid prototype model, the ability to go directly from the native CT image format to STL model seemed to offer significant reduction in process time over the point cloud to surface model methodology. Both Materialise and ARACOR were generous to offer evaluation copies of their software products for use and evaluation during the project time frame.

The Archimedes software was installed on a Silicon Graphics (SGI) workstation under the direction of the Information Technology (IT) department. At the time of this evaluation, SGI was the only supported hardware platform for Archimedes. The Materialise software was installed in DOS mode on a 100 MHz Pentium PC in the CT lab. Materialise would also run on the SGI platform, but the PC was more accessible to CT lab operations.

The valve was disassembled into its various components and scanned for total of 574 scan images. The valve body, the outlet adapter, and the end plug were individually scanned at every 1/2 mm on the SMS CITA-101B system with a 1 x 1 mm aperture. The remaining components were grouped together and scanned every 3/4 mm on the SMS CITA-201 linac system with a 3/4 x 3/4 mm aperture. The valve components are listed in Figure 3-72. All of the scan images were reviewed for completeness and the data stored in the native SMS image format for subsequent processing. Some sections had to be rescanned because of missed pulses from the linac or "rollover" of the 420 KV source. Figure 3-73 below shows a CT scan image.

Figure 3-72. Pressure Relief Valve Component Scans

Component	# Scans	Image Size	Pixel Size	Z-Aperture	Z-Step
Valve Body	197	876 x 711	0.08 mm	1 mm	1/2 mm
Outlet Adapter	89	511 x 531	0.08 mm	1 mm	1/2 mm
Plug	52	511 x 531	0.08 mm	1 mm	1/2 mm
Piston	76	120 x 119	0.29 mm	3/4 mm	3/4 mm
Spring	73	109 x 104	0.29 mm	3/4 mm	3/4 mm
Inlet Adapter	51	123 x 120	0.29 mm	3/4 mm	3/4 mm
Spring Plate	12	99 x 99	0.29 mm	3/4 mm	3/4 mm
Valve Seat	12	99 x 99	0.29 mm	3/4 mm	3/4 mm
Pivot	12	99 x 99	0.29 mm	3/4 mm	3/4 mm

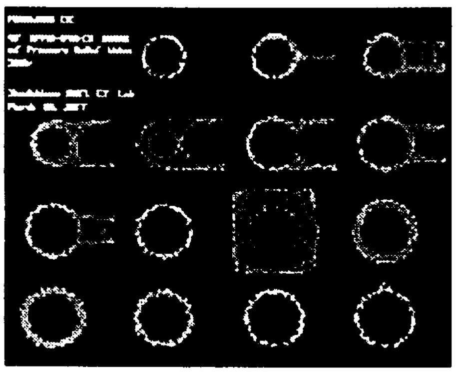

Figure 3-73. CT Scan Image of Hardware

Once the CT scans were completed, the data had to be converted to Materialise and Archimedes supported image formats. Archimedes required that all of the scan slices be in one, contiguous 16-bit or 8-bit integer file. To accomplish this, the SMS export feature was used to create 16-bit integer files for each individual scan. The UNIX concatenate function was then used in a programmed loop to append the files together by component. A header file was also created for each component to relate image rows, columns, pixel size, and vertical step size to the analysis software. Archimedes could then read these file pairs to process the data and generate a representative STL model.

The Archimedes software had some other specific requirements which partially dictated CT scanning parameters. Scan slices had to be consecutive and evenly spaced; no gaps or missing slices. This meant that even uninteresting regions such as a simple cylinder had to scanned at the same interval as more complex regions of the part. In one case the entire part had to be rescanned because of one bad scan that went undetected before the part was removed from the fixture. This was not the case with the Materialise software. Materialise reads in each scan as a separate image and obtains scan height and other image parameters from the header of the file being read. This enables scans to be made at irregular intervals and in any order. Though it was not tested, it may have allowed variation in image size as well.

While the Materialise software could also not read the native SMS floating point image files, it did include a conversion utility program, CT-Convert, which could read the exported 8-bit or 16-bit integer files. CT-Convert was used to input image row size, column size, pixel size, vertical spacing, etc., which was used to convert the each 16-bit integer file into a proprietary image format stored in a "patient" directory. Following this process, directories were created for each of the pressure valve components.

Materialise's Interactive Medical Image Control System (MIMICS) was then used to perform threshold based feature segmentation and generate a 3D volumetric datafile. The 3D datafile could then be read by Materialise's CT-Modeller (CTM) module to create the required STL model.

Imageware's RPM™ software was used as the standard by which to verify the STL model. Experience with the DTM laser sintering machine has shown RPM to be highly successful at producing an acceptable model. Though both ARACOR and Materialise claimed that their software produced "good" STL models and the STL model definition seems to be straightforward and well defined in industry, there appears to be a discrepancy between the algorithms used to check for open edges and multiply connected polygons. RPM reported thousands of open edges in the first attempt for both the Archimedes and Materialise STL models. Filtering options were then used to both reduce the data and further process the model before testing it with RPM.

On average, Materialise CT-Modeller was able to reduce the original STL models from several megabytes to a few hundred kilobytes. The number of reported open edges dropped dramatically from several thousand to only a dozen or so. The few remaining reported problems were easily correctable with the tools provided within RPM. Unfortunately, difficulty accessing the SGI workstation from an X-terminal in the CT lab prevented much experimentation with the filtering options provided within Archimedes. ARACOR offered to process the largest of the models, the valve body, to help meet schedule deadlines. The reduced model that was finally received was nearly 92 megabytes is size. The RS6000 system on which RPM was installed did not have sufficient resources available to handle a file that large. As of this writing, no determination of the resultant Archimedes STL model acceptability could be made. Materialise produced a model only 3-1/2 megabytes in size with few enough reported errors to correct and use for the demonstration. The difference in file sizes is probably due to differing parameters used in the filtering operation. This single sample should not be used to compare the capabilities of the two software packages. More controlled experiments with each of the systems still need to be made.

Results of the demonstration conclude that, although further work is required to fine tune the process for reverse engineering, it is conclusive that reverse engineering via computed tomography is greatly enhanced with the proper conversion software. Figure 3-74 below shows the CAD image of the scanned hardware and the final rapid prototype hardware next to the existing hardware that was used for reverse engineering.

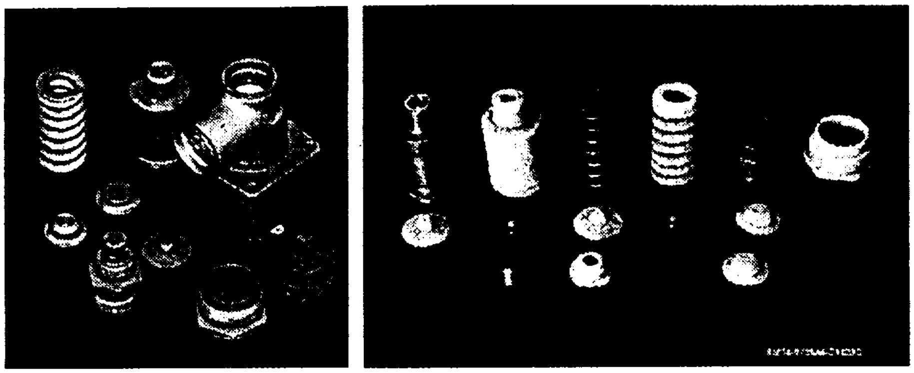

Figure 3-74. CAD Image of the Scanned Hardware and the Final Rapid Prototype Hardware Next to the Existing Hardware

Evaluation of Reverse Engineered Casting

Dimensional. The gas generator housing that was cast under Task 3 of this program was evaluated for dimensional and mechanical characteristics.

Dimensional data were gathered by the use of a Zeiss coordinate measurement system, which was set up to measure the outside profile of the gas generator body at discrete locations along the "Z" axis. One problem encountered was that the original model (STL file) utilized additional "machine stock" on the flange face. This extra material was not true or perpendicular to the gas generator body. Unfortunately, this was the only face used to orient the part, and made repeatable measurements very difficult to obtain.

Three gas generator bodies were measured using this system:

- The original polycarbonate casting pattern
- The subsequent casting derived from that pattern, and
- A polycarbonate pattern which was fabricated after an upgrade to the DTM Sinterstation.

The upgrade consisted of new galvanometers to the laser system which greatly reduced (if not eliminated) the "mirroring" of details on the surface of the sintered part.

Measurements of the parts indicated a great improvement towards the bottom (lower "Z" axis) where the tangent angle created by the forward flange face did not have a large impact. Visually, the difference between the parts was more dramatic. The mirroring observed in the first pattern was eliminated in the pattern fabricated after the galvanometer upgrade.

Metallurgical. Mechanical and metallurgical analysis of the cast gas generator housing was performed to assess the casting integrity as compared to conventionally cast Inconel 718. A materials evaluation plan was established to section tensile specimens from the casting and compare the results of the as-heat treated condition to the as-heat treated, homogenized and HIP'ed condition. Each specimen fracture surface was then studied using a scanning electron microscope to determine the effect of porosity. Metallographic samples of each condition were prepared to assess the healing effects of the HIP.

Tensile specimens were sectioned from the exhaust end (the long nozzle end) of the casting due to its consistent cross section and the semi-flat configuration which allowed for evaluating the properties of one zone.

The tensile results for the two conditions tested are shown in Figure 3-75. Specimens marked L and U are for standard solution heat treat and age and specimens marked T are for homogenization heat treated, HIP'ed and then solution and aged (samples marked T). Rocketdyne's Material Properties Manual data from cast-to-size Inconel 718 bars are included for reference. As can be seen, a significant increase in strength is obtained when the parts were HIP'ed. This is attributed to healing of the internal porosity. The cast-to-size bars are stronger, as expected, because of the gas generator configuration takes longer to cool and has a larger grain size.

Figure 3-75. Cast Inconel 718 Tensile Data

Temp (°F)	ID	UTS	YS	Elongation	RA	Comments
70	T-1	158.0	139.9	10.0	19.9	RA not accurate for flat specimens.
	T-2	162.0	141.9	11.0	34.3	RA not accurate for flat specimens.
	T-3	146.2	127.5	10.0	30.5	RA not accurate for flat specimens.
	T-4	156.8	141.0	9.0	27.4	RA not accurate for flat specimens.
		155.8	**137.6**	**10.0**	**28.0**	
70	L-1	127.2	100.3	6.2		No HIP or homogenization.
	L-4	124.6	98.9	6.5		No HIP or homogenization.
	U-01	134.5	98.4	9.3		No HIP or homogenization.
	U-03	130.9	97.7	8.1		No HIP or homogenization.
		129.3	**98.8**	**7.5**		
70	1-1	163.0	148.0	11.0	24.0	Data fromRocketdyne's Materials Properties Manual
	1-2	165.0	151.0	14.0	28.0	
	1-3	161.0	153.0	11.0	33.0	
	6-47	167.0	156.0	8.5	23.0	
	6-46	162.0	152.0	7.5	31.0	
		163.6	**152.0**	**10.4**	**27.8**	

Analysis of the specimen was performed on samples from each heat treat condition. The L and U specimen were analyzed and revealed significant levels of porosity that weakened the structure resulting in lower than anticipated mechanical properties. Figure 3-76 shows a typical fracture surface on the L samples. Figure 3-77 shows fracture surface analysis of the "T" specimen which had been HIP'ed. These specimens were considerably stronger.

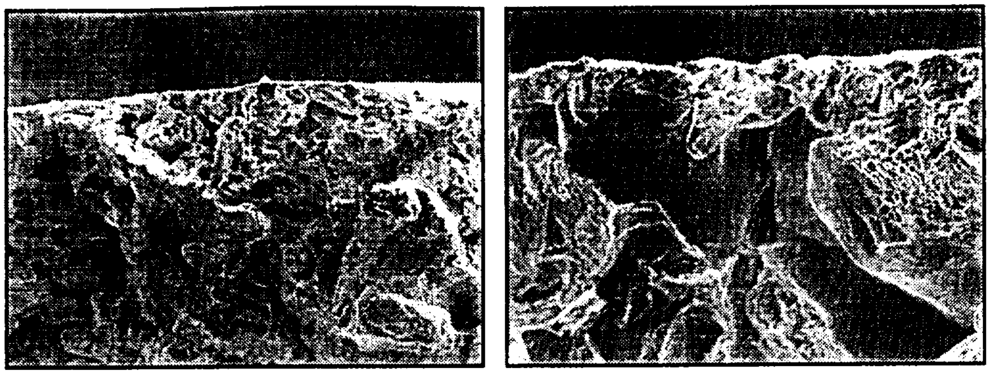

Figure 3-76. Fracture Analysis of pre-HIP and Homogenization Specimen (L Sample) Reveals Extensive Presence of Voids Due to Casting Shrinkage. The View on the Right is Magnified at 750X

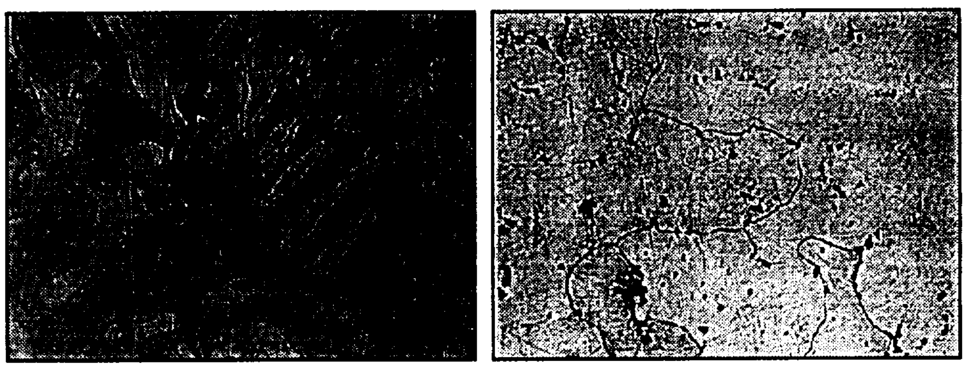

Figure 3-77. Significant Reduction in the Porosity Levels are Evident in the 100X Metallography Samples Shown of Samples Before and After Homogenization and HIP'ing

Metallography on T specimens further confirmed the elimination of much of the porosity (Figure 3-78).

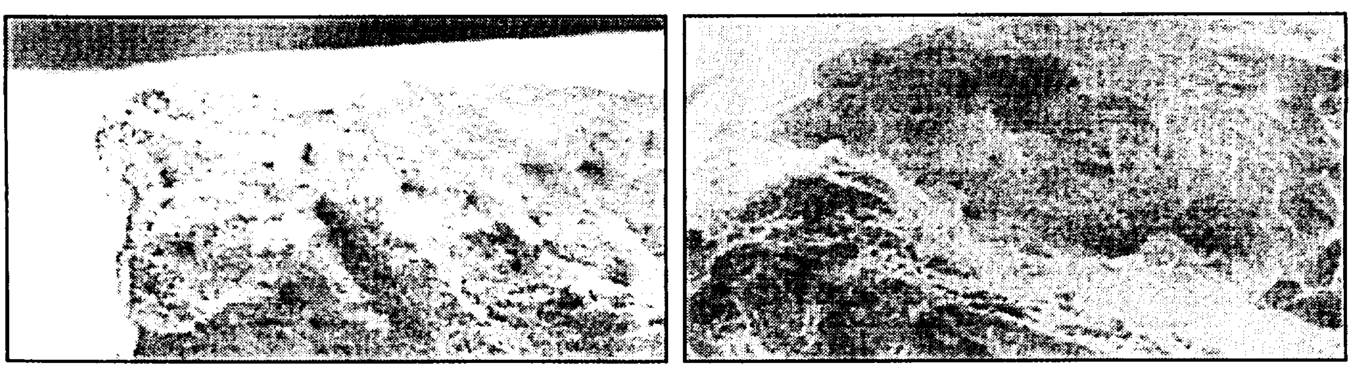

Figure 3-78. Fracture Analysis of Post-HIP and Homogenization "T" Specimen Reveals Little to No Porosity Due to Shrinkage. The View on the Right is of the Initiation Site Magnified at 600X

In conclusion, a methodology was established for producing castings using reverse engineering that produces a dimensionally accurate and metallurgically sound product.

Validation of the Thermally Controlled Solidification Process. The last effort performed by Rocketdyne in this task was focused on validating the TCS process (see Task 3) for Rocketdyne hardware. Two components, a turbine discharge housing and a center jet body, were selected for fabrication and evaluation

Fabrication of Turbine Discharge Housing. The first design selected for this effort was a 23" tall housing with a 22" diameter discharge flange and a 16" diameter inlet flange which was considered uncastable by conventional casting technology. The wall thickness were approximately 1/8" thick with about 1" thick flanges. The component is intended for use on turbopumps for an advanced rocket engine and functions as a 90° turbine exhaust gas flow elbow to interface with roll control nozzle ducting.

Based on the Lockheed Martin effort discussed in Task 3, PCC's TCS technology for the application to rocket engine hardware was evaluated. An electronic design was coordinated with PCC process engineers and electronically sent to an FTP address. PCC then converted the electronic design into a stereolithography (STL) format which was used in a SLA prototyping machine, located at PCC, to produce the "wax" pattern. The rapid prototype pattern was then gated in preparation for the molten alloy filling process and invested using a ceramic shell method that PCC had established for the TCS process.

Figure 3-79 below shows the final casting adjacent to the SLA pattern used to produce the casting with the TCS process. With the exception of a few minor defects that were weld repaired, the casting was in excellent shape and was considered a deliverable quality casting on the first attempt.

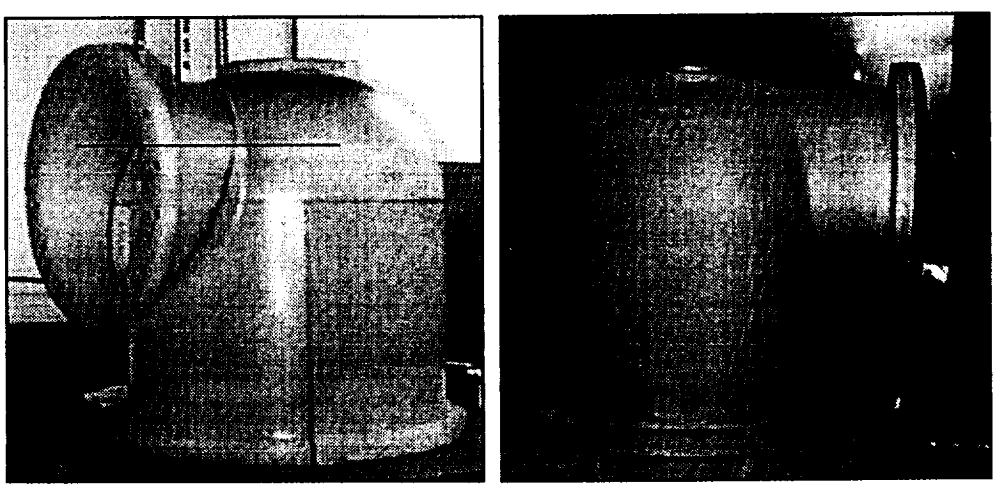

Pattern *Casting*

Figure 3-79. SLA Pattern and Casting of the Turbine Discharge Housing Cast using PCC's TCS Process

By demonstrating this part could be cast, a weight savings of approximately 200 pounds per part is achieved.

The direct cost savings that can be realized are approximately $25,000 per pump ($50,000 per engine). This takes into account only the fabrication cost savings and not other costs associated with weight penalties saved, reduced envelope requirements, and ease of assembly and access port accessibility.

Prior to confirming the success of this process, the program plans were to use a centrifugal cast billet that would have been machined and welded to a shape that retained only the internal and mating surfaces. With the success of this effort, the program has converted to this fabrication technique.

Center Jet Casting. The center jet casting was produced as a demonstrator for an advanced programs turbopump design. The function of the component produced is as a fluids mixer in which a fluid enters through the side inlet elbow and mixes in the housing with the other fluid.

Although the component requirement had already been met by machining the part from a solid billet, a decision was made to reproduce the part using the TCS process in an effort to assess cost and schedule savings should the part be put into production.

A modified electronic file was delivered to PCC where a decision was made to cast the part in two pieces rather than the original one-piece design. The separately cast pieces would then be welded together at PCC and delivered to Rocketdyne in the assembled condition. PCC electronically segmented the file into two pieces that were then converted into STL formats. The STL files were then loaded into the rapid prototyping machine located at PCC and a pattern of each file was made.

The patterns were then gated and assembled in a typical method used in the investment casting process. The ceramic invested assembly was then cast in a similar method that has been previously described for the TCS process. Figure 3-80 shows the resulting castings and after fit up and welding.

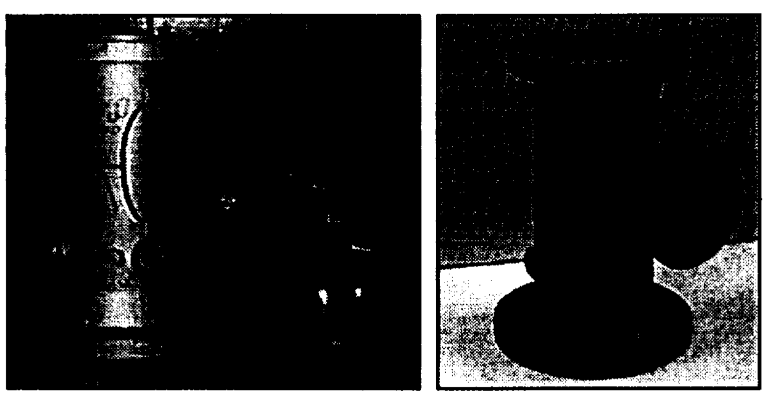

Cast Parts Prior to Welding *Finished Assembly*

Figure 3-80. Center Jet Casting Produced Through the TCS Process

Multipiece, conventionally fabricated aerospace grade hardware can be redesigned for casting and rapid prototyping "wax" patterns made for producing those castings.

The TCS process had been validated for rocket engine castings and, as a result of the success demonstrated on the AITP program, it will be used for producing production hardware.

3.4.2.5 Rapid Casting (Lockheed Martin). Per the approach set forth by the Cooperative Agreement with the Precision Casting Consortium for the Aerospace Industry Technology Program, the demonstration components were to be characterized metallurgically and mechanically, and performance tested via pressurization tests (e.g., operating, proof, and burst pressures). Chemical analysis was performed to verify that the compositions of each CF-8C stainless steel LO_2 Tank Elbow casting met the requirements of ASTM A743. No apparent abnormalities in the chemical compositions were observed, as shown in Figure 3-81.

Figure 3-81. Chemical Compositions for Each Casting Lot, as Measured by PCC, as Compared to the Requirements of ASTM A743 for the CF-8C Casting Alloy

Lot No.	C	Mn	Si	Cr	Ni	Co	Mo	Cb	Al	Fe	N2	W
005	0.03	0.65	0.6	18.5	10.7	0.03	0.02	0.6	0.01	63.5	0.007	0.05
006	0.04	0.8	0.6	18.3	10.6	0.02	0.02	0.6	0.02	62.7	0.007	0.05
007	0.04	0.8	0.6	18.3	10.6	0.02	0.02	0.6	0.02	62.7	0.007	0.05
ASTM A743	*0.08 max*	*1.50 max*	*2.0 max*	*18.0-21.0*	*9.0-12.0*	*8 x C - 1.0*	---	---	---	*Bal.*	---	---

Metallographic analysis of specimens taken from Lot 006 showed a duplex ferrite-in-austenite microstructure of the cast CF-8C alloy (Figure 3-82). The amount of ferrite varied from 8 to 15%, averaging 12%, which is typical of cast CF-8C. Grain size measurements were performed using a Beuhler Omnimet II image analyzer and the equivalent circular diameter method. A total of nineteen measurements were taken. The average grain size varied from 0.020 to 0.052 in., with some portions of the casting exhibited even larger grains. The secondary dendritic arm spacing ranged from 0.0013 to 0.0029 in., averaging 0.0015 in. The microstructure of the TCS cast CF-8C as compared to that of conventionally cast CF-8C (also shown in Figure 3-82) shows that the TCS casting has slightly larger secondary dendritic arm spacing and larger concentrations of ferrite.

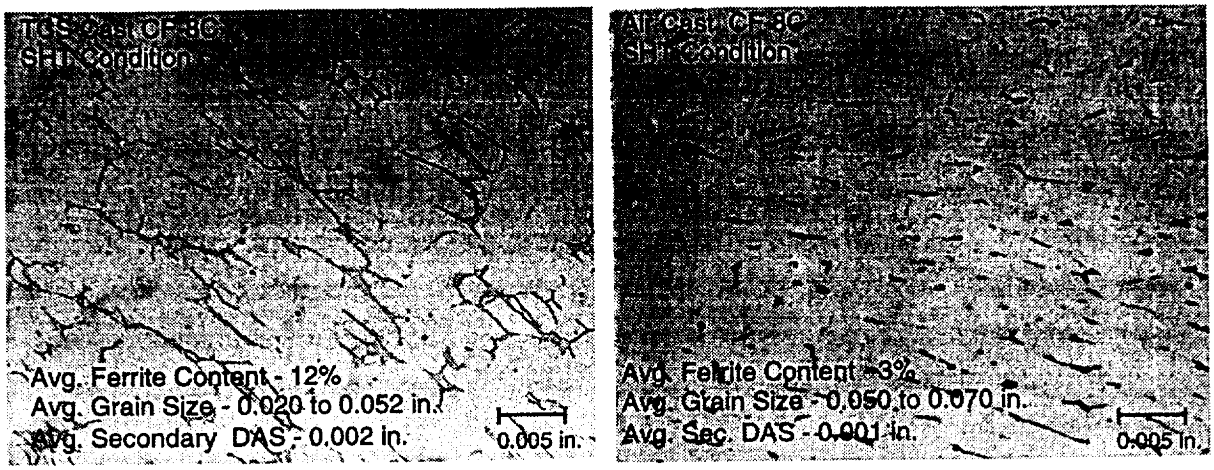

Figure 3-82. Photomicrograph of Representative TCS Casting (left) and Conventional Air Casting (Right) Showing Duplex Ferrite-in-Austenite Microstructure of CF-8C. (TCS Casting Etch: 10% Oxalic, Electrolytic - Air Casting Etch: 20% NaOH, Electrolytic)

Tensile specimens were excised from Lot 006. The specimen configurations (subsized) for the room temperature and -320°F specimens are provided in Figure 3-83. Results for tests performed at room temperature and -320°F are provided in Figure 3-84. The average room temperature test results of samples excised from Lot 006 exceeded the minimum requirements per AMS 5362 (i.e., minimums of 30 ksi yield strength, 70 ksi ultimate tensile strength and 30% elongation). The average room temperature properties for Lot 006 were 35.1 ksi yield strength, 75.2 ksi ultimate tensile strength and 44.2% elongation. These results are comparable to the "typical" published room temperature tensile properties for cast CF-8C. The average -320°F temperature tensile properties were 41.2 ksi yield strength, 128.7 ksi ultimate tensile strength, and 18.0% elongation.

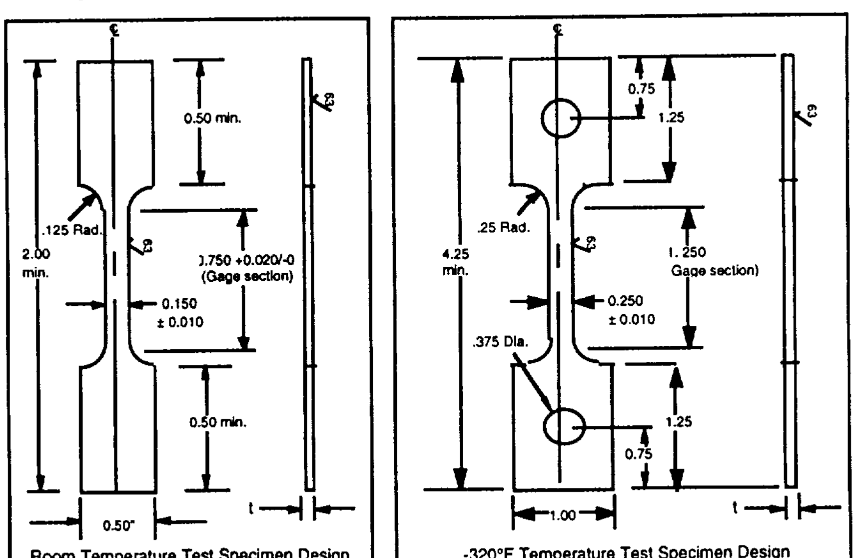

Figure 3-83. Test Specimen Configurations for Performing the Room Temperature and -320°F Tensile Tests of Lot 006 [TCS LO_2 Tank Elbow Casting (CF-8C SHT Condition)]

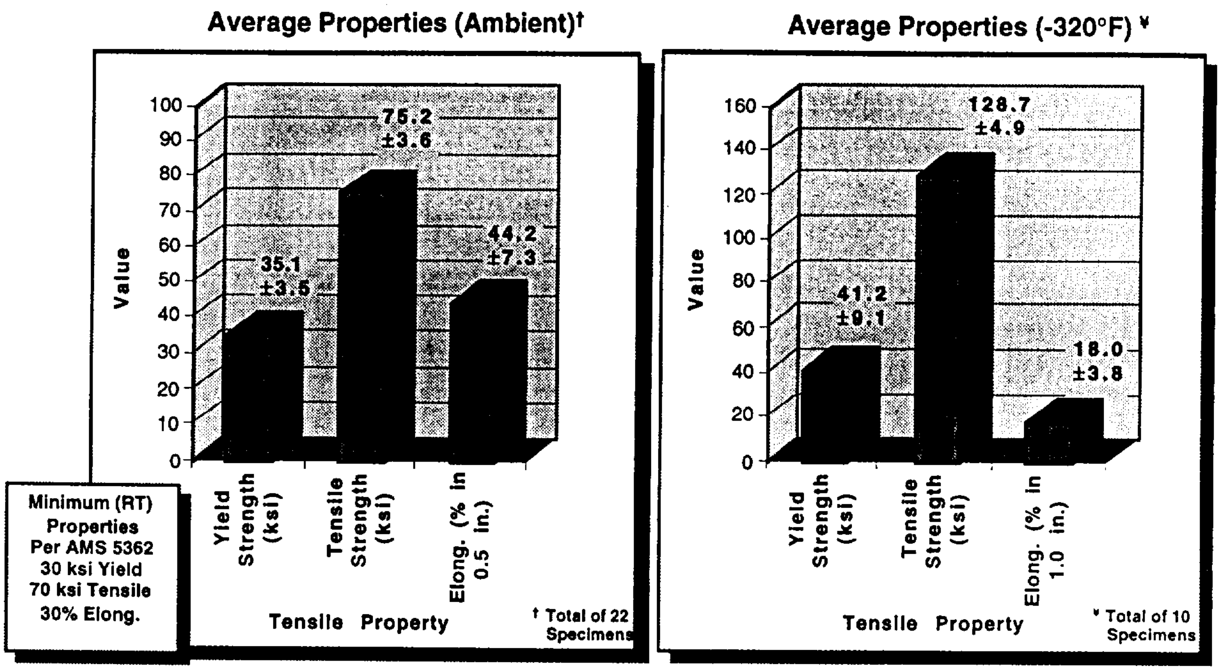

Figure 3-84. Average Test Results for Excised Tensile Specimens Taken from Lot 006 [TCS LO_2 Tank Elbow Casting (CF-8C SHT Condition)] Tested at 70°F and -320°F. Note that the Minimum Required Tensile Properties at Room Temperature per AMS 5362 were Met or Exceeded

Lot 005 of the TCS cast LO_2 Tank Elbows was pressure tested using the test conditions shown in Figure 3-85. These tests were conducted at Lockheed Martin Astronautics' Engineering Propulsion Lab in Denver, CO. Figure 3-86 shows the test setup, i.e., test fixture, instrumented casting (thermocouples and strain gages), and pressurization system (pressure lines, fill and drain, etc.). Upon successful hydrostatic proof testing, conducted at 70°F, 127 psi, with a 5 minute hold time, the thin-walled casting was drained and dried. The part was then filled with LN_2 and pressurized to the designed burst pressure of 213 psi and held at pressure for 30 seconds. At this point, the casting was pressurized until failure, which occurred at 304 psi. Note that the designed operating pressure was 85 psi, therefore the component failed at 3.6 times the operating pressure. The failure mode/mechanism is shown in Figure 3-87, which can best be described as the component extruding itself out of the test fixture. Note that the casting after completion of the burst test was completely intact.

Figure 3-85. Test Conditions for Pressurization Testing of 0.055 in. Thick Wall, 11 ID LO_2 Tank Elbow Casting (CF-8C SHT Condition) (Lot 006)

Test	Pressure (psi)	F.S.	Hold Time (min.)	Test Medium	Temp. (°F)
Proof	128	1.5	5	Deionized Water	70
Visual/Leak	30	---	As Req.	Deionized Water	70
Helium Leak	8	---	As Req.	Gaseous Helium	70
Burst	213	2.5	0.5	LN_2	-320
Destructive Burst	TBD @ Failure	---	---	LN_2	-320

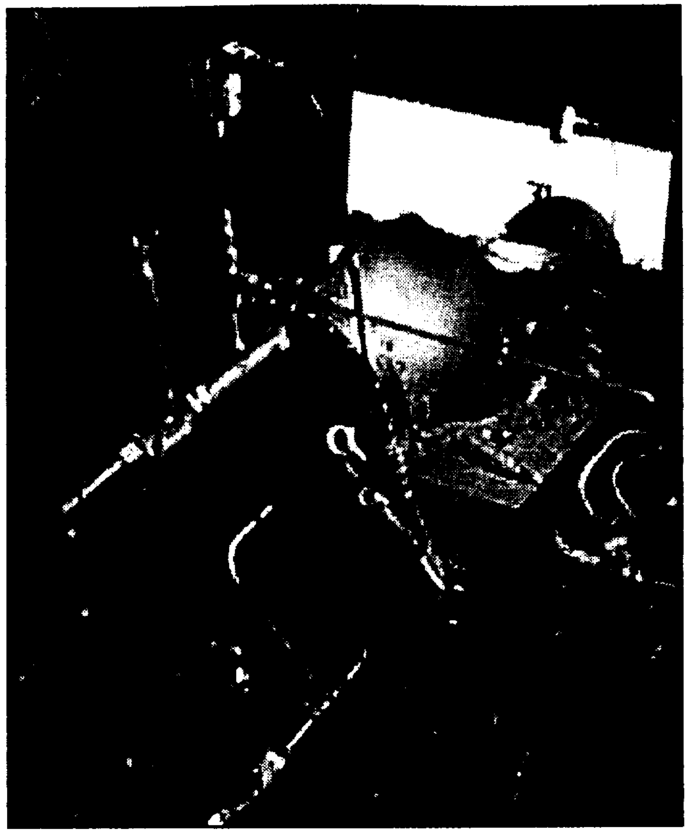

Figure 3-86. Pressurization Test Setup for Testing the TCS Cast 0.055 in. Thick Walled, 11 in. ID LO_2 Tank Elbow (Alloy CF-8C, SHT)

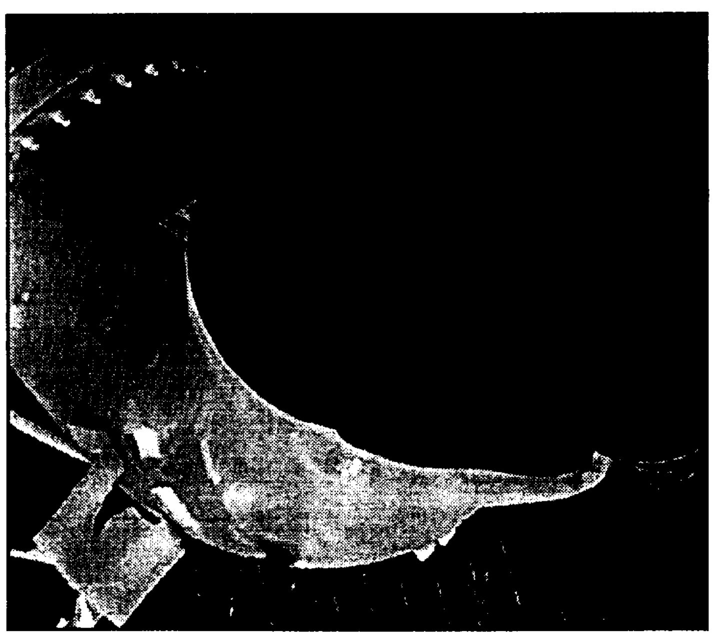

Figure 3-87. Photograph of the TCS Cast 0.055 in. Thick Walled, 11 in. ID LO_2 Tank Elbow (Alloy CF-8C, SHT) Following Successful Burst Testing. Test Completed at 304 psi vs the Designed Burst Pressure of 213 psi. Note that the Thin-Walled Casting is Completely Intact

Summary of TCS Process Development Study. A process has been developed to produce large, low cost, thin-walled propellant feedline components to pressure vessel quality standards utilizing SLA rapid prototype patterns, low expansion shell systems and the Thermally Controlled Solidification process. This process is applicable to thin-walled propellant feedline components having a variety of configurations. The 11 in. OD thin-walled LO_2 Tank Elbow TCS casting represented a thin-walled castability record for its combined size of over 800 in.^{2} with a wall thickness of 0.055 in. for Precision Castparts Corp. It was the first time that a large SLA pattern with a thin-wall had been successfully combined with a low expansion shell system. It was also the first time that an "air" alloy had been cast in the new large capacity TCS furnace. PCC also developed new high temperature mold supports for use with the TCS casting process. Mechanical property characterization test results of specimens excised from a "production-like" TCS casting also showed that the minimum tensile properties (per AMS 5362) could be met and/or exceeded via a casting process which generally has slow cooling characteristics. Also, the integrity of the thin-walled casting was further substantiated via the pressurization testing, which showed that the predicted burst pressure was exceeded by 140%.

Figure 3-88 provides a comparison of the recurring cost (normalized) for the 11 in. ID LO_2 Tank Elbow fabricated via the conventional process (formed and welded) and investment casting. It is assumed that in a production mode, cost analysis would show that the total number of builds would justify the fabrication of the wax injection mold or use of "soft tooling" for production of the investment casting patterns, therefore the cost estimate does not include the cost for STL patterns. The cost per completed casting includes dye penetrant inspection, radiographic inspection, dimensional inspection, heat treatment, weld repair, and final machining per the requirements of the engineering drawing. As compared to the conventionally fabricated 11 in. ID, 321 stainless steel Atlas IIAS LO_2 Tank Elbow's actual cost, the casting approach provides a 55% recurring cost reduction. Upon

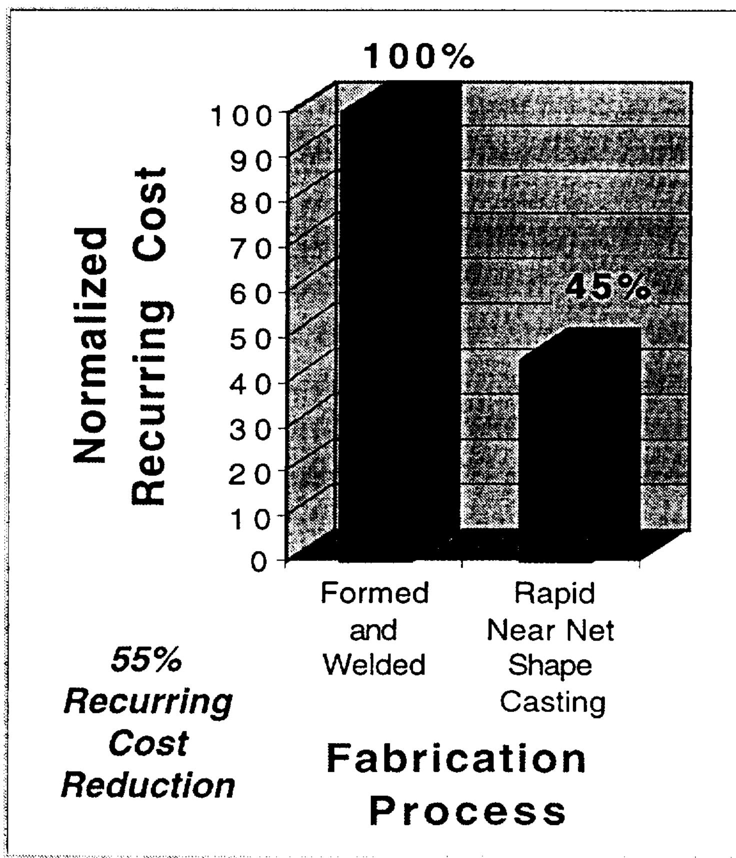

Figure 3-88. Comparison of the Recurring Cost (Normalized) of the 11 in. LO_2 Tank Elbow Fabricated Both Conventionally and as a Casting

additional development and application of the TCS process, it is presumed that the recurring cost savings inherent to this process will further improve.

The development cycle for fabrication of the thin-walled LO_2 Tank Elbow using the Rapid, Near-Net Shape Casting approach versus conventional methods was significantly reduced, as shown in Figure 3-89. Following some initial development of the TCS process for casting large, thin-walled structures using STL patterns, it is estimated that the total development cycle for components with similar configurations (e.g., thin-walled, extended feed distances, etc.) could be easily completely in twenty weeks or less. As compared to the development cycle of forty weeks for fabrication of the component with conventional processes (e.g., formed and welded), the Rapid, Near-Net Shape Casting approach results in a 50% reduction in development cycle.

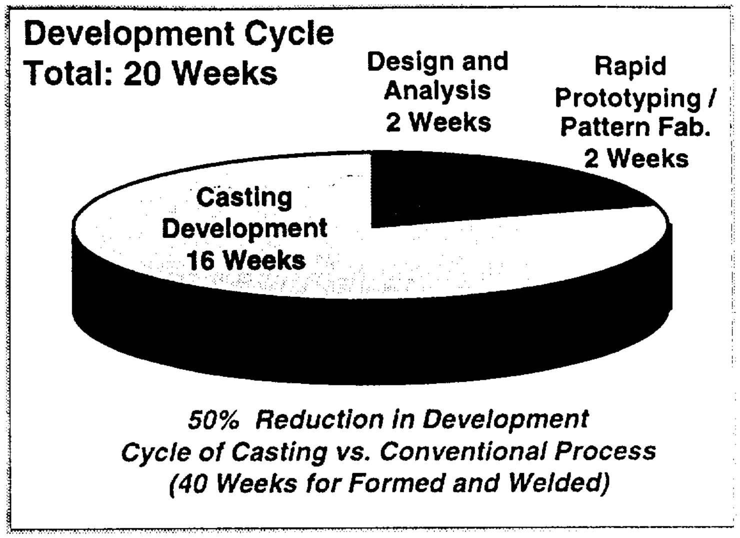

Figure 3-89. Estimated Cycle for Development of the Thin-Walled 11 in. ID LO_2 Tank Elbow Casting Using the Rapid, Near-Net Shape Casting Approach

Technology Transfer to Various Lockheed Martin Applications. As part of the technology transfer effort of Aerospace Industry Technology Program, the Rapid, Near-Net Shape Casting process was evaluated and/or utilized for various Lockheed Martin Astronautics' applications (Figure 3-90). The approach for producing low cost components in a short development cycle was successfully implemented on several programs including Defense Systems and Atlas IIAR, and has significant potential for application on others. The cost to fabricate the stainless steel outlet nozzles for Atlas II-AR's Cryogenic Testing of Propulsion Module and RD-180 Hot Fire Test Stands was reduced from \$50k to 14.3k per part. The weight of the cast aluminum (A357-T6) Reaction Wheel Bracket for Defense Systems was reduced by 58% with a cost savings per each unit of approximately 80% over the previous welded component design. The proposed cast design for the 51 in. OD Outlet Sump for EELV showed a potential life cycle cost savings using the conventional investment casting process greater than \$10.5M.

Key Conclusions. The following key conclusions were reached as a result of the investigation reported here:

- It was demonstrated that conventionally fabricated launch vehicle components can be converted into low cost, single piece castings in a shortened development cycle using the Rapid, Near-Net Shape Casting process.

- **Atlas II-AR**
  - **Nozzles for Cryogenic Testing of Propulsion Module and RD-180 Engine Hot Fire Test Stand**
  - **Feedlines**
- **Defense Systems**
  - **Reaction Wheel Bracket**
- **Commercial Applications**
  - **CommLink's Two Axis Gimbal**
- **EELV**
  - **Sump Outlets**
  - **Propulsion Module Heat Shields**
  - **Feedlines**
  - **Support Brackets**
- **RLV**
  - **Feedlines**
  - **Brackets**

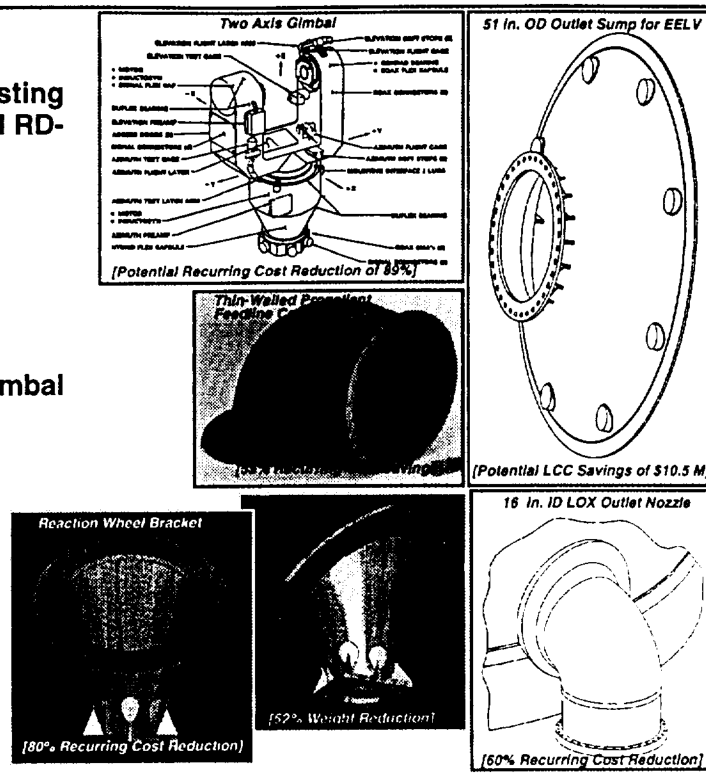

Figure 3-90. Examples of Various Lockheed Martin Applications Evaluated for or Fabricated with the Rapid, Near-Net Shape Casting Process

- While advanced casting simulation software shows significant technical merit and potential for decreasing the cost and cycle of casting development, its application to thin-walled castings having extended feed distances requires additional study.
- Rapid prototyping, particularly the STL process using the QuickCast™ technique, is a cost and schedule effective means of fabricating thin-walled patterns for investment casting development. Its use in a production environment is determined by cost analysis, i.e., dependent upon the recurring cost of patterns, total number of builds, and cost to design and machine hard tooling.
- Use of the conventional or "static" investment casting process for fabricating stainless steel propellant feedline components is dependent upon the component design, particularly wall thickness, feed distance, etc. Attempts to cast a 0.100 in. thick, 11 in. OD LO_2 Tank Elbow resulted in significant misrun due to reduced fluid flow of the molten metal through the thin-walled cross section and higher than expected amounts of heat loss.
- A process was developed to cast large, low cost, thin-walled (0.055 in.) propellant feedline components to pressure vessel quality standards utilizing STL patterns, a new low expansion shell system, and the recently developed Thermally Controlled Solidification process. Preliminary mechanical property characterization test results of specimens excised from a "production-like" TCS casting showed that the minimum tensile properties (per AMS 5362) could be met and/or exceeded via a casting process which generally has slow cooling characteristics. Also, the structural integrity of the thin-walled casting was further substantiated via the pressurization testing, which showed that the predicted burst pressure was exceeded by 140%.

3.4.3 Casting Design Guidelines (Robinson Products)

As part of the AITP Precision Casting consortium's program, Robinson Products' was tasked with preparing guidelines for castings. The result of this effort is presented in Appendix C. It includes both general guidelines and the application of specific technology developed under this program.

4.0 SUMMARY

A two-year program was conducted to develop and commercially implement selected casting manufacturing technologies to:

- Enable significant reductions in the costs of castings,
- Increase the complexity and dimensional accuracy of castings, and
- Reduce the development times for delivery of high quality castings.

Many of the process problems in producing cost effective, near net shape castings are common whether or not the casting design is for 10 space launch vehicles, 100 aircraft, or 100,000 automobiles. The alloys, tolerances, quality criteria, and production volumes certainly differ, but the fundamental physics required to quantitatively understand and control the manufacturing processes is the same. The management of the companies in this Cooperative recognized this and committed to jointly develop the innovative manufacturing technologies necessary for their companies to compete world-wide in future markets.

The overall objective of this program was to develop technology to increase the competitiveness of the U.S. casting industry. Several barriers had been identified that would have to be overcome to meet this overall objective. Tasks were set up to address each barrier and the key accomplishments are each task are presented below.

TASK 1.0 – ADVANCED SIMULATION TECHNOLOGY FOR CORE MOLDING

The objective of this effort was to investigate and apply computer aided engineering (CAE) tools and methods in the design and manufacture of air blown sand cores, associated core box tooling and real-time process controls.

At Ford, an experimental core machine was designed and built, real-time non-destructive test methods were evaluated, methods to evaluate resin bond strength were explored, sensors for monitoring all aspects of the core blow process were investigated and control and data acquisition systems were evaluated. Best practices for these efforts and the integrated controls and measurements systems were transferred to the Cleveland Casting Plant (CCP) in the second year.

The University of Alabama measured physical properties that affected transport and reaction of catalyst gas in a resin core including permeability and effective diffusivity. A resin binder was selected and equipment designed and built and screening experiments were conducted to determine which core properties had major impacts on transport properties.

Auburn University developed a system for quantifying compaction characteristics and permeability of resin coated silicon aggregate as a function of pressure, particle size, particle angularity, and resin coatings. Experimental instrumentation was designed and fabricated and viscosity measurements made.

The NASA-LeRC Computational Materials Laboratory assessed two-phase flow to understand granular flow in the core filling process. The complexity of the numerical techniques made this approach impractical.

Ford worked with UES and Aracor to study sand density during filling analytically and anchored the models with computed tomography. Finally, Ford designed and built a core box with clear windows to photograph the sand core filling process. This system was used during the second year to develop experimental data on core filling.

TASK 2.0 – INTELLIGENT PROCESS CONTROL OF CORE MOLDING

The Task 2.0 effort included both experimental and analytical thrusts to better understand the core injection molding and sintering processes. The primary focus of the experimental efforts was to characterize the process parameters that have a strong impact on dimensional control issues of injection molded cores during their fabrication. Findings from the experimental efforts at Howmet and PCC were transitioned into the production core making facilities with favorable results.

UES was chartered to evaluate and develop analysis methods and tools within ProCast that can be used to analytically predict the core injection molding process and provide insight into coupled fluid flow and heat transfer effects such as particle segregation (density variations), core porosity, and non-fill problems. It was found that the ceramic particle density variations within injection molded cores could not be adequately correlated to basic flowfield results. In order to accurately predict particle density variations a multiphase flow model is required. Auburn developed an empirical data base to evaluate dimensional changes occurring in ceramic core materials during the sintering stage of core processing.

GE and ARACOR developed the software and hardware to enable the use of 2.5D X-Ray techniques to enable near, real-time, three-dimensional evaluation of cores and/or castings during the production cycle. These tools allow direct comparison of actual part geometric data to known reference or CAD solid models and theoretically could be used to eliminate out of specification parts earlier in the casting production cycle and reduce casting scrap rates.

TASK 3.0 – RAPID, NEAR-NET SHAPE CASTING

The objective of this task was to shorten the cycle time for the fabrication of high quality castings by utilizing rapid prototyping technology.

Rocket engine and launch vehicle components that had previously been manufactured using conventional machining and welding techniques were selected. Two different approaches were used to achieve electronic designs of the hardware. The first approach used reverse engineering to produce a CAD file; the second approach applied the more traditional CAD techniques to generate an electronic model of a systems component. CAD models, created with each technique, were used to generate STL files for the fabrication of rapid prototype patterns. These patterns were used in the second year to produce investment castings.

Rocketdyne also investigated Selective Laser Sintering (SLS) to produce metallic components directly from the CAD. The objective of this effort was to evaluate the feasibility of using Rapid Prototyping as a means of forming a green part which could be subsequently sintered to high density and near net shape. Selective Laser Sintering of metals was demonstrated to be a potential method of Free Form Fabrication of parts and dies, but much work is still needed to refine the process as a production viable tool.

TASK 4.0 – TECHNOLOGY TRANSFER AND IMPLEMENTATION

The task was established to help provide a path to insure that as the technology was developed on this program it would be transferred into production. Ford, Howmet, PCC, Rocketdyne, and Lockheed Martin each had tasks to make sure the technology was implemented.

Ford focused on implementing technology developed during the evaluation of their experimental core machine. The key piece of technology that was transferred into production was the laser inspection device to insure core boxes were clean.

Howmet and PCC each used the statistical data acquired during measurement of the cores to improve the dimensional control of their ceramic cores. This technology was implemented on several different cores.

Rocketdyne and Lockheed Martin each focused on how to apply rapid prototyping to produce castings. Rocketdyne implemented novel software to help produce rapid prototyping patterns and both Rocketdyne and Lockheed Martin, in conjunction with PCC, implemented thermally controlled solidification (TCS) technology to produce castings for production. TCS casting is a technique which uses rapid prototype patterns and a thermal gradient furnace to make extremely thin-walled casting. Finally, technology demonstrated on this program to make metallic rapid prototype parts at Rocketdyne will be used to produce injectors for an Air Force program.

APPENDIX A

MULTI-PHASE TRANSPORT MODELING

Whether considering processes such as core blowing or wax slurry injection, particle segregation is of concern. Segregation can be due to differences in particle size, density and shape. However, differences in particle size will normally dominate the resulting segregation. This paper describes a mathematical model which can predict particle segregation in densely packed granular flows. The basis of this model comes from Ph.D. thesis of Syamlal.[1]

Mathematical Model

It is assumed that the particle population is characterized by a continuous distribution of particle sizes, shapes and densities. These continuous distributions are then approximated by discrete groups. In all, m groups are considered. Each group is characterized by its diameter (d_k), density (ρ_k) and sphericity (ϕ_k). Sphericity is defined as,

$$\phi = \frac{surface\ area\ of\ a\ sphere\ of\ equal\ volume}{surface\ area\ of\ the\ particle} = \frac{(36\pi)^{\frac{1}{3}}\ V_p^{\frac{2}{3}}}{S_p}$$

where, V_p and S_p are the volume and surface area of the particle. It is assumed that these m particle groups are suspended in a fluid phase. The fluid phase density is denoted as ρ_f. Using these definitions, the bulk density of our mixture can be computed as,

$$\rho_{bulk} = \epsilon_f \rho_f + \sum_{k=1}^{m} \epsilon_k \rho_k$$

[1]Syamlal, M. 1985, Multiphase hydrodynamics of gas-solids flow. Ph.D. Dissertation, Illinois Institute of Technology, Chicago, Illinois.

where, ϵ_f represents the volume fraction of the fluid phase and ϵ_k represents the volume fraction of granular phase k. Since we are considering a saturated mixture, the volume fractions must sum to unity.

$$\epsilon_f + \sum_{k=1}^{m} \epsilon_k = 1$$

The mass balance for each phase can be formed using a slightly modified form of our familiar single phase continuity constraint. Note that there is no mass transfer between groups being considered.

For the fluid phase,

$$\frac{\partial}{\partial \tau}\left(\epsilon_f \rho_f\right) + \nabla \cdot \left(\epsilon_f \rho_f V_f\right) = 0$$

For the k-th granular phase,

$$\frac{\partial}{\partial \tau}\left(\epsilon_k \rho_k\right) + \nabla \cdot \left(\epsilon_k \rho_k V_k\right) = 0$$

The terms V_f and V_k represent the velocity of the fluid and k-th granular phase. Using the same approach, the momentum equations are written as,

For the fluid phase,

$$\frac{\partial}{\partial \tau}\left(\epsilon_f \rho_f V_f\right) + \nabla \cdot \left(\epsilon_f \rho_f V_f V_f\right) =$$

$$-\epsilon_f \nabla P + \epsilon_f \rho_f g + \nabla \cdot \left(\epsilon_f \mu_f \nabla V_f\right) + \sum_{k=1}^{m} F_{fk}\left(V_k - V_f\right)$$

For the k-th granular phase,

$$\frac{\partial}{\partial\tau}\left(\epsilon_k \rho_k V_k\right) + \nabla \cdot \left(\epsilon_k \rho_k V_k V_k\right) =$$

$$-\epsilon_k \nabla P + \epsilon_k \rho_k g + \nabla \cdot \left(\epsilon_k \mu_k \nabla V_k\right) + F_{kf}\left(V_f - V_k\right) + \sum_{j \neq k}^{m} F_{kj}\left(V_j - V_k\right) - \nabla P_s$$

Going from left to right, the momentum terms account for the following phenomena:

$\frac{\partial}{\partial\tau}\left(\epsilon_f \rho_f V_f\right)$ represents the temporal acceleration of the fluid phase.

$\nabla \cdot \left(\epsilon_f \rho_f V_f V_f\right)$ represents the spatial acceleration of the fluid phase.

$-\epsilon_f \nabla P$ represents the pressure force acting on the fluid phase.

$\epsilon_f \rho_f g$ represents the body force acting on the fluid phase..

$\nabla \cdot \left(\epsilon_f \mu_f \nabla V_f\right)$ represents the viscous force acting on the fluid phase.

$\sum_{k=1}^{m} F_{fk}\left(V_k - V_f\right)$ represents the inter-phase drag force acting on the fluid phase.

The F_{fk} coefficient in the inter-phase drag term is computed considering the drag forces that are acting on particles suspended in a viscous fluid. From basis fluid dynamics, we can compute the drag force per unit volume as,

$$\frac{F}{V} = \frac{\frac{1}{2}\rho_f U^2 (C_D)_k A_f}{V} = \frac{3}{4}\frac{\rho_f U^2 (C_D)_k}{d_k}$$

Weighting this expression by the presence of the fluid and k-th granular phase, the F_{fk} term becomes,

$$F_{fk} = \frac{3}{4}\frac{\epsilon_f \epsilon_k \rho_f (C_D)_k}{d_k} \left|V_f - V_k\right|$$

The drag coefficient, $(C_D)_k$, is computed as follows:

A correction factor derived by Syamlal & O'Brien[2] is used to relate the drag coefficient of an isolated particle to a multiparticle systems.

$$(C_D)_k = \frac{(C_D)_{ip}\left(\frac{Re_k}{V_r}\right)}{V_r^2} = \frac{(C_D)_{ip}\left(Re_k^{'}\right)}{V_r^2}$$

The drag coefficient for an isolated particle, $(C_D)_{ip}$, is computed using the correlation developed by Haider and Levenspiel[3],

$$(C_D)_{ip}\left(Re_k^{'}\right) = \frac{24}{Re_k^{'}}\left(1 + A\left(Re_k^{'B}\right)\right) + \frac{C}{1 + \frac{D}{Re_k^{'}}}$$

The coefficients, A, B, C, and D can be expressed as a function of the particle sphericity,

$$A = \exp\left(2.3288 - 6.4581\,\phi + 2.4486\,\phi^2\right)$$

$$B = 0.0964 + 0.5565\,\phi$$

$$C = \exp\left(4.905 - 13.8944\,\phi + 18.4222\,\phi^2 - 10.2599\,\phi^3\right)$$

$$D = \exp\left(1.4681 + 12.2584\,\phi - 20.7322\,\phi^2 + 15.8855\,\phi^3\right)$$

$$Re_k^{'} = \frac{Re_k}{V_r} = \frac{d_k\,|\,V_f - V_k\,|\,\rho_f}{\mu_f V_r}$$

The term, V_r is the ratio of the terminal velocity of a group of particles to that of an isolated

---

[2]Syamlal, M. and O'Brien, T. J. 1988, A generalized drag correlation for multiparticle systems. Powder Technology.

[3]Haider A. and Levenspiel O., Drag Coefficient and Terminal Velocity of Spherical and Nonspherical Particles, Powder Technology, 58 (1989) 63-70.

particle. A correlation developed by Garside and Al-Dibouni[4], relates the terminal velocity ratio as a function of particle volume fraction and the particle Reynolds number.

$$V_r = 0.5\left[A - 0.06\,Re_k + \sqrt{0.0036\,Re_k^2 + 0.12\,Re_k(2B - A) + A^2}\right]$$

$$A = \epsilon_f^{4.14}$$

$$B = 0.8\,\epsilon_f^{1.28} \quad , \epsilon_f \leq 0.85 \quad or\ B = \epsilon_f^{2.65} \quad , \epsilon_f > 0.85$$

Turning our attention to the k-th granular phase momentum equations, we have:

$\frac{\partial}{\partial \tau}\left(\epsilon_k \rho_k V_k\right)$ is the temporal acceleration of the k-th granular phase.

$\nabla \cdot \left(\epsilon_k \rho_k V_k V_k\right)$ is the spatial acceleration of the k-th granular phase.

$-\epsilon_k \nabla P$ is the pressure force acting on the k-th granular phase.

$\epsilon_k \rho_k g$ is the body force acting on the k-th granular phase.

$\nabla \cdot \left(\epsilon_k \mu_k \nabla V_k\right)$ is the viscous force acting on the k-th granular phase.

$F_{kf}\left(V_f - V_k\right)$ is the fluid drag force which acts on the k-th granular phase. (Note that $F_{fk} = F_{kf}$)

$\sum_{j \neq k}^{m} F_{kj}\left(V_j - V_k\right)$ represents the particle to particle drag forces. Here again, a complication relation has been derived by Syamlal.

$$F_{kj} = \frac{\alpha(1+e)\,\epsilon_k \rho_k \epsilon_j \rho_j (d_k + d_j)^2\,|V_{kj}|\left[1 + 3\left(\frac{\epsilon_{kj}}{\epsilon_k + \epsilon_j}\right)^{\frac{1}{3}}\right]}{2\,(d_k^3 \rho_k + d_j^3 \rho_j)^2\left[3\left(\frac{\epsilon_{kj}}{\epsilon_k + \epsilon_j}\right)^{\frac{1}{3}} - 1\right]}$$

The coefficient of restitution is represent by the letter e. α is used as a fitting parameter. The term, ϵ_{kj} is known as the maximum solids volume fraction of a random closely packed structure.

---

[4]Garside J. and Al-Dibouni, M. R. 1977 Velocity-voidage relationships for fluidization and sedimentation. Ind. Engng. Chem. Process Des. Dev., 16, 206-214.

It can be computed using the correlations developed by Fedors and Landel[5]

For $X_k \leq \dfrac{\Phi_k}{\Phi_k + (1 - \Phi_k)\Phi_j}$,

$$\epsilon_{kj} = \left[(\Phi_k - \Phi_j) + (1 - a)(1 - \Phi_k)\Phi_j\right] \frac{\left[\Phi_k + (1 - \Phi_j)\Phi_k\right]X_k}{\Phi_k + \Phi_j}$$

and for $X_k > \dfrac{\Phi_k}{\Phi_k + (1 - \Phi_k)\Phi_j}$,

$$(1 - a)\left[\Phi_k + (1 - \Phi_k)\Phi_j\right](1 - X_k) + \Phi_k$$

where,

$$a = \sqrt{\frac{d_j}{d_k}}, \qquad (d_k > d_j)$$

and

$$X_k = \frac{\epsilon_k}{\epsilon_k + \epsilon_j}$$

The final term in the particle phase momentum equations considers the solid stresses brought on when the particle distributions try to exceed their maximum packing density. This can be accomplished by using a strong retarding function, like

---

[5]Fedors, R. F. and Landel, R. F. 1979 An empirical method of estimating the void fraction in mixtures of uniform particles of different size. Powder Technology 23, 225-231.

$$\nabla P_s = \epsilon_k C_1 \exp\left[C_2(\epsilon_{jk} - \epsilon_k)\right] \nabla \epsilon_k$$

The constants C_1 and C_2 can be determined via numerical experimentation.

Solution Strategies

The mathematical model that has been outlined thus far defines the conservation of mass and momentum for the fluid and each of the granular phases. Since there are m granular phases and one fluid phase, m + 1 unknown volume fractions and velocities (with components u, v, and w) exists at each computational node. In addition, the pressure must be determine at each node. The defining equation for each of these unknowns are,

Equation	Defines
Fluid conservation of mass	Volume fraction of the fluid phase
Fluid conservation of momentum	Velocity of the fluid phase
k_th particle conservation of mass	Volume fraction of the k-th granular phase
k_th particle conservation of momentum	Velocity of the k-th granular phase
Saturated mixture assumption	Pressure

As the number of unknowns is extremely large, a segregated solution approach is considered here. To solve for pressure, the conservation equations are summed across all the phases to yield equations which eliminate the volume fractions. For the conservation of mass, the summing process yields,

$$\frac{\partial}{\partial \tau}\left(\rho_{bulk}\right) + \nabla \cdot \left(\rho_{bulk} V_{bulk}\right) = 0$$

where,

$$V_{bulk} = \frac{1}{\rho_{bulk}} \left[\epsilon_f \rho_f V_f + \sum_{k=1}^{m} \epsilon_k \rho_k V_k \right]$$

For the conservation of momentum,

$$\frac{\partial}{\partial \tau} \left(\rho_{bulk} V_{bulk} \right) + \nabla \cdot \left(\rho_{bulk} V_c V_{bulk} \right) = -\nabla P + \rho_{bulk} g + \nabla \cdot \left(\mu^* \nabla V_{bulk} \right)$$

where,

$$V_c = \frac{\left[\epsilon_f \rho_f V_f V_f + \sum_{k=1}^{m} \epsilon_k \rho_k V_k V_k \right]^o}{\left[\epsilon_f \rho_f V_f + \sum_{k=1}^{m} \epsilon_k \rho_k V_k \right]^o}$$

and,

$$\mu^* = \frac{\left[\epsilon_f \mu_f \nabla V_f + \sum_{k=1}^{m} \epsilon_k \mu_k \nabla V_k \right]^o}{\left[\nabla V_{bulk} \right]^o}$$

The o superscripts indicate that these terms will be evaluated using the latest values. Also note the all the inter-phase drag terms and the solid stress terms drop out since these forces sum to zero.

Discretized forms of the momentum equations can be formed to yield the velocity - pressure coupling that is required. The equations take the form of,

$$u_{bulk} = \hat{u}_{bulk} - \Gamma_x \frac{\partial P}{\partial x}, \quad v_{bulk} = \hat{v}_{bulk} - \Gamma_y \frac{\partial P}{\partial y}, \quad w_{bulk} = \hat{w}_{bulk} - \Gamma_z \frac{\partial P}{\partial z}$$

Once these equations have been placed into our continuity constraint, a Poisson pressure equation can be constructed and solved. Once the pressure field has been computed, the phase continuity and momentum equations can be solved iteratively for ρ_f, ρ_k, V_f, *and* V_k until convergence.

APPENDIX B

MODELING OF CASTING DEFORMATIONS —

SOFTWARE GUIDE

Modeling of Casting Deformations — Software Guide

April 19, 1996

Rajiv Gupta and Art Pope
General Electric Research & Development
Schenectady, NY 12301
{gupta,pope}@crd.ge.com

Contents

1 Introduction 2

2 Deformation Modeling Scheme 3

3 Application of Deformation Models 4

4 File Formats 6

4.1 Part model 6

4.2 Deformation model 7

4.2.1 Configuration control information 7

4.2.2 Deformation mode definition 9

4.2.3 Coordinate system definition 10

4.2.4 Feature group definition 11

4.3 Deformation parameter set 12

5 Software Components 13

5.1 `DefSolve` 13

5.2 `DefApply` 14

5.3 `PartDiff` 15

5.4 `EulerToAxis` 15

A Formal Specification of Deformation Model **16**
A.1 Structure of a deformation model 16
A.2 Structure of a deformation mode 17
A.3 Deformation transformations 18
A.3.1 Rigid-body transformation 18
A.3.2 Uniform scaling 18
A.3.3 Orthogonal scaling 19
A.3.4 Twist and unwrapping 19
A.3.5 Bend and shell bulging 19

1 Introduction

Foundries are unable to monitor and control adequately the internal and external dimensions of their cores and castings. This is partly attributed to a lack of suitable methods for describing how a part's actual geometry differs from its intended geometry. The objective of this work is to develop a representation for describing deformations of cast parts in order to permit accurate quantification, monitoring, and control of part geometry.

A deformation representation must be useful for accurately describing a wide variety of castings and their possible deformations. It must allow actual deformations to be computed readily from measurements of a part, such as measurements obtained from X ray images or coordinate measurement machines. Finally, it must yield information that is useful both for understanding deformations and for correcting them.

To meet these requirements, we have developed a parameterized model for characterizing various deformations in investment castings. The model derives from experience in casting precision aircraft engine parts, but it is expected to be applicable to a wide range of other castings.[1] We have also developed and implemented algorithms to process X-ray images for the purpose of generating a deformation description.

This report describes the parameterized deformation model and its associated software.

[1]Note that only distortions in shape are addressed—not, for example, defects of material composition or of grain structure.

2 Deformation Modeling Scheme

A list of casting deformations compiled through discussions with investment casting experts reveals that, despite a proliferation of terminology, only a limited variety of deformations occur commonly. These common deformations are not arbitrarily complex, but rather each can be characterized by a small number of simple, intuitive parameters.

Our approach has been to identify an extensible repertoire of these simple deformations, called deformation modes, and to model a part's overall deformation as a series of consecutive applications of deformation modes. Each mode is controlled by parameters whose values may be determined from part measurements.

Here we present an overview of this deformation modeling scheme and an initial repertoire of deformation modes. A more precise, mathematical definition may be found in appendix A. Additional information about the modes and an empirical test of their adequacy are documented in a separate report [1].

Deformation modes are classified as core defects, which affect only a part's interior surfaces, and part-body defects, which may affect both exterior and interior surfaces.

Core defects include:

- rigid-body displacement of the core with respect to the overall part
- rigid-body displacement of one section of the core with respect to the overall core

Each rigid-body displacement is characterized by six parameters: three for rotation and three for translation. The remaining deformation modes summarized below are each parameterized in a similar fashion. Part-body defects include:

- rigid-body displacement of a section of the part with respect to the overall part
- shrinkage or expansion of a part section, either uniformly in all directions or by differing amounts along each of three principle axes
- twist of a part section, defined as rotation about some axis with the degree of rotation varying (uniformly or otherwise) with position along the axis
- unwrapping of a part section, defined similarly to twist but allowing portions of the part to rotate in opposite directions

- bending of a section of the part, defined as shift of the part in a direction perpendicular to some axis, by an amount that varies (uniformly or otherwise) with position along that axis
- shell bulging, defined as a displacement of a local region of surface, in a direction normal to the surface, by an amount characterized by a functional form such as a Gaussian

An appropriate deformation model, comprising a series of deformation modes, must be chosen for each type of part to be described. Deformation of a typical turbine airfoil part would be described by a combination of several modes; these would include, for example, twist, unwrapping, and bending deformations defined with respect to the part's stacking axis, plus displacement of core sections and shrinkage.

3 Application of Deformation Models

With the establishment of an appropriate deformation model, any common deformation of an individual part can be described precisely by a small set of deformation parameters. We have devised and partially implemented methods of computing such parameters from part measurements. The deformation parameter estimation problem is formulated as an optimization problem in which parameter values are chosen to minimize the discrepancy between actual part measurements, and measurements predicted by a deformed model of the part's geometry. When working from X-ray images, the images may be used to first recover information about the part's 3-D geometry before estimating deformation parameters, or interpretation of the images can be incorporated into the optimization problem itself. To date, we have implemented the first of these two alternatives.

The software developed to date supports the activities illustrated in figure 1. It includes:

- a program, `XFL`, for estimating the 3-D positions of a part's features from X-ray images, with the aid of a CAD model of the part
- a program, `DefSolve`, for estimating deformation parameter values, given 3-D positions of features, a part model, and a deformation model
- a program, `DefApply`, for applying a deformation model to a part model, given deformation parameter values, to obtain a deformed model of the part
- a program, `PartDiff`, for reporting the differences between two part models

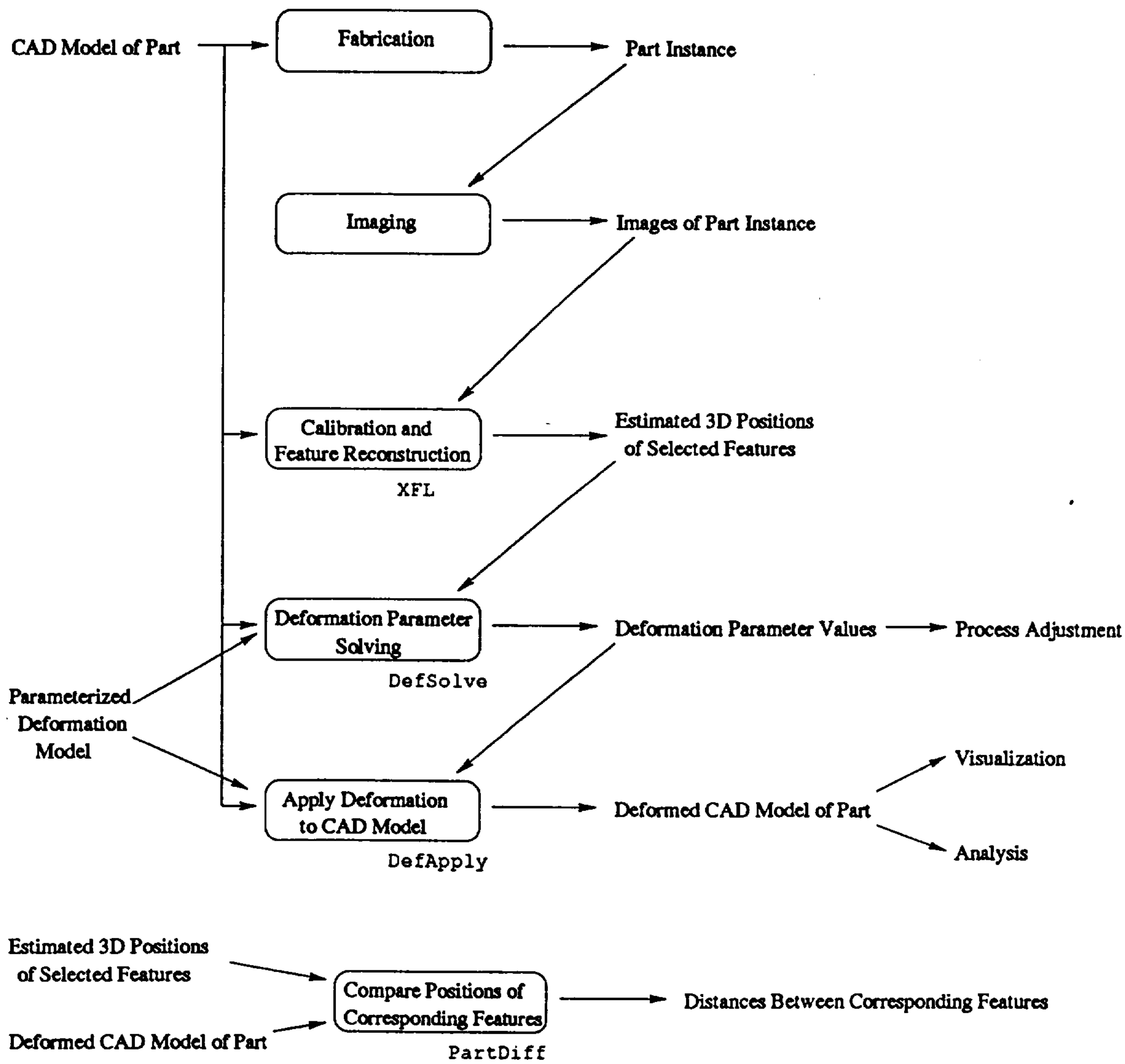

Figure 1: Use of a deformation model for characterizing a part's geometry. The roles of software components such as XFL and DefSolve are described in the text. Solution of deformation model parameters supports refinement of fabrication processes and comprehension of actual part geometry.

XFL is used to reconstruct information about a part's 3-D geometry, which is needed to estimate deformation parameter values; similar information may also be obtained from other sources, such as a coordinate measurement machine. `DefSolve` uses the reconstructed geometric information to estimate parameter values. `DefApply` can be used to synthesize a deformed model of the part for analysis, comparison to the original CAD model, and visualization of any deformations. `PartDiff` can be used to compare a deformed model of a part with a reconstruction of it, to determine how accurately a deformation model represents the part's actual geometry. All of these programs are currently restricted to features that are either points or line segments.

4 File Formats

This section documents file formats used to represent part models, deformation models, and deformation parameter sets.

4.1 Part model

A *part model* is a description of a part's geometry. Sometimes a part model is referred to as a design part model, reconstructed part model, or deformed part model to distinguish its source. These terms have the following meanings:

design part model	a part model describing the intended, ideal, or nominal form of a part (i.e., a CAD model of a part)
reconstructed part model	a part model describing the form of a part, as determined by reconstruction from images or other measurements
deformed part model	a part model describing the form of a part, obtained by applying a deformation model to a design part model

A single ASCII text file representation, called *point/line format*, is currently used for all three types of part models. As its name suggests, this format is restricted to representing just points and line segments. The format is organized as a series of lines, each terminated by a newline character. Parameters on a line are delimited by whitespace (any string of space or tab characters). Lines beginning with the character # or ! are ignored as comments.

A point is represented by a text line of the form *identifier* x y z

where *identifier* is a unique label associated with the point, and x, y, and z are the coordinates of the point. Identifiers are arbitrary strings of alphanumeric characters; coordinates are decimal floating point numbers.

A line is represented by a text line of the form

identifier x_0 y_0 z_0 x_1 y_1 z_1

where *identifier* is a unique label associated with the line segment, and the remaining parameters are the coordinates of the segment's endpoints.

Programs exist for converting between point/line format and IGES format.[2]

4.2 Deformation model

Deformation models are represented in files using a human-readable text format called *deformation model text format* (DMTF). Figure 2 shows an example of a DMTF file.

The format is organized as a series of lines, each terminated by a newline character. Parameters on a line are delimited by whitespace (any string of space or tab characters). Leading whitespace on a line is ignored. A parameter that is a string should be enclosed in " characters if it contains any whitespace, and a backslash should be used to escape any " character within the string; the string may not contain a newline character. A string parameter that does not contain any whitespace need not be enclosed in " characters (examples: `red`, `line-1`, and `rot_x`). Blank lines and anything on a line following a # or ! character are ignored as comments.

4.2.1 Configuration control information

A DMTF file begins with configuration control information in the following format:

`name`	*deformation-model-name*
`part`	*part-model-name*
`version`	*version-string*

[2]The programs are currently `iges_to_ptline` and `ptline_to_iges` in `/projects/xhl/XHL1.1/utilities`.

```
# Deformation model for AITP PIT part.
name            "PIT Deformation Model"
part            "PIT Part"
version         1.0
comment         "Just an illustration"

# Deformation mode 1: rigid-body transformation of entire core
begin_mode      core_shift
  cs            part                    # defined in part coordinate system
  domain        core                    # applies to features of core
  type          rigid                   # rigid-body transformation
  r1x           core_rx
  r2y           core_ry
  r3z           core_rz
  tx            core_tx
  ty            core_ty
  tz            core_tz
end_mode

# Deformation mode 2: shrinkage of core about core center
begin_mode      core_shrinkage
  cs            core_cs                 # defined in core coordinate system
  domain        core                    # applies to features of core
  type          uniform_scale           # uniform scaling transformation
  sx            shrink_x
  sy            shrink_y
  sz            shrink_z
end_mode

# Group: features of core
begin_group     core
  member        208
  member        236
  member        264
  member        220
  member        215
end_group

# Coordinate system: centered on core
begin_cs        core_cs
  parent        part                    # defined wrt part coord sys
  r1x           0                       # simple translation along Z
  r2y           0
  r3z           0
  tx            0
  ty            0
  tz            2.13764
end_cs
```

Figure 2: Example of deformation model text format file.

`comment`	*comment-string*

Each of the above parameters may be an arbitrary string; they are not currently used by software. The remainder of the file defines a sequence of one or more deformation modes, plus any coordinate systems and groups of part model features needed in the definition of those deformation modes.

4.2.2 Deformation mode definition

Deformation modes are defined in the file in the sequence they are to be applied to the design part model. Each deformation mode definition is of the following format:

`begin_mode`	*deformation-mode-name*
`cs`	*coordinate-system-name*
`domain`	*group-name*
`type`	`rigid` | `uniform_scaling` | etc.
parameter-role-1	*parameter-name-1*
parameter-role-2	*parameter-name-2*
etc.	
`end_mode`	

The *deformation-mode-name* string parameter assigns a name to the deformation mode; deformation mode names must be unique. The coordinate system used to define the deformation mode is specified by the *coordinate-system-name* string parameter. The domain of the deformation is the part feature or group of part features specified by the *group-name* string parameter.

The `type` entry in the deformation mode definition specifies the type of transformation used to model the deformation mode. The remaining entries establish a correspondence between generic transformation parameters (identified by *parameter-role*) and specific, unique deformation parameters (identified by *parameter-name*). The allowable transformation types and their associated parameters are listed in table 1. Parameter-defining entries must occur in the order shown in the table. Thus, for example, an orthogonal scaling transformation is specified as:

`type`	`orthogonal_scaling`
`sx`	*name-assigned-sx-parameter*
`sy`	*name-assigned-sy-parameter*

Table 1: Syntax for specifying deformation transformations and their parameters.

Transformation	Section	Keyword	Parameter	Keyword
rigid-body	A.3.1	`rigid`	r_x	`r1x`
			r_y	`r2y`
			r_z	`r3z`
			t_x	`tx`
			t_y	`ty`
			t_z	`tz`
uniform scaling	A.3.2	`uniform_scaling`	s	`s`
orthogonal scaling	A.3.3	`orthogonal_scaling`	s_x	`sx`
			s_y	`sy`
			s_z	`sz`
uniform twist	A.3.4	`uniform_twist`	ϕ_θ	`r`
uniform bending	A.3.5	`uniform_bending`	ϕ_w	`r`

Column 1: a type of transformation. Column 2: section of this report in which the transformation type is formally defined. Column 3: keyword used in a `type` entry to specify this type of transformation. Column 4: parameter of the transformation (see the referenced section). Column 5: keyword used as a *parameter-role* to identify this parameter.

`sz` *name-assigned-sz-parameter*

The names assigned to deformation parameters are defined in an associated deformation parameter set (see section 4.3).

4.2.3 Coordinate system definition

Coordinate systems, which may be referenced by deformation mode definitions, are defined in the following ways:

1. A coordinate system called `part` is predefined to be the part coordinate system.
2. A coordinate system may be defined by the part model. CAD systems such as Unigraphics, and exchange formats such as IGES, support the definition of coordinate systems. However, the point/line format currently used to represent part models cannot represent these coordinate systems. Consequently, coordinate systems defined

within part models are currently not available to the deformation model.

3. A coordinate system may be defined by entries in the DMTF file, as described below.

A coordinate system definition of the following form may appear anywhere in a DMTF file:

`begin_cs`	*cs-name*
`parent`	*parent-cs-name*
`r1x`	*rx*
`r2y`	*ry*
`r3z`	*rz*
`tx`	*tx*
`ty`	*ty*
`tz`	*tz*
`end_cs`	

This defines a new coordinate system called *cs-name*, which is related to another named coordinate system, *parent-cs-name*, by means of a coordinate transformation. The transformation, which transforms coordinates from the *cs-name* coordinate system to the *parent-cs-name* one, is composed of a rotation followed by a translation. Rotation is about *cs-name*'s X, Y, and Z axes, in that order, by the angles *rx*, *ry*, and *rz* according to the right-hand rule. Translation is along *cs-name*'s X, Y, and Z axes by the amounts *tx*, *ty*, and *tz*. All coordinate systems must be defined, directly or indirectly, in terms of the part coordinate system, which has the name `part`.

4.2.4 Feature group definition

Groups of features, which may be referenced by deformation mode definitions, are defined in the following ways:

1. A group called `part` is predefined to include all features of the part.
2. A group may be defined by the part model. CAD systems such as Unigraphics, and exchange formats such as IGES, support the definition of feature groups. However, the point/line format currently used to represent part models cannot represent these groups. Consequently, groups defined within part models are currently not available to the deformation model.

```
#
# Initial estimates of AITP PIT part deformation parameters.
#
core_rx   0   1
core_ry   0   1
core_rz   0   1
core_tx   0   1
core_ty   0   1
core_tz   0   1

shrink_x  1   1
shrink_y  1   1
shrink_z  1   1
```

Figure 3: Example of a deformation parameter set text format file.

3. A group may be defined by entries in the DMTF file, as described below.

A feature group definition of the following form may appear anywhere in a DMTF file:

`begin_group`	*group-name*
`member`	*identifier-1*
`member`	*identifier-2*
etc.	
`end_group`	

This defines a group called *group-name*, and lists its members as *identifier-1*, *identifier-2*, etc. Each member may be the identifier of a part feature (i.e., the identifier of a point or line segment as found in a part model point/line format file), or the name of another group. Any group or feature may be a member of any number of groups, although circular (recursive) group definitions are not allowed.

4.3 Deformation parameter set

Deformation parameter values are represented in files using a human-readable text format called *deformation parameter set text format* (DPSTF). DPSTF files are used to represent both initial (a priori) distributions of parameter values, and final estimates of parameter values. Figure 3 shows an example of a DPSTF file containing initial estimates of the deformation parameters referenced by the model listed in figure 2.

The DPSTF format is organized as a series of lines, each terminated by a newline characters.

Each parameter is described by a line of the form:

parameter-name value std-dev

where *parameter-name* is the parameter's name (an alphanumeric word), and *value* and *std-dev* are decimal floating point numbers. Whitespace (any string of space and tab characters) separate the three words. Blank lines and anything on a line following a # or ! character are ignored as comments.

If the file describes initial distributions of parameter values, the distribution of *parameter-name* is taken to be Gaussian with mean *value* and standard deviation *std-dev*. If the file describes final estimates of parameter values, the estimate of *parameter-name* is reported as *value* and *std-dev* has no interpretation.

5 Software Components

The following programs are available.[3]

5.1 `DefSolve`

The `DefSolve` program solves for deformation parameter values by comparing a design part model with a reconstructed part model. In addition to the two part models, it requires a deformation model and a deformation parameter set specifying the initial (a priori) distributions of the deformation parameter values. The program is invoked as follows:

`DefSolve` *design-pm reconstructed-pm def-model* < *initial-dps* > *final-dps*

The arguments *design-pm* and *reconstructed-pm* are the filenames of point/line format files containing the design (CAD) part model and reconstructed part model. *Def-model* is a DMTF file containing the deformation model, and *initial-dps* is a DPSTF file specifying the initial parameter value distributions. Final estimates of the parameter values are written to the DPSTF file *final-dps*.

[3]These programs are currently installed in `/project/xms/xms-1.0/bin` for SPARCstations running Solaris 2.4.

The program estimates the deformation parameter values of each deformation mode in sequence. Parameters are estimated by solving an optimization problem of the form

$$\hat{\phi} = \arg\max_{\phi} \sum_i d(\hat{\mathbf{x}}_i, \tilde{\mathbf{x}}_i(\phi))^2 + \sum_j \left(\frac{\phi_j - \mu_j}{\sigma_j}\right)^2$$

Here, ϕ is a vector of deformation parameter values. The a priori distribution of parameter ϕ_j, the j^{th} element of ϕ, has mean μ_j and variance σ_j^2. The reconstructed position of the i^{th} feature is $\hat{\mathbf{x}}_i$, and its position as predicted by the design model, deformation model, and deformation parameter values ϕ is $\tilde{\mathbf{x}}_i(\phi)$.[4] The distance between two features, $d()$, is measured as follows:

- the distance between two points is simply their Euclidean distance
- the distance between two line segments is the mean of the Euclidean distances of each endpoint of the deformed feature from the infinite line extending through the reconstructed feature

The optimization problem is solved using an iterative method. During operation, the program reports its progress as illustrated by the following example:

```
% DefSolve design.pl reconstructed.pl def-model.dm < initial.dps > final.dps
Deformation mode #1 (core_shift)
  number of iterations: 11
Deformation mode #2 (core_shrinkage)
  number of iterations: 10
%
```

5.2 DefApply

The DefApply program applies a deformation to a part model. The deformation is specified by a deformation model and an associated set of deformation parameter values. The program may be used, for example, to produce a version of a design part model that has been deformed according to deformation parameters estimated by DefSolve. The program is invoked as follows:

DefApply *def-model final-dps* < *design-pm* > *deformed-pm*

[4]The deformed line segment is defined as that joining the deformed positions of the two endpoints.

The arguments *def-model* and *final-dps* are the names of DMTF and DPSTF files supplying the deformation model and its parameter values. A part model is read from the point/line format file *design-pm*, deformed, and written to the point/line format file *deformed-pm*. Here's an example:

```
% DefApply def-model.dm final.dps < design.pl > deformed.pl
%
```

5.3 PartDiff

The PartDiff program will compare two part models represented as point/line format files. It reports the distances between corresponding features (those with the same identifier) and lists any features that are found in one part model but not the other. Here's an example:

```
% PartDiff deformed.pl reconstructed.pl
Primitives of deformed.pl not found in reconstructed.pl:
    201
    202
Primitives of reconstructed.pl not found in deformed.pl:
    244
    254
Separation between corresponding primitives:
    101                 0.0106896
    102                 0.0106654
    103                 0.0113429
    104                 0.0104581
    105                 0.00921212
    mean                0.0105234
%
```

5.4 EulerToAxis

The command

EulerToAxis *r_x r_y r_z*

will convert the roll-pitch-yaw angles r_x, r_y, and r_z (specifying succesive rotations about X, Y, and Z axes, in radians, according to the right-hand rule) to a rotation axis direction and rotation amount. For example:

```
% EulerToAxis 1 1 1
Axis: 0.271004 0.923642 0.271004
Angle: 1.33275 (76.3611 degrees)
%
```

A Formal Specification of Deformation Model

This appendix specifies, in formal terms, the scheme devised for representing parameterized deformations of castings. This scheme is a refinement of that described in [1].

A.1 Structure of a deformation model

A *deformation model*, D, represents a transformation from the nominal, or intended, geometry of a part to its actual, or deformed, geometry. Thus D is function that maps points from one 3–D space to another.

To simplify the task of specifying different deformations for different components of a part, D's domain is defined to include both the coordinates of a point and information about where the point lies on the part. This allows, for example, deformations to be modeled separately for a part's internal and external surfaces.

Formally, D is of the form

$$D(\phi) : \Re^3 \times Q \mapsto \Re^3,$$

where ϕ is a collection of deformation parameters, $\Re^3$ is the space of 3–D point coordinates, and Q is a set of identifiers for the part's various components or geometric primitives.

A deformation model D is a sequence of deformation modes, each denoting a particular deformation of selected components of the part. The deformation modes are applied in sequence to establish the overall deformation of the part. For example, the first deformation mode might specify a rigid shift of a casting's core with respect to its nominal position. A second deformation mode might then specify a twist of the entire casting, including the shifted core. D is defined formally as

$$D(\phi) \quad = \quad D_m(\phi_m) \circ \ldots \circ D_1(\phi_1),$$

where $D_1, \ldots, D_m$ are the deformation modes, applied in that sequence, and $\phi_1, \ldots, \phi_m$ are their corresponding parameters. Each D_i is of the form

$$D_i(\phi_i) : \Re^3 \times Q \mapsto \Re^3.$$

A.2 Structure of a deformation mode

Deformation modes of all types are collected under a single definition that is simple and concise, yet general enough to represent any of the deformations specified in [1]. A deformation mode D_i is characterized by the following:

- A *deformation coordinate system*, which is a local coordinate system defined with respect to the part coordinate system.[5] Points are represented using homogeneous coordinates. The deformation coordinate system is represented by a 4×4 matrix, U_i, that maps points from the part coordinate system to the deformation coordinate system.
- A *deformation transformation*, which maps points from their nominal positions to their deformed positions within the deformation coordinate system. The deformation transformation is represented by a 4×4 matrix, V_i. For simple, linear deformations, the elements of V_i depend only on the deformation parameters; for other deformations, elements of V_i may be functions of the coordinates of the point being mapped.
- A *deformation domain*, Q_i, listing the part components or geometric primitives to which the deformation applies.

D_i is thus of the form

$$D_i(\mathbf{x}, q; \phi_i) \quad = \quad \begin{cases} U_i^{-1} V_i U_i \mathbf{x} & q \in Q_i \\ \mathbf{x} & \text{otherwise.} \end{cases}$$

In simple cases, V_i depends only on the deformation parameters ϕ_i:

$$V_i \quad = \quad V_i(\phi_i).$$

[5]Coordinate systems are right-handed and Cartesian unless noted otherwise.

More generally, V_i may also depend on the coordinates of the point being transformed:

$$V_i = V_i(\phi_i, U_i\mathbf{x}).$$

Neither U_i nor Q_i depend on the deformation parameters, but rather they are fixed for a particular deformation mode and part model.

A.3 Deformation transformations

The matrix representation of the deformation transformation, V_i, takes a particular form for each type of deformation transformation. Those listed in [1] are catalogued below.

A.3.1 Rigid-body transformation

A rigid-body transformation is characterized by a rotation followed by a translation. For parameterization, the rotation is decomposed into successive rotations about the deformation coordinate system's X, Y, and Z axes by the angles r_x, r_y, and r_z. The translation is represented by a 3-element vector, $\mathbf{t}$. With the rotation represented as a 3×3 orthonormal matrix of elements $r_11, \ldots, r_33$, the overall transformation is represented as

$$V_i = \begin{bmatrix} r_{11} & r_{12} & r_{13} & t_x \\ r_{21} & r_{22} & r_{23} & t_y \\ r_{31} & r_{32} & r_{33} & t_z \\ 0 & 0 & 0 & 1 \end{bmatrix}.$$

A.3.2 Uniform scaling

Uniform scaling is characterized by a single scale factor, s.

$$V_i = \begin{bmatrix} s & 0 & 0 & 0 \\ 0 & s & 0 & 0 \\ 0 & 0 & s & 0 \\ 0 & 0 & 0 & 1 \end{bmatrix}.$$

A.3.3 Orthogonal scaling

Orthogonal scaling is characterized by separate scale factors, s_x, s_y, and s_z, for the three axes of the deformation coordinate system.

$$V_i = \begin{bmatrix} s_x & 0 & 0 & 0 \\ 0 & s_y & 0 & 0 \\ 0 & 0 & s_z & 0 \\ 0 & 0 & 0 & 1 \end{bmatrix}.$$

A.3.4 Twist and unwrapping

Twist is a rotation about some axis, where the degree of rotation depends on position along the axis. Unwrapping is a more general form of rotation, where the degree of rotation depends on additional components of position (points on opposite sides of the axis rotate in opposite directions). Both deformations are represented by a V_i of the form

$$V_i(\mathbf{y}) = \begin{bmatrix} \cos\theta(\mathbf{y}) & -\sin\theta(\mathbf{y}) & 0 & 0 \\ \sin\theta(\mathbf{y}) & \cos\theta(\mathbf{y}) & 0 & 0 \\ 0 & 0 & 1 & 0 \\ 0 & 0 & 0 & 1 \end{bmatrix},$$

where $\theta(\mathbf{y})$ is the rotation about the deformation coordinate system's Z axis of a point whose coordinates, in that system, are $\mathbf{y}$. If the deformation is pure twist, then $\theta(\mathbf{y})$ is of the restricted form $\theta(\mathbf{y}) = \theta(y_z)$.

It is necessary, for tractability, to define a small number of more specific forms that $\theta(\mathbf{y})$ may assume. One of these, for uniform twist, is defined as

$$\theta(\mathbf{y}) = \phi_\theta \, y_z,$$

where ϕ_θ is a deformation parameter representing rate of twist. Other specific forms of $\theta(\mathbf{y})$ may be defined in future.

A.3.5 Bend and shell bulging

Bend is a displacement in a plane perpendicular to some axis, where the displacement depends on position along the axis. Shell bulging is similar, except that the displacement depends on additional components of position. Both deformations are represented by a V_i of the form

$$V_i = \begin{bmatrix} 1 & 0 & 0 & w_x(\mathbf{y}) \\ 0 & 1 & 0 & w_y(\mathbf{y}) \\ 0 & 0 & 1 & 0 \\ 0 & 0 & 0 & 1 \end{bmatrix},$$

where $w_x(\mathbf{y})$ and $w_y(\mathbf{y})$ are the X and Y components of displacement in the deformation coordinate system, for a point whose coordinates are $\mathbf{y}$. If the deformation is pure bend, then these functions are of the restricted form $w_x(\mathbf{y}) = w_x(y_z)$ and $w_y(\mathbf{y}) = w_y(y_z)$.

It is necessary, for tractability, to define a small number of more specific forms that $w_x(\mathbf{y})$ and $w_x(\mathbf{y})$ may assume. One of these, for uniform bending, is defined as

$$w_x(\mathbf{y}) = \phi_w \, y_z, \quad \text{and} \quad w_y(\mathbf{y}) = 0,$$

where ϕ_w is a deformation parameter representing rate of bend. Other specific forms of these functions may be defined in future.

References

[1] Gupta, Rajiv and Martin Lee. "A parametrized model for deformations in investment casting of aircraft engine parts." GE CR&D Technical Report, Sept. 6, 1995.

APPENDIX C
CASTING DESIGN GUIDELINES

MARCH 17, 1997

BY:

MICHAEL ROBINSON/
Patricia McKee

ROBINSON PRODUCTS, INC.
3141 HUNTINGTON ROAD
SHAKER HEIGHTS, OH 44120-2409

TR-97020

TABLE OF CONTENTS

Page

INTRODUCTION 4

BENEFITS OF THE CONVERTING WELDED AND ASSEMBLED COMPONENTS INTO CASTINGS VIA REVERSE ENGINEERING 4

BENEFITS OF CONVERTING 4

BENEFITS OF REVERSE ENGINEERING 4

BENEFITS OF SOLIDIFICATION MODELING 5

Saves time by reducing the number of casting experiments needed 5

Saves time by reducing the number of identifying potential process problems early 5

Produce acceptable (sound and high qualify) with fewer experiments 5

Reduces costs by reducing materials, labor and other costs associated with experiments 5

FABRICATION CONVERSION TO CASTING 6

COMPONENT SELECTION CRITERIA 6

Existing Design 6

New or Modified Design 7

CASTABILITY ANALYSIS 7

COST ANALYSIS 8

COMPONENT DESIGN 8

CAD MODELING AND TOOLING 8

NDE 9

CASTING DESIGN GUIDE 9

GENERAL RULES TO CASTING DESIGN 9

ROCKET CASTING OBJECTIVE 9

. Select Commercial Software Package 9

CT Scan Component 10

. Convert into CAD format 10

USE OF RAPID NEAR NET SHAPE 10

Objective 10

Inspect Patterns 10

Optimum gating and riser locations 10

Methods Employed 10

CASTING PROCESS GUIDE 11

FACTORS AFFECTING THE CHOICE OF PROCESS 11

GENERAL DESCRIPTION OF BASIC MOLDING PROCESSES 12

Sandcasting 12

Shell molding 13

Diecasting *13*
Permanent mold casting *14*
Investment casting (lost wax) *14*
GENERAL DESCRIPTION OF BASIC CORE PROCESS 14
FOUNDRY PROCESSES 16
ALLOYS 17
GATING AND RISERING 18
Thermal Controlled Solidification (TCS) process *19*
Case Study - the LO_2 Tank Elbow *19*
REVERSE ENGINEERING THE INVESTMENT CASTING PROCESS 20
Process flow for Reverse Engineering *20*
Process flow for Conventional Casting *21*
RAPID PROTOTYPING **21**
WHAT IS NEEDED 21
HOW IS IT USED 22
LIMITATIONS 23
COSTS .... ERROR! BOOKMARK NOT DEFINED.
APPENDIX: GLOSSARY OF FOUNDRY TERMS **24**
REFERENCES **26**

INTRODUCTION

Casting product performance requirements are increasing in response to customer demands for lighter weight, higher strength, and lower cost. The ability of the U.S. foundry industry to meet these demands with shorter, more flexible product cycles is placing tremendous competitive pressures on the industry. Since the cost effectiveness of castings actually increases as castings become larger and more complex, one of the most promising capabilities requiring development is the cost-effective, rapid near net shape casting of large parts.

The overall objective of rapid near net shape casting is to shorten the cycle time for the fabrication and casting of high quality castings. It is the intent that this technology be commercially implemented to accomplish three (3) primary goals:

1. recognize significant reductions in the costs of castings
2. increase the complexity and dimensional accuracy of castings, and
3. reduce the development times for delivery of high quality castings

While many of the process problems in producing cost effective castings are common, regardless as to the quantity or application, the alloys, tolerances, quality criteria and production volumes will differ. These differences have been recognized and addressed.

BENEFITS OF THE CONVERTING WELDED AND ASSEMBLED COMPONENTS INTO CASTINGS VIA REVERSE ENGINEERING

Benefits of Converting

1. Reduced complexity - reduces the number of individual parts to make an assemble.
   A. Handling time is reduced
   B. Handling costs are reduced
   C. Part accuracy is increased
   D. Fewer drawings needed.
      (1) Time to track components is reduced
      (2) Cost to develop drawing is reduced
      (3) Time to make drawings is reduced
4. Cost Savings
5. Time to design and cast is significantly quicker than traditional casting processes.
6. Example used in program:
   Assembly had 50 parts
   Casting assemble had 3 parts

Benefits of Reverse Engineering

Although many of the benefits of switching to casting from welded and assembled components has been documented (see appendix), the high cost to develop a casting provides a barrier to conversion. But, even larger barriers are the time to develop the tooling and the time and cost to develop a process to manufacture a good casting. An expensive tool has to be made and gating added. Then, many times the tooling has to be redone to provide an acceptable casting.

Reverse engineering now breaks both of those barriers. It takes an actual assembly and develops a computer aided design (CAD) file via computed tomography (CT). A cloud of points is generated from a CT scan. The points are converted to an 3-D drawing, then into a sterolithogrpahy (STL) file which can be used to make a SLS pattern. This pattern is used to make castings and run experiments to develop the process. Changes can be quickly made to the 3-D drawing and redesigned patterns produced to proceed to an acceptable casting.

Using the CT scan method to generate the CAD file can reduce the months of efforts to produce an acceptable CAD model to weeks or in some cases days. This has the potential to make what seems impractical very possible.

An example of cost savings and time.. A part that was analyzed showed these dramatic results:

Type of Casting Development	Cost for 1st Casting	Time to 1st Casting	Tool development
Traditional casting approach	$ 100,000	8 Months	yes
Reverse Engineering approach	$ 10,000	1 Month	no

Benefits of Solidification Modeling

The 3-D CAD model that is built to produce the SLS pattern can be used for solidification modeling to run experiments to test the process. Simulations are all done on the computer. Sometimes changes can be made before the first SLS pattern is produced.

Solidification modeling provides the following advantages:

- Saves time by reducing the number of casting experiments needed
- Saves time by reducing identifying potential process problems early
- Produce acceptable (sound and high qualify) castings with fewer experiments
- Reduces costs by reducing materials, labor and other costs associated with experiments
- Allows greater use of simultaneous engineering

The product engineer can make changes to the design and the foundry engineer can identify the possible shortcomings in the manufacturing process in an early phase of the product design cycle. This is a major benefit.

FABRICATION CONVERSION TO CASTING

Using the proven technology of near net-shape castings to replace formed, welded components is a significant paradigm shift. This shift to cast components has benefits that are greater than the technical challenges posed by the process. The benefits are:

1. Potential component cost reduction
2. Reduced time to get component into production
3. Reduction in the number of elements per component
4. Leverage of rapid prototyping and modeling to improve quality and reduce product design cycle.

All of the candidates considered by the consortium are forged and welded items that represent sub-systems or assemblies. *Thus, the casting has a* **geometry** that *is more complicated than the individual forged components..* To jump-start the conversion process, the entire forged candidate subsystem was reverse engineered by computed topography to generate an electronic file that was converted into a CAD format in order to integrate casting design features. The resulting CAD database was used for solidification modeling purposes and rapid prototype development.

This overview documents the decision making process in the evaluation, and conversion of fabricated components into a casting which could assist other manufacturers interested in converting fabricated parts to casting.

COMPONENT SELECTION CRITERIA

Existing Design

One recommendation is to have the candidate component reverse engineered from an existing forged assembly or sub-assembly. The chosen cast component must maintain the strength and dimensional tolerances of the original assembly while remaining within the confines defined by the engine or application.

Selection criteria is a function of the project constraints and practical application of the technology. Table 1 defines the constraints of the five (5) selection criteria:

TABLE 1: SELECTION CRITERIA AND CONSTRAINT MATRIX

CRITERIA	CONSTRAINT
Availability	Component must be available for CT Scan or CAD Model
Future Application	Component must have potential in [illegible] [illegible] welding, etc.
Cost Savings	Component must show substantial potential for cost savings i.e., welded assemblies, machined parts.
Complexity	Component must be a technical challenge. This fabrication represents state of the art in manufacturing capability.
Performance	Cast components must meet performance requirements

[Examples of Departments that should be involved in the selection process include:]
An Integrated Product Team to be involved in the selection process should include:

- Manufacturing Engineering
- Quality Engineering
- Design Engineering
- Marketing
- Metallurgical Engineering and Testing
- Project Engineering

These components may be given high, medium, or low ratings for each of the selection criteria. Based on the ratings, the best candidate component is chosen.

New or Modified Design

When a new or modified part is used in new applications, the criteria used in the above table can be applied also. Instead of using an existing part for scanning, a 3-D CAD design should be made available. Most manufacturers are moving toward making models of all new parts. To leverage rapid prototyping, a model is required.

CASTABILITY ANALYSIS

Based on the alloy and configuration, an estimate of the probability of success should be made. This may include, but is not limited to:

1. Definition of foundry facilities required.
2. Ability to redesign casting shape to reduce weight.
3. Simulation of potential casting determines:
    - A. Metal flow
    - B. Shrink problems.
    - C. Metallurgy
    - D. Final properties

COST ANALYSIS

In justifying the conversion, the trial and error alone of fabrication many times offsets the cost of converting.

An estimated cost and time to convert to a casting must be evaluated and compared to the cost of fabricating the same part. (Note many times the number of parts required to make a sub-assembly can be significantly reduced causing tremendous cost savings. The cost to produce the casting becomes very important.)

COMPONENT DESIGN

Most fabrications or forging are not designed to be optimum cast components. Given limitations of time and performance the part should be designed to ease the casting process. Developing a casting process to make this application can have significant effects on foundry efficiency.

CAD MODELING AND TOOLING

Having a model available to make rapid tooling can dramatically save time when making a test casting. Use of rapid tooling processes provides the foundry a very fast and cost effective approach to verifying the viability of the chosen process which may or may not have been simulated.

One may perform solidification modeling on the CAD as discussed in part II above. The results of the simulation would determine if the CAD files need to be modified to improve castability before the prototype tool is made.

NDE

The ability to determine the quality of the casting made by non-destructive methods should be carefully considered.

CASTING DESIGN GUIDE

General Rules to Casting Design

While almost any shape can be cast, successful casting begins with good design.

- Generally, rounded surfaces and generous radii produce superior castings
- Extensive flat surfaces are extremely difficult to cast accurately
- Rapid changes of section should be avoided
- Take care with material selection and the correct grade of material used for any given metal thickness
- The shape of the casting should be such as to avoid shrinkage cavities
- Ideally it should be possible to draw the pattern from the sand without the use of loose pieces
- Cores should be balanced and properly supported, preferably at both ends and even the sides

Some general rules to follow:

1. Specify close tolerances only where necessary
2. Avoid heavy sections whenever possible
3. Be aware that changes of section promote stresses during cooling and overall tolerances may be affected

Rocket Casting Objective

The objective is to apply advanced technologies to rapidly fabricate low-cost, high-quality rocket engine castings.

Selection criteria are a function of the project constraints and practical application of the technology. Table 1 (pg. 5) defines the constraints of the five (5) selection criteria:

Select Commercial Software Package

It is necessary to select a Conversion Commercial Software Package. The evaluation criteria for this can be as follows:

1. Interface between existing equipment (SMS CT) and reverse engineering system
2. Functionality of the reverse engineering system
3. Interface between reverse engineering system and CAD systems

CT Scan Component

The component must next be CT scanned. Scanned images are converted into a point data file using the software package previously selected. Based on the component, hundreds of files may result from the scan, from which a surface model must be created based on the given data.

Convert into CAD format

USE OF RAPID, NEAR-NET SHAPE

Objective. The objective of rapid near net shaping is to reduce cycle time for fabricating high quality castings. It is used to fabricate patterns directly for investing and to fabricate temporary tooling for direct wax injection. While there are several rapid prototype processes for fabricating patterns for investing available, the optimum RP process for a specific component needs to be outlined.

Inspect Patterns. Patterns should be inspected for the following:

1. surface finish
2. part distortion
3. dimensional accuracy
4. repeatability

Optimum gating and riser locations. Optimum gating and riser locations can be determined from solidification modeling.

Methods Employed. Two different approaches were used to meet the objective. Approach I used Reverse Engineering while Approach II used the more conventional method of directly drawing a CAD file.

1. Approach I - Reverse Engineering rapidly produces a CAD file from an existing part. The following steps were taken:

- define existing part
- generate electronic fine using CT
- convert into engineering CAD database
- reengineer part into a castable design
- generate STL file
- produce RP pattern
- invest pattern

2. Approach II
    a. identify component
        - o selection criteria
        - recurring and nonrecurring costs
        - part reduction
        - component weight
        - material/propellant capability, material properties
    b. directly draw CAD file
    c. produce prototyped "waxed" patterns for investment casting via an RP process

CASTING PROCESS GUIDE

Factors affecting the choice of process

Often more than one process is possible and in some circumstances geography or accessibility to a supplier's foundry may be considered important. Usually the economics are fairly straightforward and it is possible to devise a simple formula to assist the ultimate decision using such data as the cost of equipment, the unit cost of castings multiplied by the volume and making due allowance for any special factors.

Some of the most important factors affecting the choice of process, though not necessarily in order of importance, are as follows:

- The quantity of castings required
- Stability of the design
- The material specification
- Surface finish required
- Tolerances to be achieved

- Complexity
- The economics of machining versus castings costs
- Financial constraints on equipment costs
- Delivery requirements

General description of basic molding processes

Sandcasting. This is the oldest and most versatile of all the foundry processes. Within what is really a group of processes, there are a number of variables in regular use:

- Greensand molding
- No-bake (furane) molding
- CO_2 molding
- Loose molding
- Machine molding
- Oil sand cores
- Shell (resin bonded sand) cores
- CO_2 cores
- Furane (air setting) cores

Most foundries insist on using plated patterns, i.e. split patterns (two halves) mounted on boards or metal plates.

An important feature of plated patterns is the runner system through which molten metal passes from the downgate. Runner systems must be designed carefully to ensure correct metal flow to all parts of the mold cavity to avoid shrinkage cavities developing in the casting during the process of metal solidification.

The mold material consists of silica sand mixed with a suitable bonding agent. Clay is commonly used for so-called "greensand" molding but chemical binders are used for the production of CO_2 molds and "air set" molds. The CO_2 process involves the injection of carbon dioxide to harden the mold and, as the term implies, "air set" molds are produced using air hardening resins.

The molding material box is usually a metal frame (although wood is used for some processes and types of castings). The molding box is placed over the pattern plate and filled with sand which is compacted round the pattern to produce a cavity representing one half of the casting. Compaction is achieved by either jolting or "squeezing" the mold. Another mold of the other half is produced in like manner and the two molding boxes brought together to form the complete mold.

If the casting has hollow sections a core consisting of hardened sand (baked or chemically hardened) is used. Cores are located in cavities formed by projection on the pattern equipment known as core prints. Sometimes extra support for the core is provided by chaplets which fuse with the molten metal when the casting is poured.

High pressure molding techniques and in particular "Disamatic" molding machines have greatly improved the standards of accuracy and finish which can be achieved with certain types of castings. Normally, to take advantage of "Dismatic" production high volume is necessary.

Shell molding. Resin bonded silica sand is "dumped" on to a heated pattern plate, the heating producing a "biscuit" of fairly uniform thickness. Ejector pins enable the mold to be released from the pattern and the entire cycle is completed in seconds. The two halves of the mold, suitably cored, are glued and clamped together prior to the pouring in of the metal. Shell may be stored for long periods if desired. Because of pattern costs this method is best suited to volume production. It is then possible to take advantage of the close tolerances obtainable and designers should seek the advice of the foundry to ensure that all the benefits of the process are achieved.

Diecasting. There are three main types, normally used for zinc or light alloy castings:

1. Gravity diecasting
2. Low pressure diecasting
3. Pressure diecasting

All three processes can be used to provide extremely accurate castings and often a good deal of freedom to the designer. Die costs are considerably higher than tooling or patterns for other casting processes.

Normally gravity diecasting is used because it is more accurate than shell molding. It is preferred almost exclusively to shell molding for light alloy components.

Pressure die casting is a high volume production technique suitable for small zinc, light alloy and low melting point castings. Great care must be taken with the design to avoid porosity to which this process is prone.

Where pressure tightness is essential the user can arrange for vacuum impregnation. Sometimes the foundry is prepared to make arrangements with a suitable sub-contractor but, depending on circumstances, the user may prefer to deal directly with a local specialist company.

Permanent mold casting. This term describes the process of producing iron diecasting. The method of production is basically similar to gravity diecasting except that mold heat transfer problems differ from those of low melting point materials and, of course, the mold must be "insulated" from the casting by the deposition of the thin carbon coating on the surface of each mold cavity.

Investment casting (lost wax). This is a complete departure from the Sandcasting process in that wax impressions of the shape required are produced in a metal die. These wax "patterns" are assembled on a "tree" is then immersed in a fluidised bed of refractory particles to form the first layer of the ceramic shell. The mold is allowed to dry and the process repeated with coarser material until sufficient thickness has been built up to withstand the impact of hot metal.

The wax is then melted out for subsequent recovery and the molds pre-tested prior to casting. Most materials can be molded by this process but the economics indicate that fairly high volume is necessary and the shape and complexity of the castings should be such that savings are made by eliminating expensive machining. Unless advantage can be taken of these features, it is unlikely that the lost wax process will compare favorably with other processes. Accuracy of castings is totally dependent on the accuracy of the die and extremely fine tolerances can be achieved with an exceptionally wide range of materials.

General description of basic Core process

Some of the most critical dimensions in complex investment casting include injection molded and sintered cores. These defects are a major source of airfoil investment casting rejects. The primary problems are:

1. Distortion of the cores during the core manufacturing process
2. Inaccuracies in the placement of the finished cores in the part wax injection die
3. Distortion of the cores during subsequent casting process operations

Cores must be strong enough to survive handling, wax pattern injection, molten metal temperatures, pressures, impingement loads and thermal shock, therefore they must be manufactured out of refractory materials. They must also be compliant enough to allow the solidifying metal to contract normally and easy removal after the casting cools.

Typical Core Process Needs

Normally this method, *Ceramic molding* of production, would be applicable to high volume requirements. The yield (casting weight/metal melted ratio) is considerably higher than with sand castings and the absence of sand in the mold ensures excellent surface finish and no sand inclusions.

Injection molding involves injecting a mixture of refractory powder and proprietary carrier material into a metal mold under high pressure. Vents in the mold allow air to escape during the injection process. The extremely fragile "green" cores are then debinded from their carrier material and finally sintered at temperatures in excess of 1200 ^{0}C to obtain cores ready for insertion into wax patterns for later investment casting. Many core defects produced in these core fabrication steps can translate directly into defects and lead to higher scrap in the investment themselves. Such core defects would include, but not limited to:

- overall dimensional accuracy and stability
- low surface density
- voids
- breakage
- non-fills

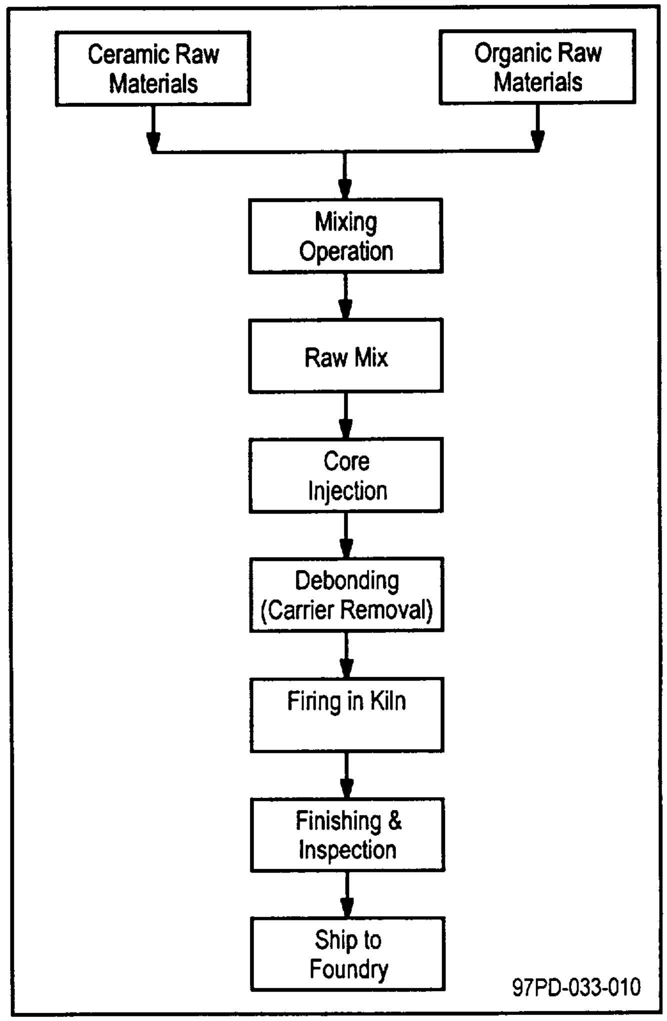

Figure 1

Typical Injection Molded Core Fabrication Process Steps

Foundry Processes

Advantages and disadvantages of various foundry process

Table 2

Advantages	Disadvantages
Sandcasting Most metals can be cast by this method Pattern costs are relatively low. The method is adaptable to large or small quantities	There are practical limits to complexity of design. Machining is often required to achieve the finished product. Dimensional accuracy cannot be rigidly controlled although good standards are possible with high class pattern equipment.
Shell molding Closer tolerances than with sand molding. Improved surface finish. Greater design latitude Better and more consistent quality	Equipment costs are relatively high. Castings tend to be more expensive but the extra cost can be more than offset by elimination of some machining operations.
Investment casting Extreme accuracy and flexibility of design. Useful for casting alloys that are difficult to machine. Exceptionally fine finish. Suitable for large or small quantities.	Limitation on size of casting. Casting costs make it important to take full advantage of the process to eliminate all machining operations.
(Shaw process) Excellent surface finish. Consistent quality.	Castings tend to be expensive. Used for relatively low volume. Dimensional accuracy broadly similar to Sandcasting, depending on standards of pattern equipment used.
Gravity diecasting (permanent mold) Good dimensional accuracy. Consistent quality Relatively inexpensive castings. Suitable for fairly complex castings in light alloys.	Relatively high cost of equipment. Commonly used for light alloy castings. Other metals can be cast using the permanent mold process but few foundries produce metals other than light alloy.
Pressure diecasting Low cost of castings. Good surface finish. Considerable design flexibility. High degree of accuracy. As with other processes inserts can be cast in if needed to enhance design capability.	Suitable for relatively low melting point and high volume. Limit on size of casting. Most suitable for small castings up to a few Kg. Equipment costs are high. Some risk of porosity. . Good sign is essential.
Centrifugal castings Improved homogeneity and accuracy in special circumstances.	Limitations on shape of castings. Normally restricted to the production of tubes or similar.

Alloys

There are several casting processes which can involve a wide range of metals. While virtually any molten metal can be poured into a mold to form a cast part, the metals considered will be contained to materials that are superalloys. This report will explore high-performance castings using superalloys.

Most of the superalloys are non-ferrous metals and are not fixed by a standards organization as are the carbon and alloy steels. They are generally known by their tradename designations. These castings are made almost exclusively by the precision investment casting method. The high-strength, nickel-base class is the predominant superbly type used for cast parts. These nickel-based superalloys may also contain materials such as boron and zirconium, which significantly prolongs life at elevated temperatures, are the most complex.

The most important property is the long-time strength at temperatures above 1200 ^{0}F and resistance to hot corrosion and erosion.

There are also the iron-base superalloys whose strengths are considerably lower at temperatures above 1200 ^{0}F, i.e. nickel-based alloys. High-temperature strengths in iron-based superalloys have been achieved by adding from 1% -3% of aluminum and titanium.

Cobalt-Base superalloys have a melting point advantage over nickel-base superalloys. Usually they are the strongest at temperatures of about 2000 ^{0}F and above. The higher the melting point, the greater the high-temperature strength of the metal. Consequently these alloys are used extensively in investment casting for aircraft turbine engine parts.

Aluminum Alloys - The casting processes most commonly used for aluminum alloys are sand, permanent, mold, die, and precision investment. Silicon is the most important alloying element for the following reasons:

1. increases fluidity of molten metal
2. promotes freedom from hot shortness (brittleness at elevated temperatures and leads to casting cracks

Copper is also added for improved strength.

Gating and Risering

Runner systems including the risers must be designed carefully to ensure correct metal flow to all parts of the mold cavity to avoid shrinkage cavities developing in the casting during the process of metal solidification.

Today there are solidification modeling programs that can take a stereolithography (STL) file used for Rapid Prototyping (RP) add the runner system and then simulate how the casting process should perform. *Trial runs on the computer can be made using potential gating.* Shrink and microstructure can be predicted. *The model can be run multiple times and gating readjusted until shrink is eliminated and micro structure is within specifications..* Given an STL file, this simulation process can now take from less than three days to several weeks to complete.

Thermal Controlled Solidification (TCS) process

An advanced casting process than controls the solidification of the casting by withdrawing the casting (especially large structures) through the hot to cold zone in the furnace. This process extends the range a gate and or risers being used can feed the casting:

Advantages of Using Gating Assembly (for large structures)

- Gating system less complex than conventional
- Metal cost decreased due to significant amount of feeding supplied by
- Decreased assembly and gating cost
- High quality

Disadvantages

- Higher capital requirements
- Special furnace requirements

Case Study - the LO_2 Tank Elbow

The casting design was generated (using SDRC IDEAS Master Series version 2.1). The casting alloy CF-8C, similar to Type 347 stainless steel, replaced the 321 CRES sheet material. The required minimum wall thickness was calculated at 0.065 in. Solidification modeling of the LO_2 Tank Elbow Casting was performed on two thickness variations: a) 0.200 in. and b) 0.100 in. nominal wall thickness.

With 0.200 in the casting was almost completely filled by the top gates, with the side gates acting as risers to feed the casting as it solidifies. Other variables such as pour velocity and gating design were modified to aid in enhancing the results. Modifying the gating design as well as the use of thermal wrap showed improved fluid and resulted in good mold fill.

Solidification modeling performed on the thinner 0.100 in. walled casting model led to the conclusion that the reduction in wall thickness had little effect on the flow pattern and solidification. The occurrence of shrink porosity or improper filling was not observed therefore indicating that a sound casting could be produced.

Reverse Engineering the Investment Casting Process

Investment Casting foundries indicated that stereolithography, using the QuickCast technique, is the preferred rapid prototyping process for directly producing consumable heat disposable patterns. QuickCast utilizes a unique build style which results in an open lattice internal structure. During burnout of the pattern from the investment shell, the quasi-hollow pattern permits the pattern to collapse inward, which greatly reduces the probability of breakage of the shell.

Process flow for Reverse Engineering

1. Select existing component
2. Reverse Engineer component
3. Generate electronic file using Computer Tomography unit (CT)
4. Convert file into CAD database
5. Produce castable design
6. Generate STL file

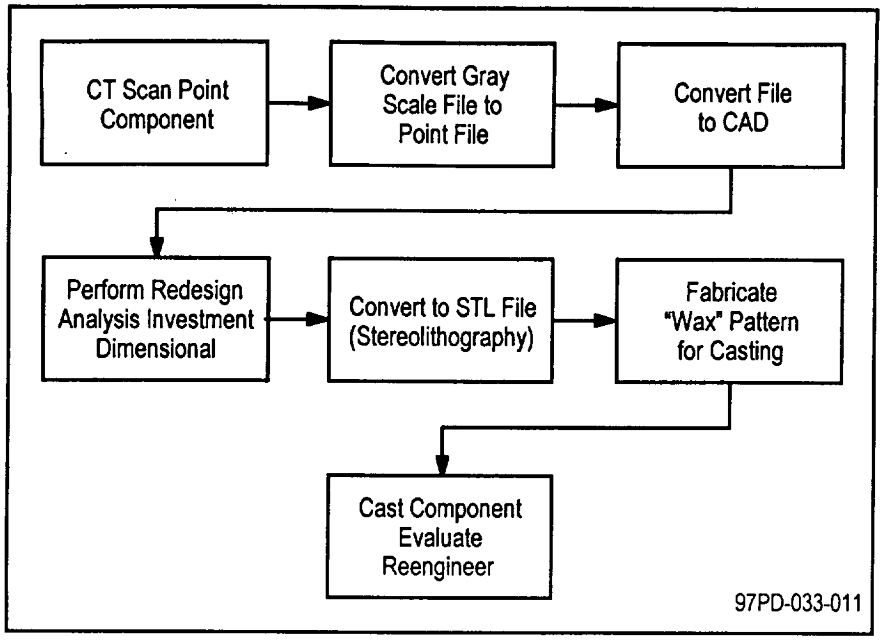

Figure 2
Approach to Reverse Engineer a Component Using a CT unit

Process flow for Conventional Casting

Similar to Reverse Engineering except the CAD file is generated through conventiona design practices.

RAPID PROTOTYPING

The objective of rapid near net shape casting is to shorten the cycle time for the fabrication and casting of high quality castings by utilizing RP (rapid prototyping) technology. While the emphasis is on launch vehicle and rocket engine components, it can apply to almost all commercial castings.

WHAT IS NEEDED

A conversion software is needed to convert the scanned images of the component into a point data file that can be translated into a CAD format. Imageware Surfacer software, used by Rocketdyne, is an acceptable one. It requires approximately 36 megabytes of memory and 20 hours to create a surface model. It provides an exact rendition of the scanned part, however modifying the part is very difficult because all of the parametric data used to build the design in Pro-E was not there, therefore the image is considered one big shape as opposed to a number of parametric surfaces.

For RP plastic injection tooling application, three techniques have been evaluated:

1. SLS (Selective Laser Sintering)
2. tool steel materials spraying technology
3. electroless nickel mold Hot Isostatic Press powder metal consolidation (HIP)

However, there are two viable RP processes to produce complex, "wax-like" patterns with acceptable surface finishes for rocket engine components:

1) Stereolithography (SLA)
2) Selective Laser Sintering (SLS) of metals. This technology produces metal components or dies directly which may be used for wax injection or the metal components may eventually be used directly. SLS was also investigated to evaluate the feasibility of using RP as a means of forming a green part, which could be subsequently sintered to high density and near net shape.

CAD models, created by reverse engineering and conventional CAD practices, can be used to generate STL (Stereolithography) files for the fabrication of RP patterns.

Reverse engineering produces the CAD file based on an existing part that has it's part shape generated by x-ray.

HOW IS IT USED

RP processes are used to produce toolless prototyped patterns from CAD files. From there the patterns are invested and the part is cast.

The application of selected RP processes to fabricate patterns directly for investing and the fabrication of temporary tooling for direct wax injection needs to be evaluated.

SLS (Selective Laser Sintering) is used to produce metallic and prototype shapes. Alloys, such as nickel-base superalloys and steels, can be used.

Several investment casting foundries indicate the stereolithography, using the QuickCast technique, is the preferred RP process for directly producing consumable heat disposable patterns. QuickCast utilizes a unique build style which results in an open lattice internal structure. During the burnout of the pattern from the investment shell, the quasi-hollow pattern permits the pattern to collapse inward, which greatly reduces the probability of breakage of the shell.

Components need to be identified for fabrication by RP and generate a casting design by conventional CAD drawing. Selection Criteria included:

- Recurring and nonrecurring costs
- Part reduction
- Component weight
- Material/propellant capability, material properties
- Qualifying/implementation cost
- Weldability/repair issues, etc.

RP is also used to make metal tooling for the sheet metal stamping industry, the plastic injection molding industry and for wax injection tooling for the casting industry.

LIMITATIONS

To date RP has been used mainly to make plastic models to verify designs and show proof of concept and produce patterns for investment casting. Fabrication of metal components directly for functional prototypes has not been successfully demonstrated for high-strength, large-scale parts. However, use of the DTM Sinterstation 2000 has allowed some success in fabricating functional metal RP parts such as a gas generator housing and a thin wall launch vehicle. Larger parts can be fabricated by joining segments. Materials needed are: investment cast wax, polycarbonate (wax filled or epoxy filled), Nylon-11 (standard and fine grades), DTM RapidTool ™ Iron/Copper Metal.

The cost to generate the CAD file needed for SLS is still one of the primary barriers of using this technology in reverse engineering.

APPENDIX: GLOSSARY OF FOUNDRY TERMS

Backing sand	The bulk of the sand in the molding box. Used to pack between the facing sand which surrounds the pattern and the molding box.
Binder	The bonding agent used as an additive to mold or core sand to impart strength or plasticity in a "green" or dry state (*see also* greensand).
Burn-on	Sand adhering to the surface of the casting which is extremely difficult to remove. Normally due to soft molds, insufficient mold coating (graphite) paint or excessive pouring temperature.
Chaplet	A small metal insert normally used to provide additional core support. Correctly used will fuse with the molten metal.
Charge	The contents of a furnace consisting of metal and fuel.
Chill	A metal insert in the sand to produce local cooling and equalize rate of cooling throughout the casting.
CO2 process	Molding sand is mixed with Sodium Silicate and the mold is injected with Carbon Dioxide gas for approximately 20 seconds to produce a hard mold or core.
Cod	A projection of sand on the outside of the mold (i.e. beyond the joint line).
Cold shut	A crack or surface imperfection due to unsatisfactory fusion of metal. Caused by insufficient fluidity, low pouring temperature, poor choice of alloy or possibly inadequate runner systems.
Contraction crack	A crack caused by restriction in the mold, normal metal contraction or stresses set up by early removal of the casting from the mold, i.e. too rapid cooling.
Cope	The top half of a mold (*see* molding box).
Core	The means of producing a cavity in a casting, i.e. the inside shape of the casting.
Core assembly	A mold built up from a number of cores. Sometimes assembled within a metal frame for extra mold strength. Cores are CO2 or air set.
Corebox	The wooden or metal mold used to produce cores (*see* also hotbox).
Coreprint	A projection on a pattern which leaves an impression in the mold for supporting the core.

Die	A metal mold frequently produced by accurate machining. Used as a permanent mold for diecasting or lost wax processes. For short-run lost wax requirements, plaster dies may be used.
Downgate	The channel from the top of the mold through which molten metal is poured into the mold cavity (*see also* runner system).
Drag	The bottom half of a mold (*see also* molding box).
Facing Sand	The sand used to surround the pattern, which produces the surface in contact with the molten metal.
Feeder	Sometimes referred to as a riser. A vertical channel in the mold (part of the runner system) which forms the reservoir of molten metal necessary to compensate for losses due to shrinkage as the casting metal cools.
Fettling	Removal of runners, risers, flash, surplus metal and sand from a casting.
Flash	Thin rough metal projecting from an unsettled casting where molten metal has seeped between mold and/or core faces.
Furnace process	Molds/cores produced with a resin bonded air setting sand. Also known as the air set (no bake) process because molds are left to harden under normal atmospheric conditions.
Gas Hole	Similar to blow holes but more evenly distributed throughout the casting. Caused by the trapping of gas in the molten metal due to use of unsuitable sand.
Gate	The junction of the channel from the top of the mold (the sprue) and the mold cavity.
Greensand	Moist clay bonded molding sand-the most commonly used mold material.
Hotbox	A term used to describe the method of producing shell cores-a similar technique to that for producing shell molds.
Hot tear	Irregularly shaped crack resulting from stresses set up by steep thermal gradients within the casting and too much rigidity of core material.
Ingate	Channels in the bottom half of the mold supplying the mold cavity with molten metal.
Join Line	The line between the two halves of the mold.
Knock-out	The process of separating the solidified casting from the mold material.
Ladle	A container for molten metal used to transfer metal from the furnace to the mold.
Mold	Normally consists of top and bottom molding boxes placed one on top of the other (cope and drag) forming a cavity into which molten metal is poured (*see also* core assembly process).
Molding Box	A rigid frame containing sand (*see also* mold).

Pattern	The wooden or metal shape used to form the cavity in the sand. A pattern may consist of one or many impressions and would normally be mounted on a board or plate complete with runner system.
Porosity	Holes in the casting due to gases trapped in the mold, reaction of molten metal with (blowholes) moisture in the molding sand or imperfect fusion of chaplets with molten metal. Surface porosity may be due to overheating of the mold or core faces but should not be confused with sand inclusions.
Runner	The set of channels in a mold through which molten metal is poured to fill the mold system cavity. The system normally consists of a vertical section (downgate or sprue) to the point where it joins the mold cavity (gate) and leading from the mold cavity further vertical channels (risers or feeder heads).
Sand Defect	Cavities or surface imperfections caused by poorly bonded or lightly rammed sand washing inclusions into the mold cavity (or from crushing).
Scrap	(a) Any scrap metal (usually with suitable additions of pig iron or ingots) to produce castings. (b) Reject castings.
Shrinkage	Contraction of metal in the mold on cooling. The term often used to describe the effect, i.e., shrinkage cavity. This results from poor design, insufficient feed metal or inadequate feeding arrangements, possibly arising form attempts to reduce cost.
Slag	Similar to sand inclusions but also containing impurities from the molten metal inclusions.

REFERENCES

Title: AN UPDATE ON PERMANENT MOLD CASTING

Author: A. P. Clark

Journal: 1st International Conference on Austempered Ductile Iron: Your Means to Improved Performance, Productivity, and Cost. ASM, P215-2, Rosemont, IL, April 2-4, 1984 (11 pages)

Abstract: Paper discusses permanent melding of ferrous metals (gray, ductile, and ADI types) and outlines the economies of producing near net shape castings through this method. Basically, the permanent mold procedure achieves far better material utilization resulting in energy, material, and labor savings, not to mention costs of sand reclamation or disposal. Of interest is the assessment of plant size and equipment required when comparing any sand casting method with permanent molding. Many examples of recent conversions to this method are shown and discussed such as gears, automobile crankshafts, suspension parts, all of which profited from the enhanced properties of clean metal

PR: 11

REPORT DOCUMENTATION PAGE

Form Approved
OMB No. 0704-0188

1. AGENCY USE ONLY (*Leave blank*)	2. REPORT DATE	3. REPORT TYPE AND DATES COVERED
	September 1997	Final Contractor Report

4. TITLE AND SUBTITLE

Precision Casting via Advanced Simulation and Manufacturing
Summary of Research

5. FUNDING NUMBERS

WU-523-22-13-00
NCC3-386

6. AUTHOR(S)

7. PERFORMING ORGANIZATION NAME(S) AND ADDRESS(ES)

Rocketdyne Division
Boeing North American, Inc.
6633 Canoga Avenue
Canoga Park, California 91303

8. PERFORMING ORGANIZATION REPORT NUMBER

E-10912

9. SPONSORING/MONITORING AGENCY NAME(S) AND ADDRESS(ES)

National Aeronautics and Space Administration
Lewis Research Center
Cleveland, Ohio 44135-3191

10. SPONSORING/MONITORING AGENCY REPORT NUMBER

NASA CR-204147
RD97-129

11. SUPPLEMENTARY NOTES

Project Managers, Robert L. Dreshfield and Robert H. Titran, Materials Division, NASA Lewis Research Center, organization code 5120, (216) 433-3198.

12a. DISTRIBUTION/AVAILABILITY STATEMENT

Unclassified - Unlimited
Subject Categories 31 and 38

This publication is available from the NASA Center for AeroSpace Information, (301) 621-0390.

12b. DISTRIBUTION CODE

13. ABSTRACT ***(Maximum 200 words)***

A two-year program was conducted to develop and commercially implement selected casting manufacturing technologies to enable significant reductions in the costs of castings, increase the complexity and dimensional accuracy of castings, and reduce the development times for delivery of high quality castings. The industry-led R&D project was cost shared with NASA's Aerospace Industry Technology Program (AITP). The Rocketdyne Division of Boeing North American, Inc. served as the team lead with participation from Lockheed Martin, Ford Motor Company, Howmet Corporation, PCC Airfoils, General Electric, UES, Inc., University of Alabama, Auburn University, Robinson, Inc., Aracor, and NASA-LeRC. The technical effort was organized into four distinct tasks. The accomplishments reported herein. Task 1.0 developed advanced simulation technology for core molding. Ford headed up this task. On this program, a specialized core machine was designed and built. Task 2.0 focused on intelligent process control for precision core molding. Howmet led this effort. The primary focus of these experimental efforts was to characterize the process parameters that have a strong impact on dimensional control issues of injection molded cores during their fabrication. Task 3.0 developed and applied rapid prototyping to produce near net shape castings. Rocketdyne was responsible for this task. CAD files were generated using reverse engineering, rapid prototype patterns were fabricated using SLS and SLA, and castings produced and evaluated. Task 4.0 was aimed at developing technology transfer. Rocketdyne coordinated this task. Casting related technology, explored and evaluated in the first three tasks of this program, was implemented into manufacturing processes.

14. SUBJECT TERMS

Casting; Sand core molding; Injection molded cores

15. NUMBER OF PAGES 172

16. PRICE CODE A08

17. SECURITY CLASSIFICATION OF REPORT	18. SECURITY CLASSIFICATION OF THIS PAGE	19. SECURITY CLASSIFICATION OF ABSTRACT	20. LIMITATION OF ABSTRACT
Unclassified	Unclassified	Unclassified	

NSN 7540-01-280-5500

Standard Form 298 (Rev. 2-89)
Prescribed by ANSI Std. Z39-18
298-102